



Cardiff  
Catalysis Institute

---

Sefydliad Catalysis  
Caerdydd

Glycerol Oxidation; An investigation into the control  
of product distribution and mechanistic pathways  
using novel supports

Thesis submitted in accordance with the requirement of Cardiff University  
for the degree of Doctor of Philosophy

**Christopher Dean Evans**

**September 2017**

## PhD Thesis Summary

The work in this thesis involves an investigation into glycerol oxidation with the aim of selectively producing lactic acid. A series of experiments was conducted so as to find an optimal set of conditions to produce high yields of lactic acid using a standard 1 wt % AuPt/TiO<sub>2</sub>. This was achieved through the sequential elimination of reaction conditions in a parameter mapping study. The high yield of lactic acid obtained from the parameter mapping study enabled the design of an experiment in which the mechanism of formation of lactic acid could be identified through <sup>13</sup>C labelling experiments. It was found that the mechanism proceeds through an intramolecular hydride shift as opposed to the previously suggested Cannizzaro reaction or benzilic rearrangement.

The results from the parameter mapping study were also used to begin a study into supercritical anti-solvent prepared perovskite materials to be used as supports for the control of product distribution in glycerol oxidation. It was found that under the same conditions used to produce high yields of lactic acid with AuPt/TiO<sub>2</sub>, a Mn based lanthanide perovskite instead produced high yields of oxidation products. Using a series of B site substitutions into a La based perovskite lattice, each was tested to observe how the B site effected the product distribution in glycerol oxidation. A correlation was found between oxygen adsorption data and affinity to the oxidation pathway. The higher the oxygen adsorption, the more oxidation products produced, and opposed to this, the lower the oxygen adsorption the higher the affinity to the dehydration pathway

## **Acknowledgements**

Conducting a PhD and writing this thesis has been an extremely rewarding experience. I feel have developed both personally and professionally and have thoroughly enjoyed my time within the Cardiff Catalysis institute

Firstly, I would like to thank the UK catalysis hub and my PhD supervisor Professor Graham Hutchings for allowing me the opportunity to conduct research in a world leading department. Regular meetings have allowed me to progress throughout, with advice helping me produce the body of work written in this thesis. I would also like to thank several prestigious professors, whom offered advice and guidance throughout; Donald Bethell and David Knight for their wisdom in organic mechanisms, Stuart Taylor for offering me opportunities beyond my PhD and Phil Davies for guiding my progress.

I would not have gotten far without the help of my post-doctoral supervisors; Dr Simon Kondrat and Dr Gemma Brett, both of who have helped me with their in-depth knowledge of the subject matter and their encouragement. I would never have completed this without you.

I would also like to thank my PhD peers who conducted their PhDs alongside me, who helped support me through the challenges we all faced; Ricci Underhill, David Crole, Gavin King, David Watson, Richard Lewis, Mark Douthwaite and Samuel Emanuel Patisson.

## Abstract

There is a major limitation preventing the use of bio-fuels as they are currently not economically viable when compared to fossil fuels. To make bio-fuels more economically attractive, new chemical processes for converting waste by-products into a valuable commodity are necessary. One of the main by-products from the production of bio-fuels is glycerol. This thesis investigates the oxidation of glycerol with the aim of selectively producing lactic acid.

Glycerol oxidation is a relatively complex reaction with two potential pathways leading to a variety of products. The oxidation pathway leads to the C3 products glyceric acid and tartronic acid, with further oxidation leading to C2 and C1 products. The dehydration pathway leads to lactic acid, through a currently unknown mechanism. The reaction scheme sets out two challenges to solve; what conditions are optimal for a high yield of lactic acid and what is the mechanism. When observing the two challenges, one begets the other. By characterising what conditions are optimal for lactic acid production, it would then be plausible that an experiment could be designed to confirm the mechanism of lactic acid formation.

Using a standard 1 wt% AuPt/TiO<sub>2</sub> catalyst, an investigation into the reaction conditions was conducted and it was found that the conditions had a significant effect on the product distribution. A progressive elimination was designed so as to progressively find the optimal conditions for the formation of lactic acid. The conditions mapped were; temperature, O<sub>2</sub> pressure, base substrate ratio, metal substrate ratio and stabilising agent used to produce the catalyst. Temperature was found to increase selectivity to lactic acid as it was increased. Increasing the O<sub>2</sub> pressure showed an increase in lactic acid selectivity up to 3 bar, at which point there was an increase in C-C scission products. By increasing the base ratio, lactic acid selectivity increased dramatically, providing an insight that would later be used to help confirm the mechanism. Higher metal substrate ratio was found to increase the C-C scission products formed. Four types of stabilising agent were used to observe the effect of stability and activity, with PVA providing a balance between stability and selectivity. The parameter map led to a series of conditions that produced a yield of 80 % lactic acid.

Using the conditions found from the parameter mapping study, an experiment was designed to attempt to confirm the mechanism of formation for lactic acid. Two current theories that lactic acid formation proceeds either *via* a benzylic rearrangement or a Cannizzaro reaction, provided an insight as to how this would be achieved, as the position of the carbon environments in lactic acid would change dependent on the mechanism followed. Through a <sup>13</sup>C labelling study, NMR spectroscopy was used to show that there was no net movement of the carbon

environments during the mechanism, discounting the benzylic rearrangement. Through a logical discussion, the Cannizzaro reaction was also discounted as technically this is an intermolecular hydride shift, with the mechanism being confirmed to be an intramolecular hydride shift.

Supercritically prepared perovskite supports were used to see if the lactic acid yield could be increased further through the change of the B site cation. Contrary to initial belief,  $\text{LaMnO}_3$  heavily favoured the oxidation pathway at the same conditions the standard  $\text{AuPt/TiO}_2$  produced a high yield to lactic acid. This was found to correlate with the oxygen adsorption to a clean lattice structure, as perovskites with high oxygen adsorption favoured the oxidation pathway whilst low oxygen adsorption favoured the dehydration pathway.  $\text{LaCrO}_3$  was found to produce a yield of up to 86 % lactic acid under the optimal conditions outlined in the parameter mapping study. The selective control of reaction products could ultimately lead to more economically viable bio-fuel production

<b>1.0. INTRODUCTION.....</b>	<b>1</b>
<b>1.1. CATALYSIS.....</b>	<b>1</b>
<b>1.2. KINETICS AND THERMODYNAMICS IN CATALYSIS .....</b>	<b>2</b>
<b>1.3. GOLD AND HETEROGENEOUS CATALYSIS .....</b>	<b>4</b>
<b>1.4. CATALYST PREPARATION METHODS.....</b>	<b>5</b>
<b>1.5. THE DIRECT SYNTHESIS OF HYDROGEN PEROXIDE.....</b>	<b>6</b>
<b>1.6. THE SELECTIVE OXIDATION OF ALCOHOLS .....</b>	<b>8</b>
<b>1.6.1. Benzyl alcohol oxidation.....</b>	<b>9</b>
<b>1.6.2. Cinnamyl alcohol oxidation .....</b>	<b>10</b>
<b>1.6.3. 1,2-Propanediol oxidation .....</b>	<b>11</b>
<b>1.7. OXIDATION OF BIO-RENEWABLE FEEDSTOCKS .....</b>	<b>13</b>
<b>1.7.1. The Energy Crisis .....</b>	<b>13</b>
<b>1.7.2. Fine chemical production from bio-renewable resources.....</b>	<b>14</b>
<b>1.7.3. Glycerol oxidation .....</b>	<b>15</b>
<b>1.7.3.1. Reaction conditions in glycerol oxidation .....</b>	<b>17</b>
<b>1.8. ORGANIC MECHANISMS .....</b>	<b>20</b>
<b>1.9. CATALYST PREPARATION USING SUPERCRITICAL FLUIDS.....</b>	<b>22</b>
<b>1.9.1. Brief introduction to supercritical fluids.....</b>	<b>22</b>
<b>1.9.2. Properties of supercritical fluids .....</b>	<b>23</b>
<b>1.9.3. Applications of supercritical fluids .....</b>	<b>25</b>
<b>i) RAPID EXPANSION OF SUPERCRITICAL SOLUTIONS (RESS).....</b>	<b>26</b>
<b>ii) SUPERCRITICAL ASSISTED ATOMISATION (SAA).....</b>	<b>26</b>
<b>iii) SUPERCRITICAL ANTI-SOLVENT PREPARATION (SAS).....</b>	<b>26</b>
<b>1.9.4. Basics of the supercritical anti-solvent process.....</b>	<b>26</b>
<b>1.9.5. Supercritical anti-solvent preparation methods .....</b>	<b>27</b>
<b>1.9.5.1 Gas anti-solvent process .....</b>	<b>27</b>
<b>1.9.5.2. Supercritical anti-solvent process.....</b>	<b>28</b>
<b>1.9.6. GAS and SAS for material preparation .....</b>	<b>29</b>
<b>1.9.7. Catalyst preparation using SC-CO<sub>2</sub> SAS preparation .....</b>	<b>30</b>
<b>1.9.8. Perovskites in catalysis.....</b>	<b>31</b>
.....	<b>31</b>
<b>1.9.9 REFERENCES .....</b>	<b>34</b>
<b>2.0. EXPERIMENTAL.....</b>	<b>43</b>
<b>2.1. MATERIALS.....</b>	<b>43</b>

<b>2.2. DEFINITIONS.....</b>	<b>44</b>
<b>2.3. SUPPORT PREPARATION .....</b>	<b>44</b>
<b>2.3.1. SUPERCRITICAL ANTI-SOLVENT (SAS) PREPARATION .....</b>	<b>45</b>
<b>2.3.1.1 Supercritical anti-solvent (SAS) apparatus .....</b>	<b>45</b>
<b>2.3.1.2 Supercritical anti-solvent (SAS) support preparation.....</b>	<b>47</b>
<b>2.3.2. FLAME PYROLYSIS (FP) PREPARATION .....</b>	<b>47</b>
<b>2.3.2.1. Flame pyrolysis (FP) apparatus.....</b>	<b>47</b>
<b>2.3.2.2. Flame pyrolysis (FP) support preparation .....</b>	<b>48</b>
<b>2.3.3. PLANETARY BALL MILL (BM) PREPARATION.....</b>	<b>49</b>
<b>2.3.3.1. Planetary ball mill (BM) apparatus .....</b>	<b>49</b>
<b>2.3.3.2. Planetary Ball Mill (BM) Support preparation .....</b>	<b>49</b>
<b>2.4. CHROMIUM (II) ACETATE PRECURSOR SYNTHESIS .....</b>	<b>49</b>
<b>2.5. CATALYST PREPARATION .....</b>	<b>50</b>
<b>2.5.1. SOL IMMOBILISATION PREPARATION .....</b>	<b>50</b>
<b>2.6. CATALYST TESTING .....</b>	<b>51</b>
<b>2.6.1. OXIDATION OF GLYCEROL IN WATER – STANDARD REACTION CONDITIONS IN A GLASS REACTOR ...</b>	<b>51</b>
<b>2.7. CHARACTERISATION .....</b>	<b>51</b>
<b>2.7.1. POWDER X-RAY DIFFRACTION (XRD) .....</b>	<b>51</b>
<b>2.7.3. THERMOGRAVIMETRIC ANALYSIS (TGA).....</b>	<b>53</b>
<b>2.7.. TEMPERATURE PROGRAMMED DESORPTION (TPD).....</b>	<b>54</b>
<b>2.7.. BRUNAUER EMMETT TELLER (BET) SURFACE AREA ANALYSIS .....</b>	<b>54</b>
<b>2.7.. MICROWAVE PLASMA ATOMIC EMISSION SPECTROSCOPY (MP-AES) .....</b>	<b>55</b>
<b>2.7.. TRANSITION ELECTRON MICROSCOPY (TEM).....</b>	<b>56</b>
<b>2.7.. NUCLEAR MAGNETIC RESONANCE (NMR) SPECTROSCOPY .....</b>	<b>58</b>
<b>2.7..1. Nuclear magnetic resonance theory .....</b>	<b>58</b>
<b>2.7..2. Nuclear magnetic resonance experimental.....</b>	<b>59</b>
<b>3.0 AN INVESTIGATION INTO GLYCEROL OXIDATION .....</b>	<b>60</b>
<b>3.1. INTRODUCTION .....</b>	<b>60</b>
<b>3.2. AIMS AND OBJECTIVES.....</b>	<b>61</b>
<b>3.2.1. OBJECTIVE .....</b>	<b>61</b>
<b>3.2.2. AIMS.....</b>	<b>61</b>

<b>3.3. CATALYST PREPARATION .....</b>	<b>61</b>
<b>3.4. CATALYST CHARACTERISATION .....</b>	<b>62</b>
3.4.1. TRANSMISSION ELECTRON MICROSCOPY .....	62
3.4.2. PHASES, LOADING AND SURFACE AREA OF THE SUPPORT .....	63
3.4.3. ISOELECTRIC POINT OF P25 TiO <sub>2</sub> .....	65
<b>3.5. CONDITIONAL PARAMETER MAPPING OF GLYCEROL OXIDATION.....</b>	<b>66</b>
3.5.1. THE EFFECT OF TEMPERATURE.....	67
3.5.2. THE EFFECT OF PRESSURE.....	70
3.5.3. THE EFFECT OF BASE RATIO.....	74
3.5.4. THE EFFECT OF METAL SUBSTRATE RATIO .....	78
3.5.5. THE EFFECT OF STABILISING AGENT AND REUSABILITY .....	80
3.5.6. OPTIMISED CONDITIONS FOR LACTIC ACID PRODUCTION .....	83
<b>3.6. THE MECHANISTIC PATHWAY TO LACTIC ACID.....</b>	<b>84</b>
3.6.1. LABELLED GLYCEROL EXPERIMENTS.....	87
<b>3.7. ONCLUSIONS .....</b>	<b>90</b>
<b>3.8. REFERENCES .....</b>	<b>92</b>
<b>4.0. PEROVSKITES FOR PRODUCT CONTROL .....</b>	<b>94</b>
<b>4.1. INTRODUCTION .....</b>	<b>94</b>
<b>4.2. SUPERCRITICAL ANTISOLVENT (SAS) PREPARATION OF PEROVSKITE TYPE MIXED METAL OXIDES .....</b>	<b>95</b>
4.2.1. PEROVSKITE SYNTHESIS AND PURITY .....	95
4.2.1.1. Thermogravimetric analysis (TGA) analysis .....	95
4.2.1.2. X-ray diffraction (XRD) analysis.....	96
4.2.1.3. Surface area analysis.....	99
4.2.2. CATALYST PREPARATION.....	100
4.2.3. CATALYST CHARACTERISATION.....	101
4.2.3.1. Transmission electron microscopy .....	101
4.2.3.2. Microwave-plasma atomic emission spectroscopy .....	103
4.2.3.3. X-ray photon spectroscopy .....	103
4.2.3.4. Ammonia temperature programmed desorption .....	105
<b>4.3. CATALYST TESTING.....</b>	<b>106</b>

4.3.1.	UNSUPPORTED PEROVSKITE SUPPORTS .....	107
4.3.2.	SUPPORTED PRECIOUS METAL CATALYST TESTING .....	107
4.3.2.1.	<i>Perovskite Supported catalysts</i> .....	107
4.3.2.2.	<i>Supported single oxide supports</i> .....	113
4.4.	SELECTIVE FORMATION OF VALUE ADDED PRODUCTS.....	114
4.4.1.	SELECTIVE CONTROL FOR THE PRODUCTION OF GLYCERIC AND TARTRONIC ACID.....	114
4.4.1.1.	<i>Effect of metal ratio on selectivity</i> .....	115
	.....	116
4.4.1.2.	<i>Selective formation of tartronic acid</i> .....	117
4.4.1.3.	<i>Kinetic model for AuPt/LaMnO<sub>3</sub> from initial rates</i> .....	118
4.4.2.	SELECTIVE FORMATION OF LACTIC ACID.....	120
4.4.2.1.	<i>The effect of metal ratio</i> .....	121
4.4.2.2.	<i>Selective formation of lactic acid</i> .....	123
4.5.	COMPARING SUPPORT PREPARATION TECHNIQUES.....	124
4.6.	CONCLUSIONS.....	127
4.7.	REFERENCES.....	129
5.0.	CONCLUSIONS AND FUTURE WORK.....	131
5.1.	CONCLUSIONS .....	131
5.1.2.	IDEAL CONDITIONS FOR LACTIC ACID PRODUCTION .....	131
5.1.2.	DETERMINING THE MECHANISTIC ROUTE TO LACTIC ACID .....	132
5.1.3.	CONTROLLING PRODUCT DISTRIBUTION WITH PEROVSKITES .....	133
5.2.	FUTURE WORK.....	134
5.2.1.	A SITE DOPING .....	134
5.2.2.	GLYCEROL IN FLOW .....	136

## Introduction

### 1.1. Catalysis

In the early beginnings of Chemistry, it was once possible to produce an annual report that summarised the entirety of Chemistry. This task was undertaken by the noted Swedish chemist, J.J. Berzelius, and during his summaries he observed that the addition of particular compounds in low concentrations seemed to exert a force on the reactants within the reaction aiding their decomposition. Berzelius dubbed this the “catalytic force” which was the beginning of modern catalysis<sup>1</sup>. The current definition of a catalyst is:

“A catalyst is a body or material which can induce the phenomena of catalysis. It enhances the rate of the reaction, and whilst the catalyst is immediately involved within the reaction, it is not consumed and can be recovered at the end of it.”<sup>2</sup>

Catalysts have a wide range of applications and are utilised in everyday processes, many of which are essential to the modern world, from the production of ammonia for fertiliser through the Haber process, to the control of exhaust emissions<sup>3</sup>. Biological catalysts, known as enzymes, control almost all of the reactions within living organisms in the natural world, most of which are made up of product specific proteins<sup>4</sup>. Synthesis of man-made catalysts are conducted in an effort to replicate the specific activity and product selective nature of enzymes, and are classified in two main forms, homogeneous and heterogeneous catalysts.

Homogeneous catalysts are always within the same phase as the reactant species used, such as the catalyst for the production of phenol from toluene<sup>5</sup>. Homogeneous catalysts are well documented and can provide a high degree of atom efficiency and product selectivity in a reaction and are typically formed of ligand bound metal centres with highly controlled coordination numbers. To achieve the highest possible product selectivities it is necessary to consider the metal oxidation state and stereoelectronic properties of the ligands, allowing for site specific complexes<sup>6</sup>. The main issue associated with the industrialisation of homogeneous catalysts is the separation of the catalysts from the reaction effluent post reaction.

Heterogeneous catalysts operate in a separate phase to the reactant species, an example of which would be the solid catalyst used in the gas phase reaction of hydrogen production from steam reforming<sup>7</sup>. Heterogeneous catalysts are almost entirely solid phase catalysts used in gas or liquid phase systems. The phase difference between the catalyst and reaction mixture makes the separation of both much simpler than with homogeneous catalysts, a big advantage for industrial processes. Heterogeneous catalysts tend to be single or mixed

metal oxides which can either be used alone, for example  $\text{CeO}_2$  in the total oxidation of naphthalene<sup>8</sup>, or they can be enhanced by the addition of nanoparticles to the surface<sup>9, 10</sup>. Although the ability to control specific selectivity is more difficult than in heterogeneous catalysis, industrial applications favour the ability to separate and reuse heterogeneous catalysts, and as such, they are incorporated into many industrial processes including acetylene hydrochlorination<sup>11</sup>, Fischer-Tropsch synthesis of hydrocarbons and ammonia<sup>12</sup>, steam reforming and the water-gas shift reaction<sup>13</sup> being some of the most prominent examples. Heterogeneous catalysis has many complex mechanisms that are yet to be discovered and is an extremely fruitful research topic for future developments.

## 1.2. Kinetics and thermodynamics in catalysis

One of the defining features of a catalyst is the surface structure, which is predominantly responsible for the activity of the catalyst as well as how selective a catalyst is towards particular products within a reaction. This is due to the fundamental process of diffusion that occurs on the surface involving the transfer of liquid or gas molecules. These molecules, or reactants, then bond to the surface through adsorption and can travel across the surface through surface diffusion.

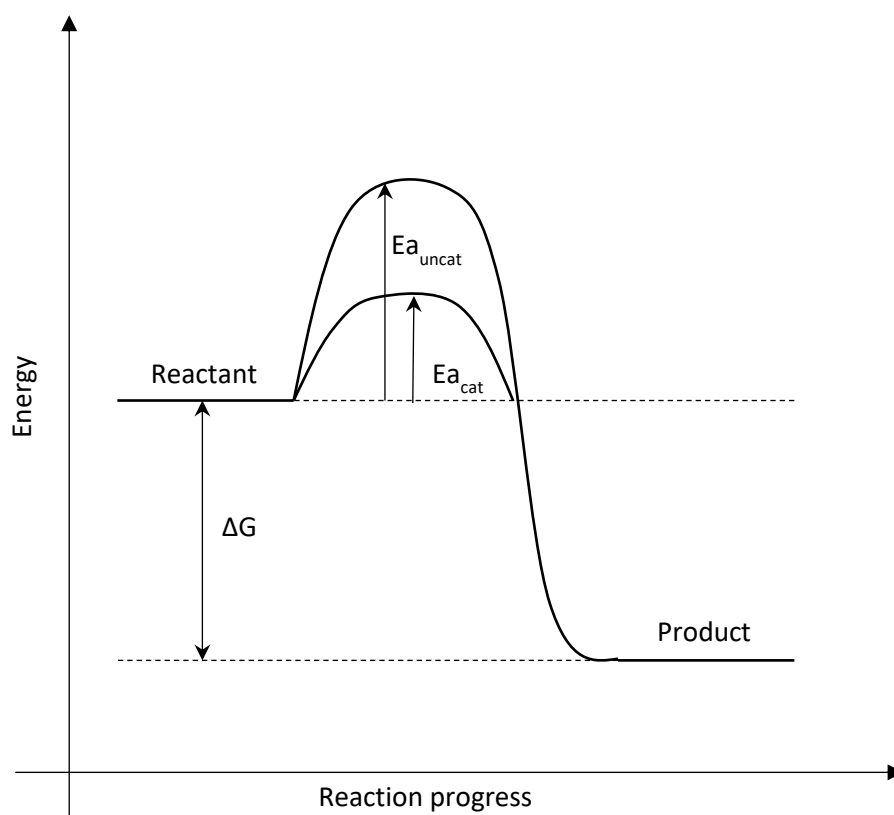


**Figure 1. 1 Energy level diagram describing a typical reaction showing the alternate, lower energy pathway as a result of adding a catalyst.**

The reactants may then dissociate and surface reactions can occur in which the adsorbed species can react together, often known as the rate determining step (RDS). The reacted molecules, or products, then leave the catalyst surface through desorption. This process offers a lower, alternate pathway for the reaction of the molecules to occur and is illustrated in Figure 1.1.

An important consideration of a catalysed reaction is that the free energy of the system is left unchanged as the catalyst itself has no effect on either the reactants or products within the system. It is also true that due to the fundamental laws of thermodynamics that the use of a catalyst also does not affect the equilibrium position of a reaction system, which means that the catalyst must equally promote both forward and reverse reactions. It can be concluded from these points that the catalyst therefore only affects the kinetics of a reaction system and not thermodynamics.

To attempt to understand the material role of a catalyst in a reaction system, knowledge of the kinetics involved within the reaction system is required. The key to deriving the kinetics of a reaction system is the identification of the rate dependency at various stages of the reaction mechanism, which, in turn enables the manipulation of conditions to optimise the reaction whether this be through conditional parameters such as temperature or pressure, reactor design or specific catalyst design. Although the simplest way of visualising this as an example is through a unimolecular system, in a real-world scenario, most reactions are bimolecular, therefore in concept, CO oxidation makes a simple, proven model to view as an example. *Haruta et al.* showed that gold catalysts were extremely effective for CO oxidation<sup>14</sup> as it was found that by supporting gold nanoparticles on iron oxide that the catalyst was superior to the previous catalysts used.

—

***Equation 1.1 Showing a stoichiometric equation for the oxidation of carbon monoxide to carbon dioxide.***

Although the CO oxidation reaction (equation 1.1) looks simple on the surface, and is being used as one of the simplest possible bimolecular reactions to consider, there is still a surprising degree of complexity involved. The mechanism of CO oxidation has been debated and expanded upon continuously over a period of 3 decades<sup>15-17</sup>, illustrating just how complex the subject of kinetics is. This is due to the large number of variables that are present within any one reaction system. As the reaction system itself gets more complex, so to do the kinetics involved,

making kinetic modelling an extremely challenging subject to pursue. One way to simplify this process without affecting the results detrimentally, is to view the kinetic change from the reactants to the products as a whole, rather than looking at each of the individual processes described in figure 1.1. The information gathered from this process can be processed by the kinetic rate equation shown in equation 1.2.

**Equation 1.2 Kinetic rate equation describing the reaction between reactants A, B and C, where;  $K$  is the reaction rate,  $k$  is the rate constant,  $cat$  is a constant,  $a$ ,  $b$ , and  $c$  represent the order of reaction with respect to the concentration of A, B and C.**

The order of a reaction is an efficient method to classify specific chemical reactions and by determining the order of reaction in respect to the concentration of reactants, A, B and C, it ultimately allows the calculation of the activation energy ( $E_a$ ) of the reaction. This is achieved by finding  $K$  through the initial rates method, followed by rearranging the kinetic rate equation to find the rate constant,  $k$ , at a range of temperatures. These values are then used to derive the activation energy through use of the Arrhenius Equation shown below (Equation 1.3). The activation energy allows us to experimentally define why a preferred reaction pathway is followed through the reaction.

---

**Equation 1.3 Arrhenius equation for derivation of the activation energy ( $E_a$ ) of a reaction where;  $k$  is the rate constant,  $A$  is the pre-exponential factor,  $R$  is the gas constant, and  $T$  is the temperature in Kelvin.**

### 1.3. Gold and heterogeneous catalysis

Gold had long been considered catalytically inactive with its primary use in organometallic and coordination chemistry. Relatively recent advances in gold catalysis by Bond *et al.* proved that, contrary to previous belief, by impregnating metal oxides with chloroauric acid, these materials showed high activity for the hydrogenation of olefins<sup>18</sup>. Following this publication, there was a decade long pause in gold catalysis research until observations by Haruta<sup>19</sup>, that gold was highly active for CO oxidation, and Hutchings<sup>20</sup>, for the hydrochlorination of acetylene into vinyl chloride. The study on CO oxidation found that the preparation method of the catalysts had an extreme effect on the activity of the catalyst and it was determined that this was due to a change in particle size of the gold dependent on the preparation method used.

Haruta and co-workers continued work showed that the selective epoxidation of propene was catalysed effectively by gold on titania<sup>21</sup>. More recently, work conducted by Prati and Rossi showed that gold supported on carbon had a remarkable ability to control the selectivity of products in the oxidation of alcohols<sup>22</sup>. Hutchings *et al.* made the significant discovery that supported gold nanoparticles were able to effectively catalyse the direct synthesis of hydrogen peroxide under non-explosive conditions<sup>23</sup>. Each of these studies had noted that the particle size of the gold had a significant effect on the activity of the catalysts produced. This has since been proven in several studies in which the activity of the catalyst is monitored whilst altering the gold nanoparticle size<sup>24-26</sup>, with the ultimate conclusion showing that gold nanoparticles of 5 nm or less exhibit the highest activity<sup>27</sup>. Control of the gold nanoparticle size is gained by using a variety of catalyst preparation methods each with specific advantages and disadvantages over one another.

#### **1.4. Catalyst Preparation methods**

Commonly known as the simplest preparation technique is the impregnation method. This technique has unsurprisingly been adopted by industries producing large amounts of catalyst due to the techniques ease of scalability, in which it is possible to produce tonnes of catalyst on a continuous basis making it extremely cost effective. Although the impregnation method produces nanoparticles within the desired activity region, the control of the particle size distribution is poor, with a bimodal distribution of smaller particles (2 – 10 nm) and larger particles (>20 nm)<sup>28</sup>. Catalysts prepared by the impregnation method have been successfully used in the direct synthesis of hydrogen peroxide<sup>29</sup> and the oxidation of polyols<sup>30</sup>.

Control over the nanoparticle size is extremely desirable, and is made possible with the deposition precipitation, DP, method. The DP method involves stirring the catalyst support in a solution containing the desired metal precursor and the pH of the solution is altered through the addition of a base. There are several factors that influence the size of the nanoparticles on the surface including concentration of the precursor solutions, altering the solutions pH, the length of time the solution is stirred for and the calcination conditions the catalyst is treated under<sup>31</sup>. The catalysts produced from the DP method exhibit smaller nanoparticles than found in the impregnation method (7 – 20 nm), consequently increasing both the activity and selectivity of the catalysts<sup>32</sup>. An important consideration when producing catalysts through the DP method is the stability of the support used in basic solutions.

A method that has been developed in more recent years, producing exceptional particle size distribution within the range of 2 – 5 nm, is sol-immobilisation. Sol-immobilisation can trace

its routes back to colloidal gold observed over a hundred years ago by Faraday, who produced a paper on the colours of colloidal gold, observing the change from ruby red to blue. The particle size of the gold in these observations ranged from 20 – 220 nm<sup>33</sup>.

The sol-immobilisation method is accomplished by forming a suspended colloid stabilised through the use of an immobilising polymer, such as PVA or PVP. A colloid is formed by reducing the metal cations to its metallic state with a reducing agent before adding the desired support to the solution to produce a catalyst with narrow particle size distribution in which all the nanoparticles are within the active range<sup>34</sup>. The reason the particle size distribution is so narrow, is that the catalysts do not need to be heat treated to reduce the metal nanoparticles, as the metal is reduced in-situ, preventing sintering when reaching the Huttig temperature (1/3 of the melting point) of the metals. This method of catalyst preparation has been shown to produce active catalysts for CO oxidation<sup>35, 36</sup> and glycerol oxidation<sup>37</sup> among other reactions.

The alloying of Au with other metals has been shown to increase the activity of catalysts for a range of oxidation reactions. Alloying Au with Cu has been shown to increase catalyst activity in CO oxidation<sup>38</sup>, whereas with Pd and Pt show an increase in activity for alcohol oxidation<sup>39, 40</sup>. There are several potential reasons for the synergistic effect observed when alloying Au with other metals, such as increased oxygen at the active site as the secondary metal is more easily oxidised than the Au, altering the band structure of Au through electronic promotion or demotion, and geometric effects observed in the alloying of the particles.

## 1.5. The direct synthesis of hydrogen peroxide

Hydrogen peroxide is a high value chemical with both industrial and household uses. H<sub>2</sub>O<sub>2</sub> is currently produced through the auto-oxidation of anthraquinone developed by BASF back in 1939. This involves the hydrogenation of 2-alkylanthraquinone, followed by exposure to oxygen reforming the 2-alkylanthraquinone and producing H<sub>2</sub>O<sub>2</sub> shown in figure 1.2.

A clear advantage of this process over the direct addition of H<sub>2</sub> and O<sub>2</sub> is that the auto-oxidation process forms high concentrations of H<sub>2</sub>O<sub>2</sub> without needing to worry over the explosive region of H<sub>2</sub> and O<sub>2</sub>. The disadvantage to this process is that the 2-alkylanthraquinone can itself be reduced in the process, leading to lower atom efficiency. This process is also a bulk scale process requiring the transport and storage of large quantities of a hazardous substance – a difficult and costly problem.

There are several reviews describing the potential uses and advantages of the direct synthesis of  $\text{H}_2\text{O}_2$ <sup>40, 41</sup>. The direct synthesis of  $\text{H}_2\text{O}_2$  avoids waste as the reaction is 100 % atom efficient with the possibility to conduct the synthesis in water, eliminating the need to remove the  $\text{H}_2\text{O}_2$  from solution.

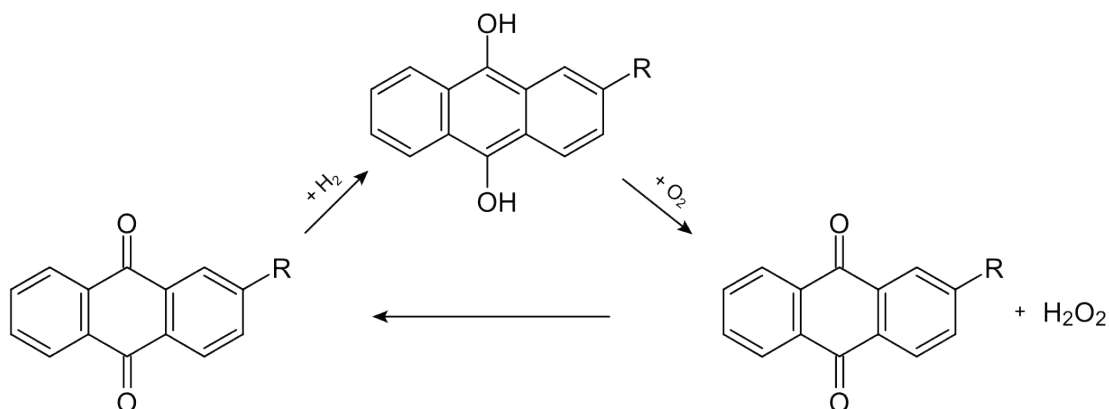


**Figure 1.2 2-Alkylnaphthoquinone auto-oxidation process.**

One of the major limiting factors to industrial production of  $\text{H}_2\text{O}_2$  is that to conduct the reaction safely, an inert carrier gas is needed for the addition of  $\text{H}_2$  to remain within a safe limit when mixing with  $\text{O}_2$ , which has an adverse effect on the production of  $\text{H}_2\text{O}_2$ <sup>42, 43</sup>. There are also competing pathways, shown in figure 1.3, which can occur and must be controlled through catalyst and reaction design. The direct synthesis is less thermodynamically favourable than the formation of water, adding another layer of complexity to what on the surface appears to be a simple reaction system.

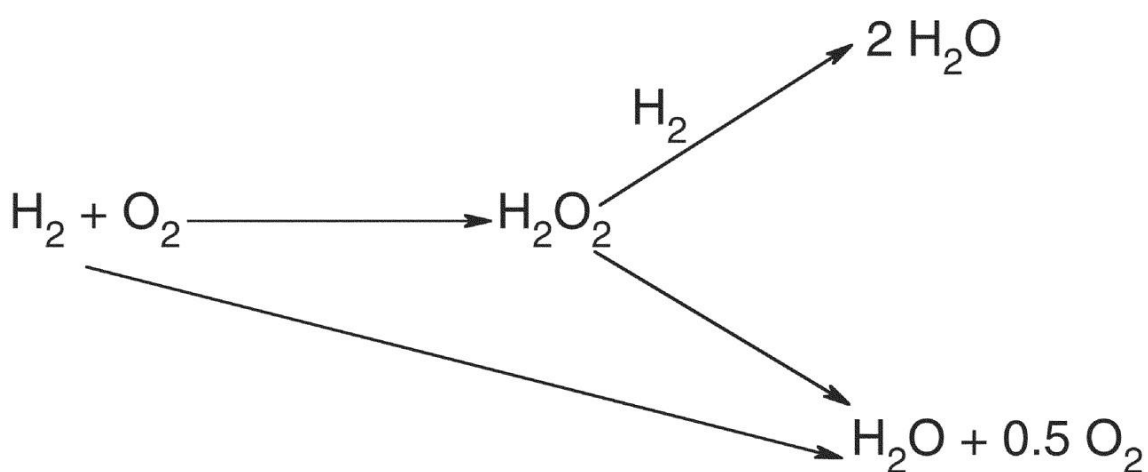


**Figure 1.3 Reaction scheme illustrating the direct production of hydrogen peroxide and the other potential unfavourable pathways.**

It has been shown by Hutchings and co-workers that Au nanoparticles supported on alumina were active for the direct synthesis of  $\text{H}_2\text{O}_2$ <sup>23</sup>, and that by alloying the Au with Pd, the activity was further enhanced. Further work by the group has shown that by altering the metal oxide support, the activity can be increased. The supports tested, reported with increasing activity, were  $\text{Al}_2\text{O}_3$ <sup>44</sup>,  $\text{Fe}_2\text{O}_3$ <sup>45</sup>, and  $\text{TiO}_2$ <sup>46</sup>. Microscopy conducted on the catalysts showed a common morphology of the Au/Pd nanoparticles – core shell structures, which have shown to exhibit increased activity in catalytic processes<sup>47</sup>. The chosen support demonstrates a clear effect on the activity of the catalyst, with significant progress being made by Edwards *et al.*, when using active carbon that had acid pre-treatment<sup>48</sup>. It was found the sequential and unfavourable reactions were lowered significantly as the pre-acid treatment of the support allowed for the formation of smaller, Pd rich alloys. These findings have led to the use of catalyst supports with fundamentally higher acidic properties including zeolites<sup>49</sup> and more recently insoluble heteropolyacids<sup>50, 51</sup>.

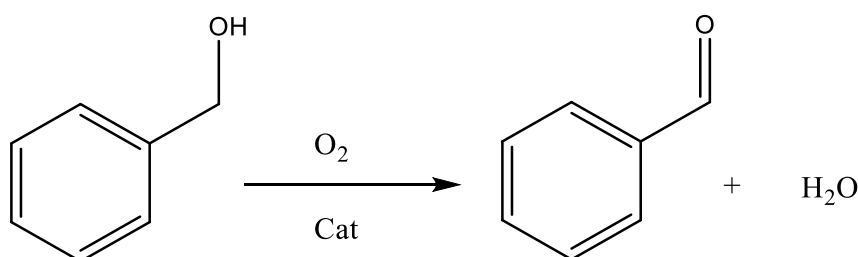
## **1.6. The Selective Oxidation of Alcohols**

Research into the selective oxidation of alcohols is of significant interest to both industry and academia as recycling objectives become increasingly important, with alcohols often being produced as side products from other reaction sources. The potential for the production of high value products from alcohols is highly plausible. Industrial reactions currently using stoichiometric equivalents of hazardous reagents to obtain the most efficient means of product production, an alternate method utilising waste products to form the value-added products with heterogeneous catalysts is a highly desirable outcome. Supported Au has been proven to be active and selective for the oxidation of alcohols<sup>52</sup> and following this observation, research into precious metals for alcohol oxidation has grown. Many alcohol substrates have been studied, successfully using Au, Pd and Pt to increase activity and selectivity. The selective oxidation of benzyl alcohol to benzaldehyde showed that AuPd nanoparticles on titania were both extremely active and selective with only small amounts of the side product, toluene evolved<sup>53</sup>. The same high activity and selectivity was also observed in the oxidation of cinnamyl alcohol to cinnamaldehyde<sup>54</sup> using the AuPd on titania catalyst. The oxidation of 1,2 propanediol to lactic acid was found to be active with Au, Pt and Pd catalysts on carbon supports<sup>55</sup>. These reactions are by no means an exhaustive list of the potential oxidation reactions, but each form a

fundamental understanding to the work conducted for this thesis and each will be discussed in further detail to set the scene.

### 1.6.1. Benzyl alcohol oxidation

Benzyl alcohol is a simple oxidation reaction, shown in scheme 1.1, with the main product aim being benzaldehyde which has its principle use in the pharmaceutical and cosmetic industries. Initial research into the activity of Au nanoparticles for the oxidation reaction showed the Au was active in the absence of a solvent producing excellent selectivity towards benzaldehyde<sup>56</sup>. Hutchings and co-workers continued research showed an increase of activity through synergistic effects when adding Pd to the Au catalysts<sup>57</sup>, a similar effect that previously observed in the direct synthesis of hydrogen peroxide. It was subsequently found that the preparation method used for the catalysts had a significant effect on the activity, with the sol-immobilised catalysts performing better than the DP and impregnation counterparts<sup>58</sup>.



**Scheme 1.1 Oxidation of benzyl alcohol to benzaldehyde**

The effect of the support has been indirectly investigated simultaneously by several research groups. Edwards *et al.* showed that AuPd supported on titania exhibited high TOF and using in depth microscopy, it was found that core shell structures were formed on the support surface, with Au (core) and Pd rich (shell), again similar to the structures found in direct synthesis of H<sub>2</sub>O<sub>2</sub><sup>54</sup>. Choudhary *et al.* found that when testing a range of supports, U<sub>3</sub>O<sub>8</sub>, MgO, Al<sub>2</sub>O<sub>3</sub> or ZrO<sub>2</sub>, were all selectively active for benzyl alcohol oxidation, although these required higher temperatures than in Edwards work to achieve higher activity<sup>59</sup>. Hutchings and co-workers later demonstrated that AuPd supported on carbon prepared by sol-immobilisation was also extremely active for benzyl alcohol as-well as for the direct synthesis of H<sub>2</sub>O<sub>2</sub><sup>60</sup>, hinting that there may be a link in the active site for these two catalytic processes.

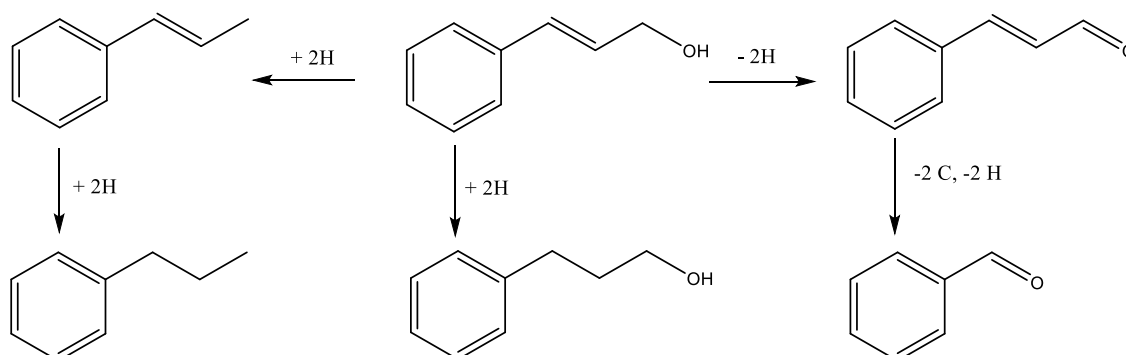
Benzyl alcohol oxidation produces a relatable model for interpretation of alcohol oxidation processes, with a limited series of products under oxidation conditions. Benzyl alcohol is either directly oxidised to benzaldehyde (shown in scheme 1.1) followed by a sequential oxidation to the ester and acid substrates or can proceed via a disproportionation to toluene. Through the addition of Pd to Au

catalysts it was found that Pd increases the disproportionation as well as increasing the rate of the oxidation reaction<sup>61</sup>. Cao *et al.* discovered that the unfavourable disproportionation of benzyl alcohol can be mitigated through the use of a magnesium oxide support, or through the addition of a base<sup>62</sup>. The leaching of the MgO support occurs readily in this reaction medium without base, as MgOH is formed from the leached MgO, subsequently increasing the basicity of the reaction solution, and therefore decreasing the formation of toluene formed. Although the leaching of the support is undesirable, it provides an important insight into how the acidic or basic nature of the support effects the reaction.

AuPd/TiO<sub>2</sub>, an acidic support, was shown by Hutchings and co-workers to produce stoichiometric amounts of benzaldehyde and toluene. This observation can be explained that the binding of the transition state to the surface of the catalyst, allowed further interaction with additional molecules of substrate, increasing the unfavourable disproportionation reaction rate. The disproportionation reaction has been shown to be hindered through the addition of Pt to the AuPd/TiO<sub>2</sub> catalyst, proposing that the Pt causes blocking of particular active sites on the catalyst surface by binding intermediate species too strongly or that Pt acts as an electronic modifier to the AuPd nanoparticles<sup>63</sup>.

### 1.6.2. Cinnamyl alcohol oxidation

Cinnamyl alcohol oxidation is another example of a simple alcohol oxidation model, however, as with benzyl alcohol, there are other reactions pathways that can occur such as hydrogenation, hydrogenolysis and decarbonylation – thus making the reaction more complicated than it initially appears. Baiker *et al.* produced a publication describing the potential complexity of the reaction network by modelling each reaction mechanism with Pd based catalysts<sup>64</sup>, described in scheme 1.2.



**Scheme 1.2** The potential reactions of cinnamyl alcohol

This investigation was preceded by an investigation into the partial oxidation of cinnamyl alcohol to cinnamaldehyde using air. It was found that Pt catalysts supported on alumina deactivated quickly after the rapid, irreversible adsorption of by-products blocked active sites upon the surface, hindering further reaction. Through the addition of Bi, this effect was eliminated, increasing the activity of the catalyst by a factor of 26, with an increase of cinnamaldehyde yield to 96 %. It was found that the Bi caused geometric blocking on the surface of the catalyst, decreasing the size of the Pt ensembles formed and therefore decreasing the hydrogenation products being formed<sup>65</sup>. Prati and co-workers had already shown Au was active for oxidising alcohols in the presence of O<sub>2</sub>, and by adding Au to Pd and Pt, it was found that the catalytic performance was improved, even under mild conditions (<60 °C and <4 bar). It was found that the addition of Au not only increased catalytic performance, but also decreased deactivation of the catalyst due to surface poisoning<sup>66, 67</sup>. Deactivation was found to be lower in the bimetallic Pt containing catalysts than in the Pd containing catalysts due to the decrease in hydrogen transfer, resulting in a higher selectivity to cinnamaldehyde.

Although the activity for both the AuPt and AuPd catalysts were similar, the Au had a more significant effect on reducing hydrogen transfer with the Pt containing catalyst showing that Pt can increase activity without the undesirable side reactions that occur in the monometallic Pt catalysts<sup>40</sup>. These findings show that the nature of the metal nanoparticles have a profound effect on the selectivity breakdown of cinnamyl alcohol oxidation, these findings that can, theoretically, applied to other oxidation reactions.

### 1.6.3. 1,2-Propanediol oxidation

Platform chemicals are chemicals that can be manipulated through various reaction conditions to form a range of products. Diols are alcohol compounds with 2 alcohol constituent groups, and are formed in large quantity from the production of bio-diesel. The chemical by-products formed are often viewed as waste chemicals as they are difficult to separate from the crude waste stream, however, as platform chemicals, these waste products have a high potential value. Through the design of efficient catalysts, it would be possible to utilise these platform chemicals, turning them into value added products and subsequently increasing the viability of the production of biodiesel.

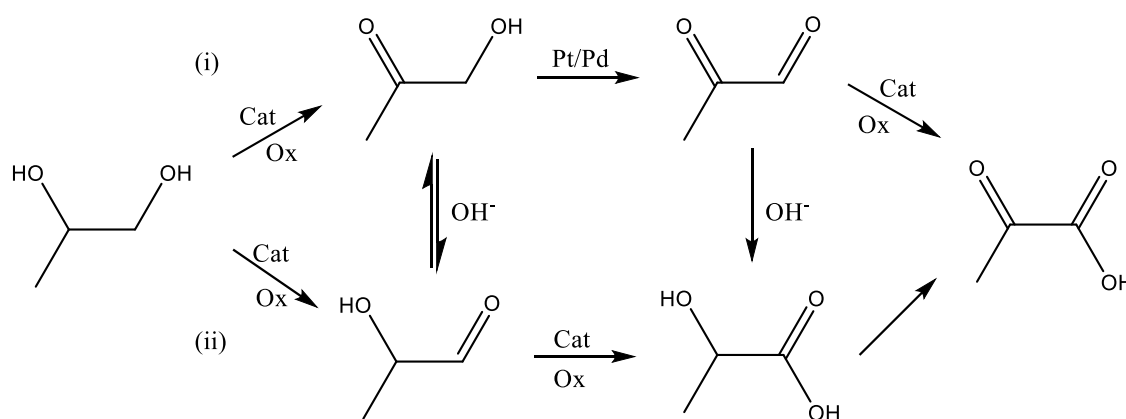
1,2-propanediol is one such waste product and a potential precursor to lactic acid *via* a selective oxidation reaction. Lactic acid is a highly desirable product for the use as a precursor to polylactic acid, a biodegradable polymer<sup>68</sup>. Prati and co-workers have previously been mentioned for the use of Au nanoparticles for selective oxidation reactions, finding that several

factors affected the activity and selectivity breakdown of the Au catalysts including the support used, how the catalyst was prepared and the conditions within the reaction system. It was also found that stoichiometric amounts of base had a favourable effect on the selective product formation, effectively reducing harsher conditions with the reaction medium and subsequently forming higher yields of the desired products<sup>22</sup>.

Furthering the advances on Au only catalysts, Hutchings and co-workers introduced Pd to the catalysts and observed a higher activity attributed to synergistic effects between the Au and Pd<sup>69</sup>, similar to the observations with the direct synthesis of hydrogen peroxide described in section 1.5. A DFT study conducted by Griffin *et al.* on AuPd/Mg(OH)<sub>2</sub> showed that the enhanced activity of the alloy was due to Au aiding the removal of strongly bound surface species, freeing active sites for the higher activity exhibited with Pd addition, increasing the rate at which the C-H bond scission occurs<sup>70</sup>. Preparation technique of the catalysts was again shown to have a significant effect on the activity of the catalysts with sol-immobilisation catalysts having higher activity than catalysts prepared through simple impregnation. This is due to the small, well dispersed nanoparticles with a low particle size distribution, formed during the sol-immobilisation process, subsequently increasing the number of active sites available on the catalyst surface<sup>71</sup>. This was not the first study that showed sol-immobilisation catalysts were more active than other preparation methods, Dimitratos *et al.* had shown they exhibited higher activity for benzyl alcohol oxidation<sup>72</sup> and Villa *et al.* observed increased activity for glycerol oxidation<sup>73</sup>. AuPt catalysts have proven to be active under ambient conditions, as long as there is a sacrificial base available<sup>74</sup>. Both AuPt and AuPd catalysts have been studied without the use of a sacrificial base, showing that although there was some activity, both the conversion of substrate and selectivity of products was greatly reduced<sup>75</sup>.

There are two logical pathways that can occur in 1,2-propanediol oxidation to form lactic acid which are (i) the direct oxidation of the primary alcohol in 1,2-propanediol to a lactaldehyde intermediate followed by a benzylic rearrangement to lactic acid, or (ii) *via* a simultaneous oxidation of both alcohol groups followed by either an intramolecular or intermolecular Cannizzaro type reaction of pyruvaldehyde. These steps require the presence of a sacrificial base

to occur favourably. These suggested reaction pathways are shown in scheme 1.3.



**Scheme 1.3** The proposed pathways for the oxidation of 1,2-propanediol to lactic acid.

## 1.7. Oxidation of bio-renewable feedstocks

### 1.7.1. The Energy Crisis

The modern world is continuously evolving technologically and has an ever-increasing population requiring a huge amount of energy to maintain growth and current living standards. Traditionally, this energy requirement is met through the use of fossil fuels – a finite resource controlling many geopolitical factors in our current world. Economic growth is intrinsically linked to the energy industry, and the current growth can only meet demand with a view to replacing fossil fuels with a renewable energy – else we face a disaster scenario in which fossil fuels will eventually be entirely consumed. The environmental impact of the energy industry cannot be understated, and utilising waste products is essential to create a sustainable environment in which the future population can live.

The rate at which current fossil fuels are being consumed has increased exponentially since the 1950s, having a considerable impact on the global climate with higher CO<sub>2</sub> emissions increasing global temperatures and having adverse effects on global ecosystems<sup>76</sup>. Such issues have preceded the search for methods of decreasing environmental impact in the production new energy sources. Many advances have been made in harnessing the elements for the production of fuels through tidal, wind and solar energy – although currently these methods do not produce anywhere near the global energy requirement<sup>77</sup>. Another potentially viable solution is through the use of nuclear power. Much research has been undertaken to increase the efficiency and safety protocols for the use of nuclear power<sup>78, 79</sup>, with two new plants being commissioned for the United Kingdom at Hinkley point in 2013. The potential energy production from nuclear power is theoretically enough to meet current energy needs, however, the nuclear waste generated is a significant problem. There is also a general uneasiness surrounding nuclear

power, stemming from the disastrous failure of plants in Chernobyl and Fukushima, which has put strain on the potential growth for nuclear power.

A possible energy source with a much lower environmental impact, not to mention a considerably safer alternative, is the production of biofuels from bio-renewable feedstock sources. There is a wide range of feedstock sources available opening a pathway to the development of fine chemicals.

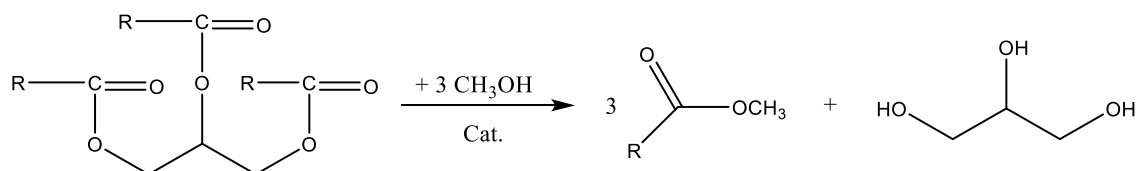
### **1.7.2. Fine chemical production from bio-renewable resources**

There are two main sources of biofuels known as the first and second generations. First generation biofuels are obtained from crop sources such as corn and sugar cane or organic waste. Through use of these crop source feedstocks, it is possible to form bio-diesel, bio gas and m/ethanol. The main issue with the formation from first generation sources is that there is an ethical dilemma, known as the food vs fuel debate. Though the processes themselves are efficient in the production of these high value renewable fuels, the use of crop sources depletes from the available crop for human consumption, potentially worsening the poverty issues in the developing world<sup>80-82</sup>. By increasing the demand for a staple crop like corn, simple economics dictates that the price would increase, with these issues essentially limiting the potential for fuel production from first generation sources.

Second generation biofuels, whose production is often described as sourced from plant biomass, actually refers to the lignocellulosic material stemming from non-food feedstocks available from plants. There is a large quantity of plant biomass produced that is wasted, despite having the potential to form fuels and fine chemicals. The simplest fuel potential for plant biomass is to burn it to produce electricity, though environmentally this has several obvious problems. The real potential in plant biomass is the formation of liquid biofuels. These biofuels are considered a much greener alternative to standard fossil fuels, with significantly lower CO<sub>2</sub> production and the second-generation sources avoid the economic and ethical issues of the first-generation sources<sup>83, 84</sup>.

Bio-diesel, one of the potential bio-fuels, is comprised of fatty acid methyl esters and can be synthesised through the transesterification of vegetable or animal fats with an alcohol using either heterogeneous or homogeneous catalysts<sup>85</sup>. The main advantage of bio-diesel is that it behaves chemically comparably to petroleum derived diesel, and is therefore a potential replacement. One of the by-products of bio-diesel production is the formation of glycerol in a ratio of 3:1, shown in scheme 1.4. Due to the highly functionalised nature of glycerol, it has been noted in literature as a platform chemical for the production of value added chemicals, including

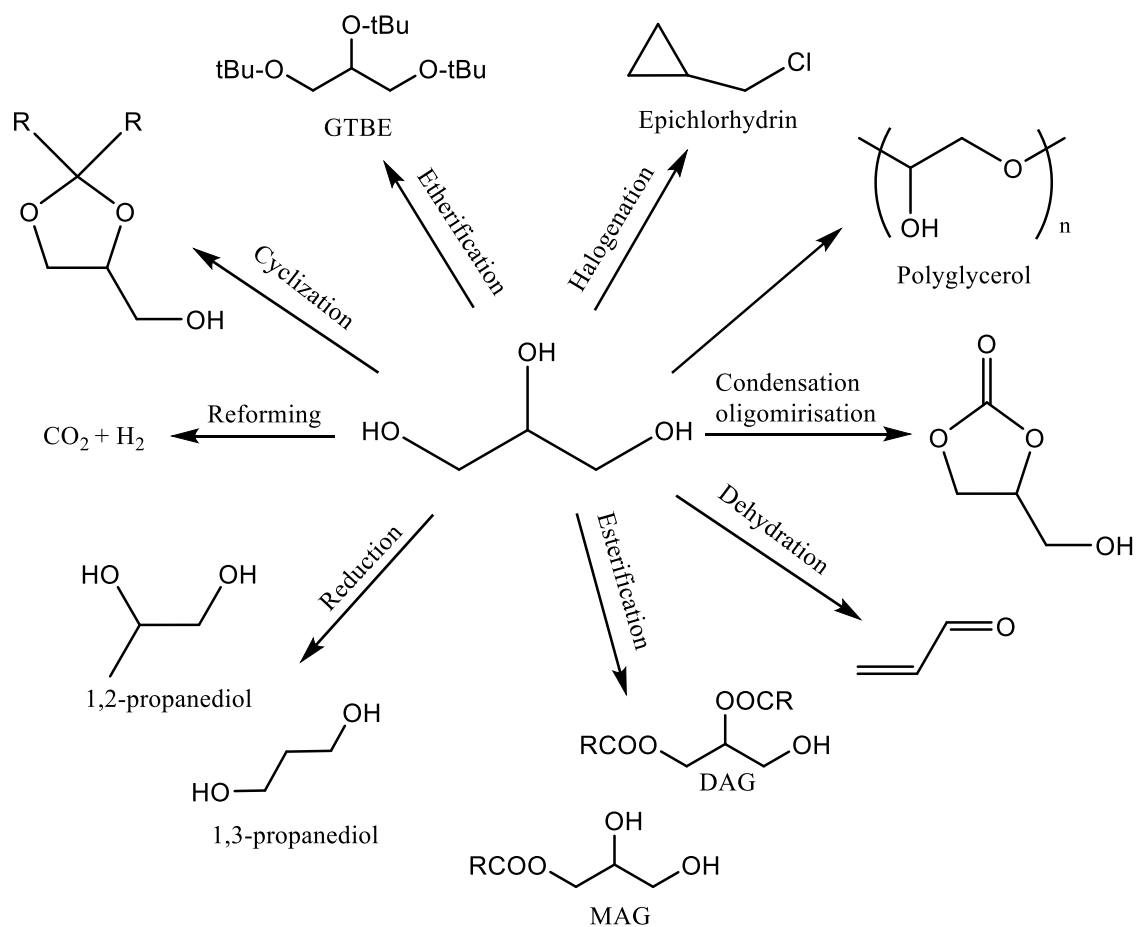
lactic acid<sup>86</sup>. If bio-diesel were to be adopted as a fuel replacement, the atom efficiency of the production would have to improve significantly, therefore the utilisation of waste products formed, such as glycerol, is an important consideration.



**Scheme 1.4** Transesterification of fats producing bio-diesel and glycerol.

### 1.7.3. Glycerol oxidation

Glycerol is a highly functionalised tri-ol containing 3 hydroxyl groups with a vast array of potential products, illustrated in scheme 1.5. By utilising glycerol in this way, it will aid the pathway towards making bio-diesel more economically viable for industrial acceptance.



**Scheme 1.5** Potential products formed from treating glycerol under various conditions.

The fine chemicals which are able to be produced from selective glycerol oxidation include glyceric acid (GA), tartronic acid (TA), lactic acid (LA), dihydroxyacetone (DHA) and glyceraldehyde (GLA). Producing catalysts that are both high in activity and selective towards particular products is of high value in this reaction and heterogeneous catalysts in particular have been proven to be excellent at the production of these fine chemicals<sup>67, 87, 88</sup>.

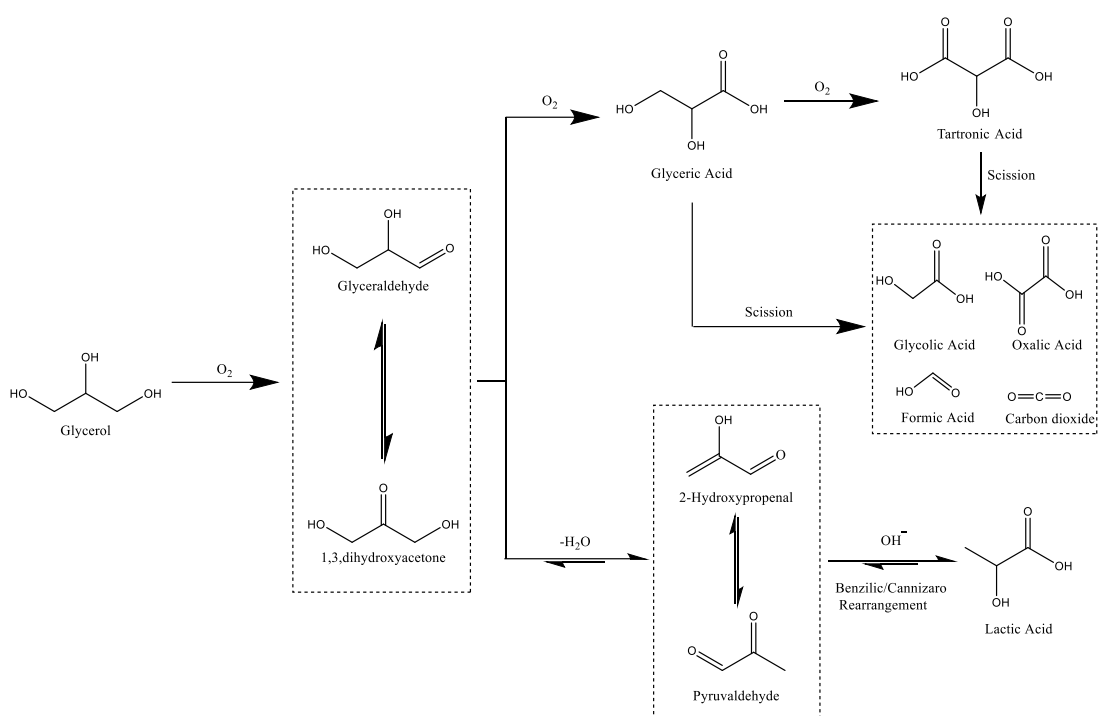
The successful selective production of DHA was first documented by Kimura *et al.*, who used Bi doping on Pt catalysts, increasing the selectivity towards DHA up to 80 % from 10 %. This success was attributed to the Bi lowering the over-oxidation of the DHA, preventing the formation of further oxidation products. Further work by Fordham *et al.* theorised that the Bi specifically orientated the glycerol substrate on the surface of the catalyst, and in proving this theory, it was highlighted that a Pd/C catalyst could be used to selectively form GA in high yields<sup>89</sup>. During this body of work, the experimental conditions used were found to have significant effects on the selectivity breakdown of the products formed. Pioneers in Au catalysis research, Prati and Rossi led the further research with Au catalysts, and as has been previously observed, the preparation method of the catalyst and support used were key components in how the catalysts performed<sup>90</sup>. Separately Hutchings and co-workers found that both Au/C and Au/graphite were effective catalysts for the selective production of GA from glycerol, although it should be noted these experiments were also carried out with a sacrificial base<sup>87</sup>. Further research by Hutchings and co-workers on the Au/graphite catalysts used TEM to show that the particle size of the Au was an important factor in the activity of the catalysts produced, with particles of >50 nm sizes rendering the catalyst completely inactive, and the optimum activity exhibited by catalysts with particles between 1 – 10 nm<sup>91</sup>. These findings were the beginning of an enormous series of publications continuing over 20 years, which has been summarised in a recent review, led by the founders of this line of research, Prati and Hutchings<sup>92</sup>.

Doping Au with other metals has already been shown to be effective for increasing activity for hydrogen peroxide and 1,2-propanediol oxidation among many other reactions. These bimetallic catalysts can boost the activity of the catalyst as well as increasing selectivity to particular products<sup>93</sup>. It has been suggested that the secondary metal added has specific effects on the catalyst. Davies and co-workers theorised that by adding Pd to Au, that the Pd aided decomposition of a peroxide formed on the catalyst surface, forming a peroxy species that could potentially lead to increased selectivity towards undesirable C-C scission products<sup>94</sup>. Hutchings and co-workers also found that when adding Pt to Au catalysts, there was an increase in C-C scission. It was also found that this could be eliminated through the use of a sacrificial base, which could show that the base is preventing the peroxy species from forming, eliminating

C-C scission. Once the base was added, selectivity to GA increased to 100 %, showing increased activity over the Au only catalysts<sup>95</sup>.

### 1.7.3.1. Reaction conditions in glycerol oxidation

A major consideration when viewing the activity and selectivity that a catalyst exhibits is the conditions the reaction is conducted under. In a typical liquid phase batch reactor, there are several conditions that can be altered; (i) temperature, (ii) gas pressure, (iii) stirring speed, (iv) metal to substrate ratio, as-well as the (v) base ratio used for glycerol oxidation specifically. The effect of altering each condition is described below (scheme 1.6.), showing the proposed reaction pathways that will be referred to throughout this thesis.



**Scheme 1.6 Proposed reaction scheme for glycerol oxidation showing both oxidation and oxidative dehydrogenation pathways.**

#### (i) Temperature

Temperature is a crucial condition to consider for glycerol oxidation. By increasing the temperature, the rate at which the glycerol is consumed increases. At lower temperatures of 30 °C, the main product formed with bimetallic AuPd catalysts has been shown to be GA<sup>96</sup>, whereas with AuPt catalysts at the same temperature showed higher undesirable C-C scission products<sup>67</sup>. By increasing the temperature to 50 °C, Prati and co-workers observed an increase in selectivity to GA with AuPd catalysts, with lower C-C scission than previously observed for the AuPt catalysts. As mentioned above, Davies and co-workers had postulated that the peroxide species

formed was the cause of C-C scission occurring, and at temperatures in excess of 50 °C, peroxide is unstable and readily decomposes, therefore eliminating the C-C scission. At further elevated temperatures of 80 – 100 °C, there is a shift in selectivity towards lactic acid, an opposing pathway to that of the sequential oxidation that can be observed in scheme 1.6.

(ii) Pressure

The oxygen pressure within the reaction may be perceived as having a simple effect on the surface, but actually has a complex role. By increasing the oxygen pressure, one might imagine that the rate of the oxidation pathway would increase linearly with pressure. Valverde and co-workers found that by altering the oxygen pressure with Au supported on various catalysts, that whilst the rate at which glycerol was converted was only slightly increased, but the effect on selectivity was much more pronounced with the selectivity to GA increasing significantly<sup>97</sup>. The effect of pressure on the reaction has not been specifically documented over a wide range of conditions for bimetallic catalysts, therefore the effects at higher temperatures are currently unknown and will be studied in this thesis.

(iii) Stirrer speed

The effect of stirring speed of a reaction can cause a physical effect known as mass transport limitation. Mass transport limitations can have a significant effect on the rate of a reaction at both the reactant conversion and product formation steps within a reaction. In a reaction where the catalyst is heterogeneous, the catalyst and reactant are in different phases and in the case of this thesis, solid catalysts with liquid phase reactants. This leads to a mass transfer or diffusion process between the reactant conversion and product formation processes. The physical reaction conducted by solid catalysts initiates when the reactant comes into contact with the active sites located on the surface of the catalyst, and the rate of mass transfer to the reactive surface, in an ideal system, will be a steady state process and will equal the rate of the reaction. If this process occurs quickly, then there will be active sites available for further substrate to be adsorbed, and essentially, the system will have no mass transport limitations. This effect can be hindered through ineffective stirring of the solution as the reactant is not mixed adequately with the solid catalyst, resulting in a slower reaction rate due to mass transport limitations<sup>98</sup>.

(iv) Metal to substrate ratio

The metal to substrate ratio is a fairly simple parameter that has the potential for high impact. Increasing the amount of catalyst in the reaction mixture will effectively increase the

number of active sites available for the reaction to occur at. The lower amount of catalyst used, however, increases the industrial viability of the catalyst as the cost of large amounts of catalyst would be expensive and more difficult to separate from the reaction mixture, also increasing the cost of the process. Ultimately, there is a balance between the activity and viability of the amount of catalyst used in the reaction.

(v) Base ratio

It has been postulated that the role of the base within the reaction medium is to act as an initiator, activating glycerol for dehydration of the hydroxyl group<sup>99</sup>. Without the presence of base, Au catalysts have been shown to have greatly reduced activity<sup>95</sup> and the base to substrate ratio within the reaction also has a notable effect on the conversion of glycerol and the selectivity profile. At temperatures between 40 – 80 °C, the most effective base for increasing selectivity to glyceric acid specifically was shown to be LiOH and NaOH for Au, Pd and Pt catalysts with nitrate analogues producing a higher yields to a scission product, oxalic acid<sup>67, 100</sup>. It has been found that using gold catalysts in the presence of base are able to produce a 100 % selectivity to glyceric acid.

The pH of the reaction medium has a substantial effect on the rate of glycerol oxidation as-well as the selectivity breakdown of the products produced, shown over a variety of studies<sup>101-105</sup>. In researching the oxidation of C3 diols, Prati and Rossi had theorised that NaOH aided the initial dehydrogenation of the alcohol group, forming the carbonyl. In the absence of base, the conversion is significantly lowered. Following Prati's theory, it can be rationalised that the cleavage of the C-H bond followed by H-abstraction is too energy intensive to occur spontaneously without the aid of a base. This rationale has been positively reinforced by work conducted by Hutchings and co-workers<sup>95</sup>. By increasing the concentration of base within the reaction, a positive effect on the selectivity to C3 products is observed, which can be attributed to the decomposition of peroxide, which as previously mentioned, is believed to increase the C-C scission products observed. A DFT study conducted by Davis *et al.* modelling surface bound hydroxide intermediates, described how the energy boundary is lowered for the C-H and O-H bond activation in the presence of Au nanoparticles. Although the formation of the initial alkoxy intermediate is able to occur in the absence of base, the energy required to activate the C-H bond is significantly lower in the presence of the hydroxyl intermediates<sup>106</sup>.

Base free glycerol oxidation has received attention in recent literature as the use of a base for industrial applications requires separation or treatment of the reaction effluent, increasing the cost of the process. Liang *et al.* had initially investigated a range of particle sizes

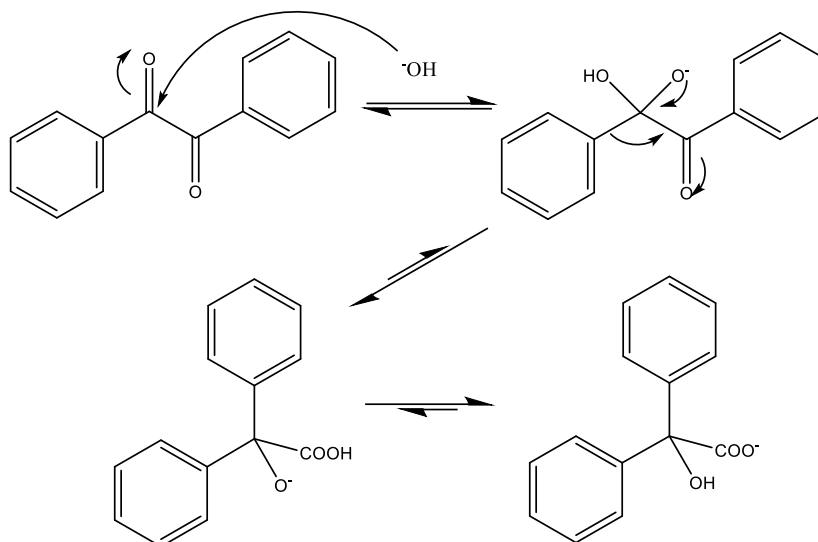
of Pt/C finding that in concordance with current work, larger particles produced lower activity, and smaller particle sizes produced some conversion of glycerol<sup>107</sup>. Further work by Hutchings and co-workers utilised AuPt bimetallic catalysts, which displayed high activity when supported on MgO<sup>96</sup>, although, this could be due to leaching of the MgO into the reaction effluent forming MgOH and therefore increasing the rate of the reaction through the introduction of a base. Ebitani and co-workers found that by using hydrotalcite as a support for Pt nanoparticles, a selectivity of 67 % to glyceric acid at 71 % conversion of glycerol could be achieved under base free conditions, stating that the acidic sites were responsible for the higher activity<sup>108</sup>. This work suggests the importance of the support used within the reaction system with basic supports promoting activity, and acidic supports increasing the selectivity to C3 products.

## 1.8. Organic mechanisms

Several organic mechanisms will be referred to in this body of work based on the theoretical mechanisms for the formation of lactic acid from glycerol, each of which are described within this section. Lactic acid was first isolated from sour milk by the Swedish chemist, Carl Wilhelm Scheele, in 1780. Berzelius discovered that lactic acid was also produced in muscles during periods of exertion, with its structure being established by Johannes Weslicenus in 1873. The commercial production of lactic acid was pioneered by German chemist, Boehringer Ingelheim in 1895 and though the commercial success of lactic acid is apparent with current average annual production growth of 10 % up to 275, 000 tonnes in 2006<sup>109</sup>, the mechanism of formation is still only speculated. Two theories are generally accepted from the scientific community, the formation through a Benzilic rearrangement<sup>110</sup> or *via* a Cannizarro type reaction<sup>111</sup>.

### 1.8.1. Benzilic rearrangement reaction

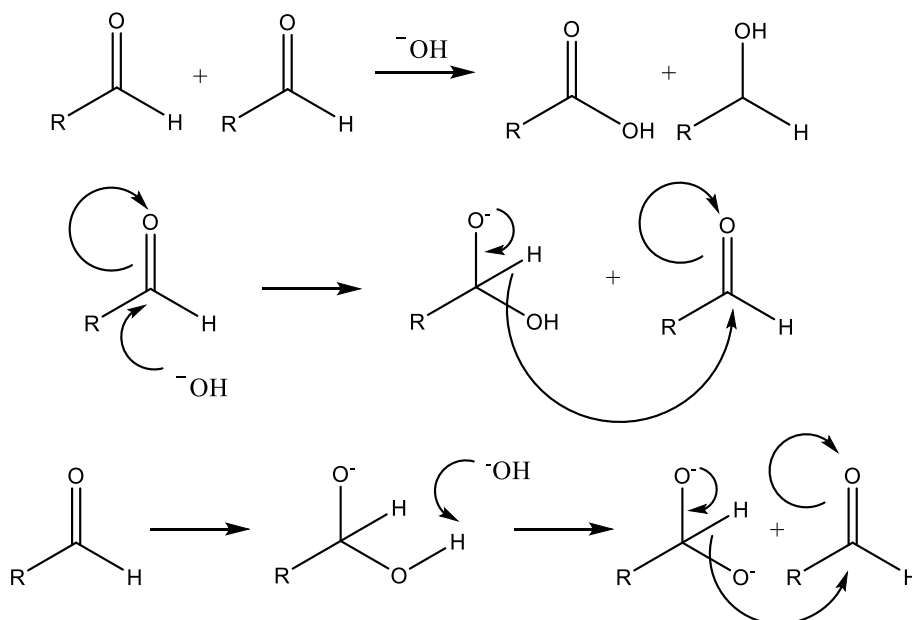
The benzilic acid rearrangement was first conducted by Justus Liebig in 1838<sup>112</sup>, and involves a rearrangement reaction of benzil with a hydroxide anion to form benzilic acid. This type of reaction is often exhibited by 1,2-diketones where the reaction product is an  $\alpha$ -hydroxy-carboxylic acid<sup>113</sup>, illustrated in scheme 1.7.



**Scheme 1.7 Mechanism for a benzilic rearrangement which proceeds through an initial hydroxide anion attack on one of the ketone groups. There is then a bond rotation which places the migrating R for secondary attack on the second carbonyl group.**

### 1.8.2. Cannizzaro reaction

The Cannizzaro reaction is named for its discoverer, Stanislao Cannizzaro, and is a chemical reaction involving a base induced disproportionation of an aldehyde that contains no hydrogen atoms within the  $\alpha$  position<sup>114</sup>, shown in scheme 1.8.



**Scheme 1.8 Mechanism for a Cannizzaro reaction in which the reaction initially proceeds through a base induced disproportionation of two carbonyl species. Stoichiometric equivalents of the corresponding alcohol and aldehyde are then formed.**

## 1.9. Catalyst preparation using supercritical fluids

### 1.9.1. Brief introduction to supercritical fluids

A supercritical fluid (SCF) by definition is a substance in which the temperature and pressure exceed their critical values,  $P_c$  and  $T_c$ . The boundary between liquid phase and gas phase converge, forming a single, supercritical phase illustrated in figure 1.4.

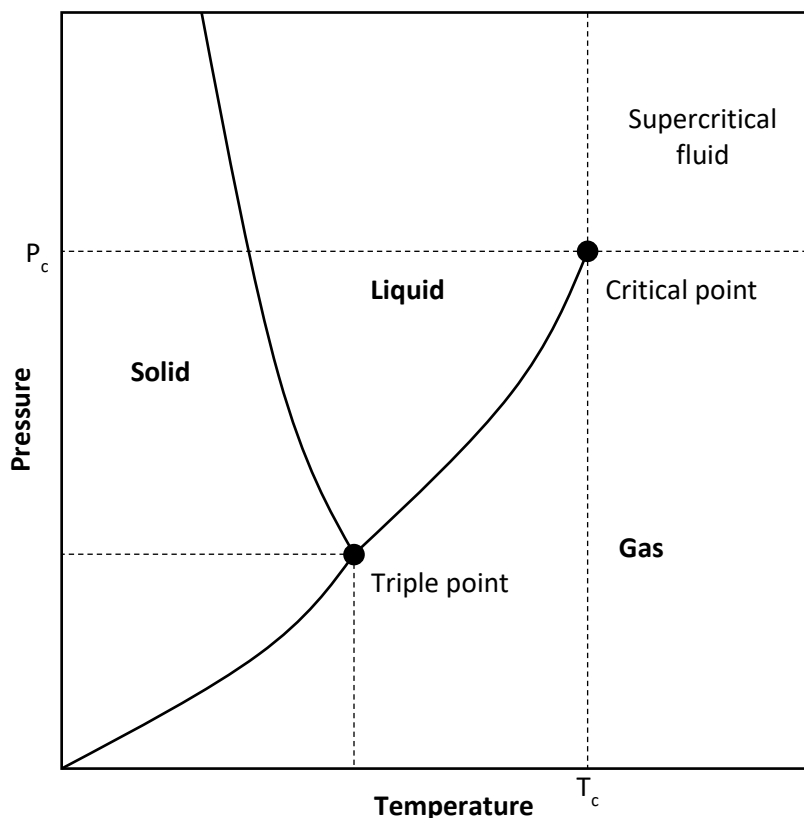


**Figure 1.4** P-T phase diagram showing the phase regions with boundaries and coexisting equilibrium.

Some examples of critical temperature, pressure and density of commonly used SCFs are shown in table 1.1 below.

**Table 1.1** Critical points of commonly used supercritical fluids

Compound	$T_c$ (°C)	$P_c$ (Bar)	$\rho_c$ (Kg m <sup>-3</sup> )
Water (H <sub>2</sub> O)	373.9	220.6	322
CO <sub>2</sub>	30.9	73.75	468
Methanol (CH <sub>3</sub> OH)	239.4	80.92	272

Ethanol (C <sub>2</sub> H <sub>5</sub> OH)	240.7	61.37	276
Nitrous Oxide (N <sub>2</sub> O)	36.4	72.55	452
Ammonia (NH <sub>3</sub> )	132.3	113.50	235
Propane (C <sub>3</sub> H <sub>8</sub> )	96.6	42.50	217
Ethene (C <sub>2</sub> H <sub>4</sub> )	9.1	50.41	214
Propene (C <sub>3</sub> H <sub>6</sub> )	91.6	56.01	233
Sulfur Hexafluoride (SF <sub>6</sub> )	45.5	37.70	735
Xenon (Xe)	16.5	58.40	1110

The P-T diagram shown in figure 1.4 only describes a single component system with any real chemical process involving at least a ternary system. The difficulty of predicting and modelling a multi-component system is considerably higher than that of a single component system as changes in the individual components will alter the liquid-vapour equilibrium resulting in changes to the critical point<sup>115-117</sup>.

### 1.9.2. Properties of supercritical fluids

SCF properties can be thought of as both liquid and gas like in nature, with the specific properties of gases and liquids being more pronounced than others<sup>118, 119</sup>. Significant changes in the properties of a SCF can be influenced with minute changes to the system parameters, and this is especially true for the region near the critical point, in which the SCF density is the most prominent factor.

The density of SCFs are found in a region between that of a liquid and gas, although, with orders of magnitude considered, SCF density tends towards comparable levels of liquid density. The density of the SCF has a direct effect on the solvation property, with higher densities enabling higher solvation. It can be suggested from this that as SCFs have comparable density to liquids, that the solvation properties should also be comparable. The general rule for increasing the density of a SCF is to increase the pressure of the system, therefore, the solvation abilities will also increase, whereas an increase in temperature displays the opposite effect. It should be noted that whilst the solvation properties are tuneable in a SCF, the solubility of a compound is heavily dependent on the nature of the compound, and so, whilst the SCF will have higher

solvation properties than the corresponding gas, thought must go into the compound being dissolved to optimise the system.

The nature of SCFs show that whilst the density is closer to a liquid than a gas, the hydrodynamic properties are much more similar to that of a gas. This property enables the SCF to have low viscosity and high diffusion rates, properties that directly increasing the molecular and macro-scale mass transfer coefficients within the system. The influence of pressure and temperature on the system again shows a profound effect on these properties, with higher pressures causing higher viscosity and lower diffusion rates opposing to higher temperatures having the opposing effect. The effect of parameters on the properties of SCFs has been extensively researched<sup>120, 121</sup>, with the general trends shown in figure 1.5.

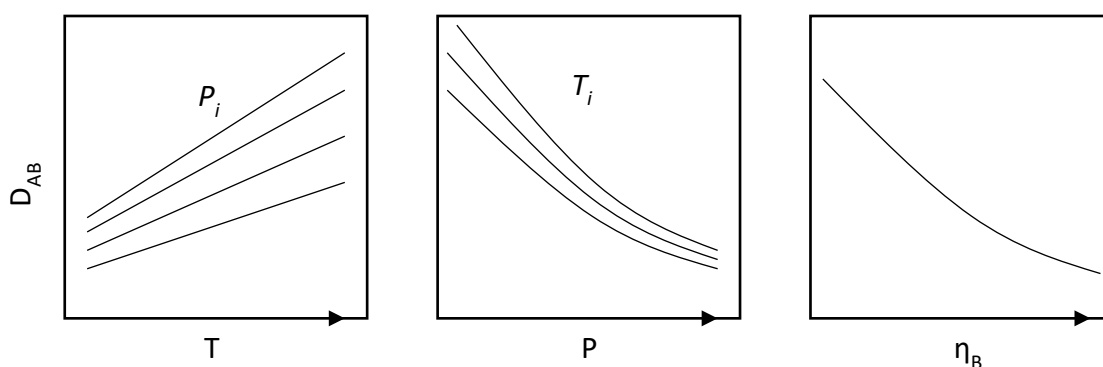


**Figure 1.5 Describing the general trend of the diffusion coefficients ( $D_{AB}$ ) with respect to temperature ( $T$ ), pressure ( $P$ ) and viscosity ( $\eta_B$ ).  $P_i$  shows the isotherms with respect to temperature, whilst  $T_i$  shows the isotherms with respect to pressure.**

An advantage of utilising SCFs is that the surface tension, a property that when related to liquids is dependent on the equilibrium position with respect to the vapour phase, tends to zero as the critical point is approached. As previously stated, the system becomes much more complicated when considered as a multi-component system, as factors including the miscibility of the compound involved and the non-equilibrium conditions have significant effects on the system<sup>122</sup>.

The desire for environmentally friendly solvents to lower environmental impact and costs on material production is an important consideration that can be potentially filled with the use of a SCF, as they are potentially recyclable components that can be easily separated and are already generated through current process waste streams. Commonly used SCFs are  $H_2O$  and  $CO_2$ , both of which when compared to solvents used in industry, are much cleaner alternatives. The issue with using  $H_2O$  in its supercritical state, is that it becomes highly corrosive with higher critical temperature and pressure needed to obtain the SCF state. Supercritical  $CO_2$  (Sc- $CO_2$ ) on

the other hand, has lower critical point conditions, is non-flammable and has a low threshold limit, a highly desirable quality for industrial applications. Sc-CO<sub>2</sub> also matches several of the criteria in the basic principles of green chemistry set out by Anastas and Warner<sup>123</sup>;

- i) Can replace toxic solvents preventing waste, rather than remediating waste.
- ii) Renewable feedstock due to natural abundance.
- iii) Can be sourced as a waste products from industrial processes.
- iv) Potential to be recycled within a flow system, preventing further waste.

### 1.9.3. Applications of supercritical fluids

SCFs have found many uses in several fields due to their unique and highly tuneable properties, the main uses are found in extraction, chromatography, a medium for catalytic reactions, and compound synthesis.

SCFs are used industrially for the extraction of medicinal compounds from plant matter, edible oils, caffeine from coffee, and treatment of waste streams<sup>124</sup>. Chromatography uses include detection of polymer additives, toxic compounds contained in foods and can be used in most applications where normal phase HPLC can be used<sup>125</sup>.

SCFs have been utilised in both homogeneous<sup>126</sup> and heterogeneous<sup>118</sup> catalytic processes. Homogeneous processes suffer from a significant disadvantage to heterogeneous catalytic processes in that the separation of phases is very difficult, a problem that can be solved as SCFs are excellent at separating compounds. As previously described, small alterations to the pressure and temperature can tune the properties of an SCF, allowing for separation of valuable homogeneous metal complex catalysts from the solution containing the products<sup>126</sup>. This makes homogeneous reactions much more efficient, increasing the industrial viability and with successful testing conducted for hydrogenation<sup>127</sup>, cyclization<sup>128</sup> and oxidation<sup>129</sup> processes. Heterogeneous catalysis has used a supercritical medium for a wide range of processes including cracking, esterification, hydrogenation, isomerisation, oxidation, amination, alkylation and Fischer-Tropsch synthesis. SCFs help lower issues with mass transfer that many heterogeneous reactions suffer with, remove the gas/liquid barrier present in the reactions and, as with homogeneous reactions, can be tuned to separate phases in both reactants and products.

SCF use in compound synthesis can either be utilised as solvents or reactants<sup>130</sup> with the advantages over traditional solvent based methods being the high tuneable nature of the SCF and the lack of waste from production, as theoretically, both the gas and solvents used within the process are completely recoverable.

There are several techniques that have been developed using SCFs in material synthesis, and these can be categorised into 3 groups;

- i) Rapid expansion of supercritical solutions (RESS)
- ii) Supercritical assisted atomisation (SAA)
- iii) Supercritical anti-solvent preparation (SAS)

This project will only be using the SAS preparation method, and therefore only brief descriptions of the RESS and SAA methods will be noted.

The principle behind the RESS technique<sup>131</sup> uses the fact that solvation power can be controlled through the applied pressure on a supercritical solvent. Initially, a solid is dissolved in a supercritical solvent, followed by rapid depressurisation (usually through a nozzle), which greatly lowers the solvation power of the supercritical solvent, causing supersaturation followed by nucleation of the solid particulate. Using the RESS method it is possible to alter the morphology of the particles formed by changing the material preparation conditions, i.e. the drop in pressure, temperature of the reaction and the physical geometry of the nozzle used. The disadvantage of RESS when compared to SAA and SAS is that as a batch system, the solubility limit of the solid being dissolved within a suitable supercritical solvent and the potential for agglomeration of the particles as the majority of particles will rapidly nucleate at the same time.

The SAA process ultimately enables the user to effectively disperse a solution into fine particles. This occurs as by choosing a supercritical solvent that is miscible with a solution, it is possible to dissolve the SCF in said solution at pressure. Upon depressurisation, the SCF will no longer be miscible with the solution, thus separating, and causing the rapid dispersion of the solution into fine droplets<sup>132</sup>.

#### **1.9.4. Basics of the supercritical anti-solvent process**

The SAS process was first described by Gallagher and co-workers<sup>133</sup> and work using a similar principle to more traditional anti-solvent processes, in which a poor solvent is used to induce particle formation through the dilution of a solution that is miscible with the solvent and the desired material. Since the method was first described by Gallagher and co-workers, many iterations of the method have been developed, although the underlying principle remains the same in which a solution with the desired material is added to a supercritical anti-solvent, which is miscible in the initial solution. The mixing of solution and supercritical anti-solvent results in a rapid supersaturation, precipitating the particles of the dissolved material.

There are several benefits of using a supercritical anti-solvent due to the inherent properties of the SCFs chosen. Firstly, the supersaturation when using a more conventional solvent occurs at a much lower rate than when using an SCF as the diffusion coefficient is much higher. This results in time scales of supersaturation between  $10^{-4} - 10^{-5}$  seconds<sup>134</sup>, resulting in smaller particles being formed. Secondly, as previously mentioned, the tuneable nature of the SCF allows for control over particle morphology and size. Thirdly, there are significant environmental problems that can be alleviated through the use of SCFs, especially in the use of the most common SCF,  $\text{CO}_2$ , instead of conventional solvents that often have undesirable qualities such as high toxicity. It is also possible to separate the organic solvents used to dissolve the material from the SC- $\text{CO}_2$  through the control of system pressure, allowing the potential to re-use solvents. Solvents are chosen based on their miscibility with appropriate SCF, and some common solvents used with SC- $\text{CO}_2$  include low chain alcohols, dimethyl formamide, and dimethyl sulfoxide.

### 1.9.5. Supercritical anti-solvent preparation methods

The supercritical anti-solvent processes differ in their modes of operation. These modes of operation are described by two main processes, the primary process developed with the batch method, gas anti-solvent (GAS) process and the secondary, and further developed process is known as the supercritical anti-solvent (SAS) precipitation method.

#### 1.9.5.1 Gas anti-solvent process

The GAS process was developed as a batch method of producing particles in the micro/nano range of a desired product by adding a solution to a sealed vessel and pumping in the desired gas anti-solvent (GAS), described in Figure 1.6 using  $\text{CO}_2$  as an example gas.

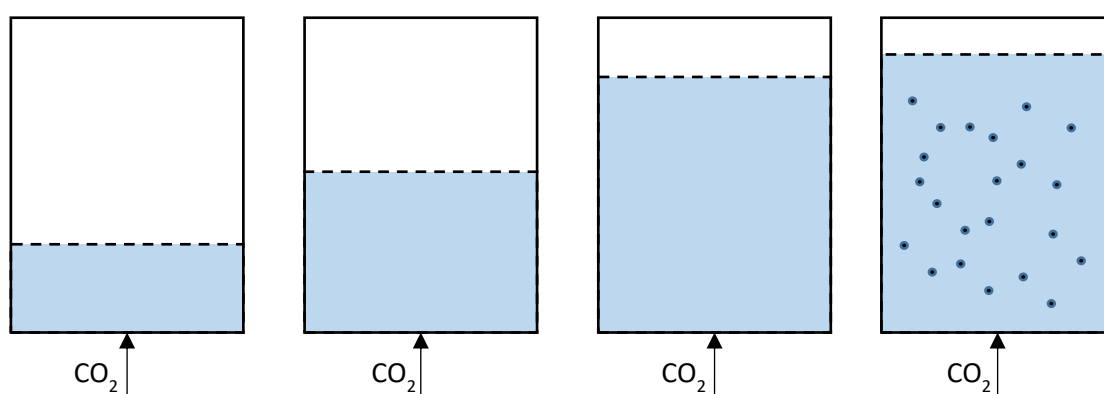


**Figure 1.6** Diagram describing the expansion of a solution during the GAS process, in which as pressure increases, the  $\text{CO}_2$  becomes increasingly miscible with the solvent causing expansion.

By adding the anti-solvent to the homogeneous single phase system, a two phase system is produced, as illustrated in figure 1.7. The separation from a single phase to a two phase system results in the precipitation of solid particles and the expansion of the solvent/anti-solvent phase. The system is then washed with the gas used to remove any residual solvent.

The GAS process is a system in which the mixture does not need to be above the critical point, only the near critical point. The properties of the particles formed through the GAS process, such as morphology and structure, are dependent on the rate of nucleation and growth

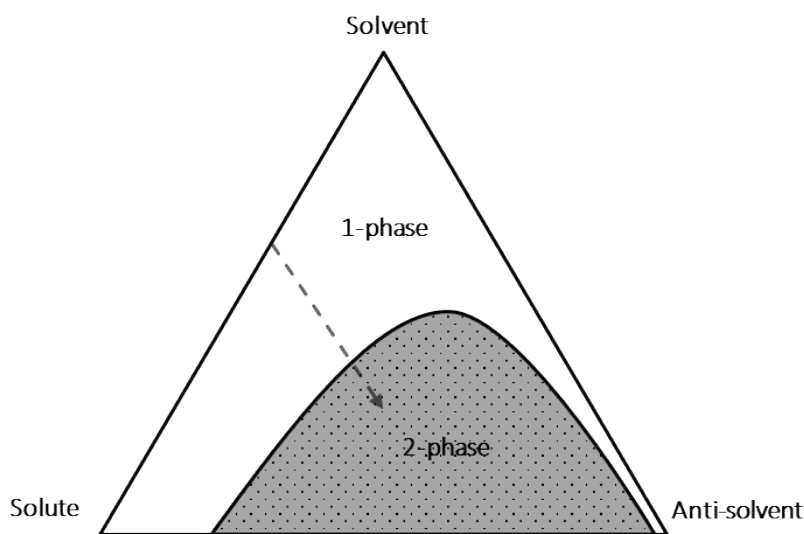


**Figure 1.7 Phase diagram describing the system change during the GAS process.**

of the particles. These factors are controlled by the degree at which the solvent and anti-solvent are soluble with each other, the maximum potential for supersaturation and the rate at which the system changes between a single phase and two phase system. As expected, the temperature and pressure of the system must be carefully considered as this changes the density of the anti-solvent, which controls its solubility, as-well as influencing the maximum potential for supersaturation.

### **1.9.5.2. Supercritical anti-solvent process**

The method for forming the novel supports used in this thesis is the supercritical anti-solvent process. This method requires a precursor solution to be added to a supercritical anti-solvent phase resulting in the rapid expansion of the solvent in the precursor solution, causing supersaturation and precipitation of the material dissolved within the precursor solution. Unlike the GAS process, the SAS process is a steady state system in which the precursor solution is continuously added to a pre-pressurised vessel containing the anti-solvent, resulting in exceptional supersaturation rates. The high rate of supersaturation directly causes the

nucleation to growth ratio to increase, resulting in the materials being formed to have much smaller particle sizes than observed in the GAS process<sup>135</sup>.

The procedure for the SAS process is semi-continuous as the precursor solution and anti-solvent are co-currently pumped into the precipitation vessel. A schematic for the SAS process can be observed in the experimental section. The mixing of precursor solution and anti-solvent is conducted through a nozzle system, increasing dispersion of the particles formed. The design of the nozzle along with the flow rate of the solvent have a significant effect on the hydrodynamics of the system. The hydrodynamics of the system have an impact on the precipitated material, and are defined by the Reynolds number, i.e. the ratio of inertial and viscous forces. By altering flow rate within specific nozzle design, the Reynolds number can be changed to alter dispersion.

Another factor that has a high degree of control over the system is the thermodynamics. The temperature and pressure of the system can have a high impact upon both the solvating power of the anti-solvent and mass transfer properties. There is a balance that is required from the pressure and temperature of the system. By increasing the pressure, or decreasing the temperature, the system increases in density, causing higher miscibility of the precursor solution and anti-solvent resulting in the production of smaller particle sizes<sup>136</sup>. The increase in density also results in a higher solubility of the material dissolved in the precursor solution, which reduces the yield of precipitated material<sup>137</sup>.

An important consideration when using SAS preparation is what happens when the precursor solution is added to the supercritical phase as this has a significant effect on the mixture critical point (MCP)<sup>138, 139</sup>. Essentially, operating at conditions near the critical point of the chosen anti-solvent can result in the system dipping into a sub-critical state, which will alter the precipitation of the desired material. This results in the SAS process being operated at considerably higher pressures than the critical point of the anti-solvent to ensure the system remains in a supercritical state consistently.

### **1.9.6. GAS and SAS for material preparation**

There are a wide range of applications for materials produced through GAS and SAS methods from the pharmaceutical industry to polymers and inorganic materials. Pharmaceuticals products being produced through anti-solvent preparation utilise the benefit of the production of nanoparticles, which can increase the bioavailability of drugs as nanoparticles can diffuse easily through the internal barriers within the body<sup>140</sup>. Polymeric

foams have been synthesised using supercritical preparation<sup>141</sup>, as-well as biocompatible polysaccharides used for encapsulating drug compounds<sup>142</sup>.

Inorganic materials produced through supercritical preparation have been used in a range of applications where particle size is an important factor, such as in semi-conductors, inorganic dyes and heterogeneous catalysts. As shown in table 1.1, there are a wide range of potential SCFs that can be considered, although the majority of studies have been conducted using CO<sub>2</sub>, H<sub>2</sub>O, ethane and ethene<sup>119</sup>. Supercritical CO<sub>2</sub> is the most widely used SCF and has many benefits such as SC-CO<sub>2</sub> being non-flammable, non-toxic, environmentally safe, and widely available at high purity, all whilst being relatively unreactive.

The production of semiconductor materials using metal acetates provides an insight to the conditions needed for precipitating oxide precursor materials, with pressure and temperature ranges (100 – 150 bar and ~40 °C) defined using SC-CO<sub>2</sub><sup>143</sup>. Similarly, experiments producing yellow pigment inorganic dyes conducted by Yuan *et al.* illustrated the effect of temperature and nozzle size on the particle size. It was found that increased temperature and nozzle size, with lower pressure, increased particle size<sup>144</sup>. For the production of metal oxides, using acetate precursors in the SAS process provides nanoparticles that can be calcined to form the desired metal oxide. The idea behind using SAS is to create a precursor that can be calcined to form a pure phase of an oxide, normally requiring much higher temperature to reach, and therefore increasing the surface area of the oxide produced.

### **1.9.7. Catalyst preparation using SC-CO<sub>2</sub> SAS preparation**

The use of SAS precipitation can be used to produce either a catalyst or catalyst support, which then has active nanoparticle metals deposited on the surface using methods such as standard impregnation or sol immobilisation. A range of support materials have been successfully produced and are documented in literature, including TiO<sub>2</sub> and CeO<sub>2</sub>.

SAS precipitated TiO<sub>2</sub> was prepared and studied extensively by Lu *et al.*, with the study finding a correlation between particle size and morphology with changes in flow rate, nozzle geometry, pressure, temperature and the concentration of the titanium acetylacetonate precursor solution. The trends found concur with the effects of changing conditions in SAS preparation described above. XRD of the precipitated material revealed that the samples were completely amorphous, where the precursor material is known to be highly crystalline. Calcination of the sample provided a highly crystalline phase of mixed anatase and rutile TiO<sub>2</sub>.

Tang *et al.* showed that SAS prepared TiO<sub>2</sub> has been shown to be significantly more

active for CO oxidation with Au deposited on the surface when compared to a standard Au/TiO<sub>2</sub> with conversion being 9 times higher. It was suggested that this was due to the increased dispersion of Au on the SAS prepared TiO<sub>2</sub><sup>145</sup>.

CeO<sub>2</sub> was prepared through SAS precipitation from the Cerium acetylacetonate precursor by Hutchings and co-workers<sup>146</sup>. The system pressure and temperature was altered from 110 -150 bar and 40 – 60 °C, with the resulting precipitates calcined at 400 °C to produce the oxide material. BET analysis was conducted on the calcined material, with the CeO<sub>2</sub> having a surface area of 30 m<sup>2</sup>g<sup>-1</sup>. Similarly to the TiO<sub>2</sub>, Au was deposited on the surface and the Au/CeO<sub>2</sub> was tested for CO oxidation, comparing the results to a standard Au/CeO<sub>2</sub>. Again, the activity for the SAS precipitated CeO<sub>2</sub> sample was higher than that of the standard sample, with the results attributed to the better dispersion of Au nanoparticles on the surface of the SAS prepared CeO<sub>2</sub>.

### 1.9.8. Perovskites in catalysis

The original perovskite material, CaTiO<sub>3</sub> was discovered in the Ural Mountains of Russia by Gustav Rose in 1839. The general structure of a perovskite can be described as an ABO<sub>3</sub> mixed metal oxide, where the A and B sites have balancing charges, although usually these are 3<sup>+</sup>, shown in figure 1.8.

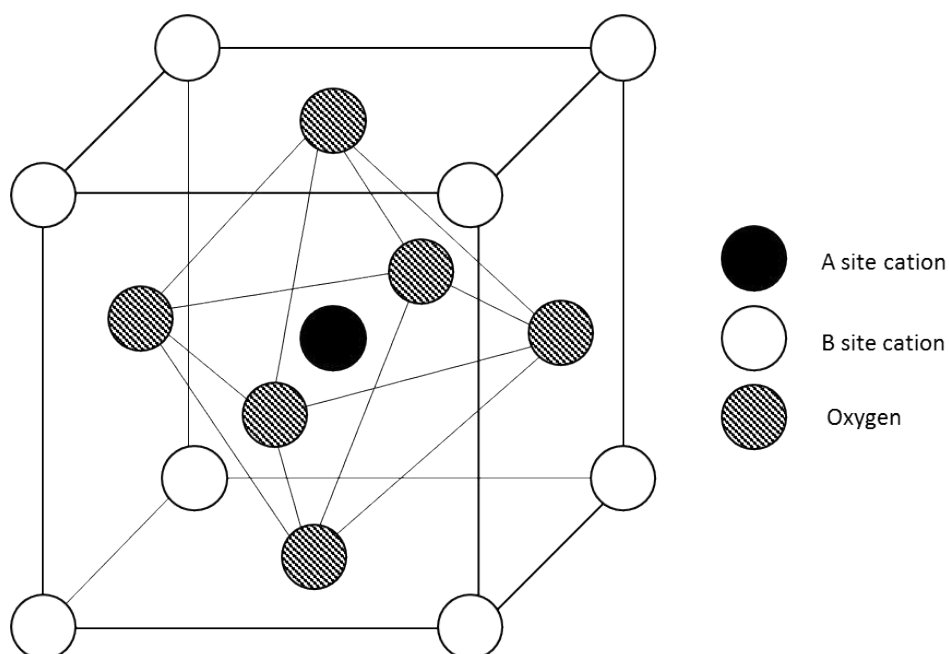


Figure 1.8 Crystal structure of a typical ABO<sub>3</sub> perovskite type mixed metal oxide.

The possible oxidation state is dictated by the ionic radius of the cation, as the perovskite structure generally has a larger A site cation, with a smaller B site cation. It was first

assumed that the  $ABO_3$  perovskite had a simple cubic structure, whereas in reality, to obtain this structure, extremely high temperatures are required. In the structure of a perovskite, the A site cation is coordinated with 12 oxygen anions, whilst the B site is coordinated with 6 oxygen anions, hence the ionic radii size difference. In order for these orientations to be met, it is often the case that the structure of the perovskite is distorted with orthorhombic and rhombohedral structures appearing most commonly<sup>147</sup>. Several attempts have been made to improve the preparation method or to synthesise perovskite structures that require lower calcination temperatures in order to increase surface area<sup>148, 149</sup>. One of the more traditional methods is the simple addition of an organic complex, such as citric acid, however, this only lowers the calcination temperature by a nominal amount. For example, the preparation of  $LaCoO_3$  involves the combustion of citric acid followed by calcination at 900 °C over a period of 6 hours under flowing air resulting in a surface area of  $9 \text{ m}^2 \text{ g}^{-1}$ . To improve upon surface area, one of the more successful methods is to prepare smaller particle sizes of the precursor, which enables the use of lower calcination temperatures to reach the perovskite phase, subsequently increasing surface area. One aspect that is important to the development of these methods is characterisation of the physical properties and structures of the perovskite type oxides formed. By altering the crystal properties of the structures, the properties of the perovskite mixed metal oxides change, and therefore should be characterised with appropriate methods. XRD, XPS, and TEM are valuable tools for defining the crystal phases, surface species and orientation of the lattice structure. The physical properties can be measured through  $NH_3$ ,  $CO_2$  and  $O_2$  TPD, which can provide information on the acid and basic surface sites as-well as information about the oxygen vacancies within the lattice structure.

Perovskites are extremely tuneable complexes, with many metals fitting the structural criteria. The tuneable nature of the perovskite has been of interest in catalysis for many years, with studies into the redox capability stretching back to the 1960s. Much of the interest then was the use of lanthanide perovskites in automotive catalysis due to the high thermal stability, electron mobility, and redox behaviour exhibited by the structure, however, perovskites weren't seen as industrially viable due to the inherent low surface area that accompanies high temperature treatment of precursors<sup>150</sup>. More recently, the application of perovskite oxides as heterogeneous catalysts has increased due to the tuneable properties and inherent thermal and hydrothermal stability. Perovskites have been applied to gas and solid phase reaction at higher temperature and liquid phase reaction at more ambient temperatures<sup>151, 152</sup>.

Perovskite catalysts have been successfully used in both NO decomposition<sup>153, 154</sup>, NO reduction<sup>155</sup> and NO oxidation<sup>156</sup>. Although each of these reactions proceed through different

pathways, the tuneable nature of the perovskite structure means that by altering the cations used, different properties can be achieved. For example, NO decomposition requires an oxygen deficient surface so as to provide a vacancy site for NO adsorption which can be achieved using  $\text{LaSrNiO}_4$ <sup>157</sup> with 94 % conversion achieved. NO reduction, however, usually requires a reducing agent such as  $\text{CO}$ <sup>158</sup> to aid conversion. The dependency on the reducing agent can be mitigated by using the redox potential of the perovskite catalysts. It has been found that by altering the B site cation, that a large difference in activity is observed as the activity is based on the redox property of the B site cation<sup>159</sup>.

Other reactions that perovskite catalysts have been used for aside from the aforementioned, are reactions such as dehydrogenation of organic substrates<sup>160</sup>, oxidative coupling of methane<sup>161</sup>, oxygen evolution<sup>162</sup> and hydrogenation of carbon oxides<sup>163</sup>. These more recent advances in material preparation have rekindled the interest in perovskites as catalysts and provide a good basis for the potential use in glycerol oxidation for the following body of work.

### 1.9.9 References

1. J. Berzelius, *Annal Chim Phys*, 1836, **61**, 146-151.
2. M. Bowker, *Oxford Chemistry Primers*, 1998, **53**, ALL-ALL.
3. C. Adams, *Topics in Catalysis*, 2009, **52**, 924-934.
4. W. C. Winkler, A. Nahvi, A. Roth, J. A. Collins and R. R. Breaker, *Nature*, 2004, **428**, 281-286.
5. G. Szonyi, in *Homogeneous Catalysis*, AMERICAN CHEMICAL SOCIETY, 1974, vol. 70, ch. 4, pp. 53-96.
6. W. Wang, G. B. Hammond and B. Xu, *Journal of the American Chemical Society*, 2012, **134**, 5697-5705.
7. B. Zhang, X. Tang, Y. Li, Y. Xu and W. Shen, *International Journal of Hydrogen Energy*, 2007, **32**, 2367-2373.
8. T. García, B. Solsona and S. H. Taylor, *Applied Catalysis B: Environmental*, 2006, **66**, 92-99.
9. A. Guimaraes, L. Dieguez and M. Schmal, *The Journal of Physical Chemistry B*, 2003, **107**, 4311-4319.
10. J. Barbier and D. Duprez, *Applied Catalysis A: General*, 1992, **85**, 89-100.
11. M. Conte, A. F. Carley, C. Heirene, D. J. Willock, P. Johnston, A. A. Herzing, C. J. Kiely and G. J. Hutchings, *Journal of Catalysis*, 2007, **250**, 231-239.
12. A. Jones and B. D. McNicol, *Journal of Catalysis*, 1977, **47**, 384-388.
13. J. Xu and G. F. Froment, *AIChE Journal*, 1989, **35**, 88-96.
14. M. Haruta, N. Yamada, T. Kobayashi and S. Iijima, *Journal of Catalysis*, 1989, **115**, 301-309.
15. K. Ramesh, L. Chen, F. Chen, Y. Liu, Z. Wang and Y.-F. Han, *Catalysis Today*, 2008, **131**, 477-482.
16. H. Y. Kim, H. M. Lee and G. Henkelman, *Journal of the American Chemical Society*, 2012, **134**, 1560-1570.
17. C. Zhang, P. Hu and A. Alavi, *Journal of the American Chemical Society*, 1999, **121**, 7931-7932.
18. G. C. Bond and P. A. Sermon, *Gold Bulletin*, 1973, **6**, 102-105.
19. M. Haruta, T. Kobayashi, H. Sano and N. Yamada, *Chemistry Letters*, 1987, **16**, 405-408.

20. G. J. Hutchings, *Journal of Catalysis*, 1985, **96**, 292-295.
21. T. Hayashi, K. Tanaka and M. Haruta, *Journal of Catalysis*, 1998, **178**, 566-575.
22. L. Prati and M. Rossi, *Journal of Catalysis*, 1998, **176**, 552-560.
23. P. Landon, P. J. Collier, A. J. Papworth, C. J. Kiely and G. J. Hutchings, *Chemical Communications*, 2002, **152**, 2058-2059.
24. V. Subramanian, E. E. Wolf and P. V. Kamat, *Journal of the American Chemical Society*, 2004, **126**, 4943-4950.
25. M. Murdoch, G. Waterhouse, M. Nadeem, J. Metson, M. Keane, R. Howe, J. Llorca and H. Idriss, *Nature Chemistry*, 2011, **3**, 489-492.
26. M. Haruta, *Catalysis Today*, 1997, **36**, 153-166.
27. M. Haruta, *The Chemical Record*, 2003, **3**, 75-87.
28. J. C. Pritchard, Q. He, E. N. Ntainjua, M. Piccinini, J. K. Edwards, A. A. Herzing, A. F. Carley, J. A. Moulijn, C. J. Kiely and G. J. Hutchings, *Green Chemistry*, 2010, **12**, 915-921.
29. D. A. Crole, S. J. Freakley, J. K. Edwards and G. J. Hutchings, *Proceedings of the Royal Society A: Mathematical, Physical and Engineering Science*, 2016, **472**.
30. E. Nowicka, M. Sankar, S. H. Taylor, D. Bethell, D. W. Knight and G. J. Hutchings.
31. M. Á. Centeno, I. Carrizosa and J. A. Odriozola, *Applied Catalysis A: General*, 2003, **246**, 365-372.
32. R. Gopinath, N. Lingaiah, N. S. Babu, I. Suryanarayana, P. S. Prasad and A. Obuchi, *Journal of Molecular Catalysis A: Chemical*, 2004, **223**, 289-293.
33. P. Mulvaney, *MRS bulletin*, 2001, **26**, 1009-1014.
34. J. A. Lopez-Sanchez, N. Dimitratos, P. Miedziak, E. Ntainjua, J. K. Edwards, D. Morgan, A. F. Carley, R. Tiruvalam, C. J. Kiely and G. J. Hutchings, *Physical Chemistry Chemical Physics*, 2008, **10**, 1921-1930.
35. J.-D. Grunwaldt, C. Kiener, C. Wögerbauer and A. Baiker, *Journal of Catalysis*, 1999, **181**, 223-232.
36. M. Comotti, W.-C. Li, B. Spliethoff and F. Schüth, *Journal of the American Chemical Society*, 2006, **128**, 917-924.
37. F. Porta and L. Prati, *Journal of Catalysis*, 2004, **224**, 397-403.
38. X. Liu, A. Wang, X. Wang, C.-Y. Mou and T. Zhang, *Chemical communications*, 2008, 3187-3189.
39. D. I. Enache, J. K. Edwards, P. Landon, B. Solsona-Espriu, A. F. Carley, A. A. Herzing, M. Watanabe, C. J. Kiely, D. W. Knight and G. J. Hutchings, *Science*, 2006, **311**, 362-365.

40. N. Dimitratos, A. Villa, D. Wang, F. Porta, D. Su and L. Prati, *Journal of Catalysis*, 2006, **244**, 113-121.
41. J. M. Campos-Martin, G. Blanco-Brieva and J. L. Fierro, *Angewandte Chemie International Edition*, 2006, **45**, 6962-6984.
42. V. R. Choudhary, A. G. Gaikwad and S. D. Sansare, *Angewandte chemie international edition*, 2001, **40**, 1776-1779.
43. P. Landon, P. J. Collier, A. F. Carley, D. Chadwick, A. J. Papworth, A. Burrows, C. J. Kiely and G. J. Hutchings, *Physical Chemistry Chemical Physics*, 2003, **5**, 1917-1923.
44. J. K. Edwards, A. F. Carley, A. A. Herzing, C. J. Kiely and G. J. Hutchings, *Faraday Discussions*, 2008, **138**, 225-239.
45. J. K. Edwards, B. Solsona, P. Landon, A. F. Carley, A. Herzing, M. Watanabe, C. J. Kiely and G. J. Hutchings, *Journal of materials chemistry*, 2005, **15**, 4595-4600.
46. J. K. Edwards, B. E. Solsona, P. Landon, A. F. Carley, A. Herzing, C. J. Kiely and G. J. Hutchings, *Journal of Catalysis*, 2005, **236**, 69-79.
47. M. B. Gawande, A. Goswami, T. Asefa, H. Guo, A. V. Biradar, D.-L. Peng, R. Zboril and R. S. Varma, *Chemical Society Reviews*, 2015, **44**, 7540-7590.
48. J. K. Edwards, B. Solsona, E. Ntainjua, A. F. Carley, A. A. Herzing, C. J. Kiely and G. J. Hutchings, *Science*, 2009, **323**, 1037-1041.
49. G. Li, J. Edwards, A. F. Carley and G. J. Hutchings, *Catalysis Communications*, 2007, **8**, 247-250.
50. S. Park, S. H. Lee, S. H. Song, D. R. Park, S.-H. Baeck, T. J. Kim, Y.-M. Chung, S.-H. Oh and I. K. Song, *Catalysis Communications*, 2009, **10**, 391-394.
51. S. J. Freakley, R. J. Lewis, D. J. Morgan, J. K. Edwards and G. J. Hutchings, *Catalysis Today*, 2015, **248**, 10-17.
52. C. Della Pina, E. Falletta, L. Prati and M. Rossi, *Chemical Society Reviews*, 2008, **37**, 2077-2095.
53. S. Meenakshisundaram, E. Nowicka, P. J. Miedziak, G. L. Brett, R. L. Jenkins, N. Dimitratos, S. H. Taylor, D. W. Knight, D. Bethell and G. J. Hutchings, *Faraday Discussions*, 2010, **145**, 341-356.
54. D. I. Enache, J. K. Edwards, P. Landon, B. Solsona-Espriu, A. F. Carley, A. A. Herzing, M. Watanabe, C. J. Kiely, D. W. Knight and G. J. Hutchings, *Science*, 2006, **311**, 362-365.
55. Y. Ryabenkova, Q. He, P. J. Miedziak, N. F. Dummer, S. H. Taylor, A. F. Carley, D. J. Morgan, N. Dimitratos, D. J. Willock, D. Bethell, D. W. Knight, D. Chadwick, C. J. Kiely and G. J. Hutchings, *Catalysis Today*, 2013, **203**, 139-145.

56. D. I. Enache, D. W. Knight and G. J. Hutchings, *Catalysis Letters*, 2005, **103**, 43-52.
57. J. Pritchard, L. Kesavan, M. Piccinini, Q. He, R. Tiruvalam, N. Dimitratos, J. A. Lopez-Sanchez, A. F. Carley, J. K. Edwards, C. J. Kiely and G. J. Hutchings, *Langmuir*, 2010, **26**, 16568-16577.
58. P. Miedziak, M. Sankar, N. Dimitratos, J. A. Lopez-Sanchez, A. F. Carley, D. W. Knight, S. H. Taylor, C. J. Kiely and G. J. Hutchings, *Catalysis Today*, 2011, **164**, 315-319.
59. V. R. Choudhary, A. Dhar, P. Jana, R. Jha and B. S. Uphade, *Green Chemistry*, 2005, **7**, 768-770.
60. J. A. Lopez-Sanchez, N. Dimitratos, P. Miedziak, E. Ntainjua, J. K. Edwards, D. Morgan, A. F. Carley, R. Tiruvalam, C. J. Kiely and G. J. Hutchings, *Physical Chemistry Chemical Physics*, 2008, **10**, 1921-1930.
61. E. Nowicka, J. P. Hofmann, S. F. Parker, M. Sankar, G. M. Lari, S. A. Kondrat, D. W. Knight, D. Bethell, B. M. Weckhuysen and G. J. Hutchings, *Physical Chemistry Chemical Physics*, 2013, **15**, 12147-12155.
62. E. Cao, M. Sankar, E. Nowicka, Q. He, M. Morad, P. J. Miedziak, S. H. Taylor, D. W. Knight, D. Bethell, C. J. Kiely, A. Gavriilidis and G. J. Hutchings, *Catalysis Today*, 2013, **203**, 146-152.
63. Q. He, P. J. Miedziak, L. Kesavan, N. Dimitratos, M. Sankar, J. A. Lopez-Sanchez, M. M. Forde, J. K. Edwards, D. W. Knight and S. H. Taylor, *Faraday discussions*, 2013, **162**, 365-378.
64. C. Keresszegi, T. Bürgi, T. Mallat and A. Baiker, *Journal of Catalysis*, 2002, **211**, 244-251.
65. T. Mallat, Z. Bodnar, P. Hug and A. Baiker, *Journal of Catalysis*, 1995, **153**, 131-143.
66. L. Prati, A. Villa, F. Porta, D. Wang and D. Su, *Catalysis today*, 2007, **122**, 386-390.
67. C. L. Bianchi, P. Canton, N. Dimitratos, F. Porta and L. Prati, *Catalysis today*, 2005, **102**, 203-212.
68. J. Lunt, *Polymer Degradation and Stability*, 1998, **59**, 145-152.
69. N. Dimitratos, J. A. Lopez-Sanchez and G. J. Hutchings, *Chemical Science*, 2012, **3**, 20-44.
70. M. B. Griffin, A. A. Rodriguez, M. M. Montemore, J. R. Monnier, C. T. Williams and J. W. Medlin, *Journal of catalysis*, 2013, **307**, 111-120.
71. N. Dimitratos, J. A. Lopez-Sanchez, S. Meenakshisundaram, J. M. Anthonykutty, G. Brett, A. F. Carley, S. H. Taylor, D. W. Knight and G. J. Hutchings, *Green Chemistry*, 2009, **11**, 1209-1216.

72. N. Dimitratos, J. A. Lopez-Sanchez, D. Morgan, A. Carley, L. Prati and G. J. Hutchings, *Catalysis today*, 2007, **122**, 317-324.
73. A. Villa, D. Wang, G. M. Veith, F. Vindigni and L. Prati, *Catalysis Science & Technology*, 2013, **3**, 3036-3041.
74. Y. Ryabenkova, P. J. Miedziak, N. F. Dummer, S. H. Taylor, N. Dimitratos, D. J. Willock, D. Bethell, D. W. Knight and G. J. Hutchings, *Topics in Catalysis*, 2012, **55**, 1283-1288.
75. J. N. Chheda, G. W. Huber and J. A. Dumesic, *Angewandte Chemie International Edition*, 2007, **46**, 7164-7183.
76. R. J. Andres, J. S. Gregg, L. Losey, G. Marland and T. A. Boden, *Tellus B*, 2011, **63**, 309-327.
77. J. Chang, D. Y. C. Leung, C. Z. Wu and Z. H. Yuan, *Renewable and Sustainable Energy Reviews*, 2003, **7**, 453-468.
78. H. Hong, Z. Hanqian, Y. Xiangqian and D. Jianhua, *Baosteel Technical Research*, 2017, **11**, 18.
79. R. B. Rebak, K. A. Terrani, W. P. Gassmann, J. B. Williams and K. L. Ledford, *MRS Advances*, 2017, 1-8.
80. S. Srinivasan, *Renewable Energy*, 2009, **34**, 950-954.
81. R. W. Harrison, *Journal of Agricultural and Applied Economics*, 2009, **41**, 493-500.
82. P. B. Thompson, *Agriculture*, 2012, **2**, 339-358.
83. S. N. Naik, V. V. Goud, P. K. Rout and A. K. Dalai, *Renewable and sustainable energy reviews*, 2010, **14**, 578-597.
84. M. A. Carriquiry, X. Du and G. R. Timilsina, *Energy Policy*, 2011, **39**, 4222-4234.
85. F. Ma and M. A. Hanna, *Bioresource technology*, 1999, **70**, 1-15.
86. Y. Shen, S. Zhang, H. Li, Y. Ren and H. Liu, *Chemistry-a European Journal*, 2010, **16**, 7368-7371.
87. S. Carrettin, P. McMorn, P. Johnston, K. Griffin and G. J. Hutchings, *Chemical Communications*, 2002, 696-697.
88. J. Xu, H. Zhang, Y. Zhao, B. Yu, S. Chen, Y. Li, L. Hao and Z. Liu, *Green Chemistry*, 2013, **15**, 1520-1525.
89. P. Fordham, R. Garcia, M. Besson and P. Gallezot, *Studies in Surface Science and Catalysis*, 1996, **101**, 161-170.
90. F. Porta, L. Prati, M. Rossi and G. Scari, *Journal of Catalysis*, 2002, **211**, 464-469.
91. S. Carrettin, P. McMorn, P. Johnston, K. Griffin, C. J. Kiely, G. A. Attard and G. J. Hutchings, *Topics in Catalysis*, 2004, **27**, 131-136.

92. A. Villa, N. Dimitratos, C. E. Chan-Thaw, C. Hammond, L. Prati and G. J. Hutchings, *Accounts of chemical research*, 2015, **48**, 1403-1412.
93. M. Sankar, N. Dimitratos, P. J. Miedziak, P. P. Wells, C. J. Kiely and G. J. Hutchings, *Chemical Society Reviews*, 2012, **41**, 8099-8139.
94. W. C. Ketchie, M. Murayama and R. J. Davis, *Journal of catalysis*, 2007, **250**, 264-273.
95. S. Carrettin, P. McMorn, P. Johnston, K. Griffin, C. J. Kiely and G. J. Hutchings, *Physical Chemistry Chemical Physics*, 2003, **5**, 1329-1336.
96. G. L. Brett, Q. He, C. Hammond, P. J. Miedziak, N. Dimitratos, M. Sankar, A. A. Herzing, M. Conte, J. A. Lopez-Sanchez and C. J. Kiely, *Angewandte Chemie*, 2011, **123**, 10318-10321.
97. S. Gil, M. Marchena, L. Sánchez-Silva, A. Romero, P. Sánchez and J. L. Valverde, *Chemical engineering journal*, 2011, **178**, 423-435.
98. R. Klaewkla, M. Arend and W. F. Hoelderich, in *Mass Transfer-Advanced Aspects*, InTech, 2011.
99. S. Demirel-Gülen, M. Lucas and P. Claus, *Catalysis Today*, 2005, **102**, 166-172.
100. A. André, P. Diamantopoulou, A. Philippoussis, D. Sarris, M. Komaitis and S. Papanikolaou, *Industrial Crops and Products*, 2010, **31**, 407-416.
101. B. N. Zope, D. D. Hibbitts, M. Neurock and R. J. Davis, *Science*, 2010, **330**, 74-78.
102. L. Roquet, E. Belgsir, J.-M. Léger and C. Lamy, *Electrochimica Acta*, 1994, **39**, 2387-2394.
103. R. Garcia, M. Besson and P. Gallezot, *Applied Catalysis A: General*, 1995, **127**, 165-176.
104. H. Kimura, *Applied Catalysis A: General*, 1993, **105**, 147-158.
105. B. Katryniok, H. Kimura, E. Skrzyńska, J.-S. Girardon, P. Fongarland, M. Capron, R. Ducoulombier, N. Mimura, S. Paul and F. Dumeignil, *Green Chemistry*, 2011, **13**, 1960-1979.
106. M. S. Ide and R. J. Davis, *Accounts of chemical research*, 2013, **47**, 825-833.
107. D. Liang, J. Gao, J. Wang, P. Chen, Z. Hou and X. Zheng, *Catalysis Communications*, 2009, **10**, 1586-1590.
108. D. Tongsakul, S. Nishimura, C. Thammacharoen, S. Ekgasit and K. Ebitani, *Industrial & Engineering Chemistry Research*, 2012, **51**, 16182-16187.
109. R. Datta and M. Henry, *Journal of Chemical Technology and Biotechnology*, 2006, **81**, 1119-1129.
110. H. Kishida, F. Jin, Z. Zhou, T. Moriya and H. Enomoto, *Chemistry Letters*, 2005, **34**, 1560-1561.

111. H. Kishida, F. Jin, X. Yan, T. Moriya and H. Enomoto, *Carbohydrate research*, 2006, **341**, 2619-2623.
112. J. Liebig, *European Journal of Organic Chemistry*, 1838, **25**, 1-31.
113. D. A. Ballard and W. M. Dehn, *Organic Syntheses*, 1941, 29-29.
114. S. Cannizzaro, *European Journal of Organic Chemistry*, 1853, **88**, 129-130.
115. J. A. Darr and M. Poliakoff, *Chemical Reviews*, 1999, **99**, 495-542.
116. A. L. Scheidgen and G. M. Schneider, *Fluid phase equilibria*, 2002, **194**, 1009-1028.
117. E. Reverchon, G. Caputo and I. De Marco, *Industrial & Engineering Chemistry Research*, 2003, **42**, 6406-6414.
118. A. Baiker, *Chemical Reviews*, 1999, **99**, 453-474.
119. A. Baiker and R. Wandeler, *Cattech*, 2000, **4**, 128-143.
120. R. Noyori and T. Ohkuma, *Pure and Applied Chemistry*, 1999, **71**, 1493-1501.
121. J. J. Suárez, I. Medina and J. L. Bueno, *Fluid Phase Equilibria*, 1998, **153**, 167-212.
122. Y. Sun and B. Y. Shekunov, *The Journal of supercritical fluids*, 2003, **27**, 73-83.
123. P. T. Anastas and J. C. Warner, *Green chemistry: Theory and practice*, 1998, 29-56.
124. M. McHugh and V. Krukoni, *Supercritical fluid extraction: principles and practice*, Elsevier, 2013.
125. L. T. Taylor, *Analytical chemistry*, 2010, **82**, 4925-4935.
126. P. G. Jessop, T. Ikariya and R. Noyori, *Chemical Reviews*, 1999, **99**, 475-494.
127. P. G. Jessop, Y. Hsiao, T. Ikariya and R. Noyori, *Journal of the American Chemical Society*, 1996, **118**, 344-355.
128. Y. Kayaki, M. Yamamoto and T. Ikariya, *The Journal of organic chemistry*, 2007, **72**, 647-649.
129. H. H. Yang and C. A. Eckert, *Industrial & engineering chemistry research*, 1988, **27**, 2009-2014.
130. F. Cansell, B. Chevalier, A. Demourgues, J. Etourneau, C. Even, V. Pessey, S. Petit, A. Tressaud and F. Weill, *Journal of Materials Chemistry*, 1999, **9**, 67-75.
131. D. W. Matson, J. L. Fulton, R. C. Petersen and R. D. Smith, *Industrial & engineering chemistry research*, 1987, **26**, 2298-2306.
132. E. Reverchon, *Industrial & engineering chemistry research*, 2002, **41**, 2405-2411.
133. P. M. Gallagher, M. Coffey, V. Krukoni and W. Hillstrom, *The Journal of Supercritical Fluids*, 1992, **5**, 130-142.
134. S. Bristow, T. Shekunov, B. Y. Shekunov and P. York, *The Journal of Supercritical Fluids*, 2001, **21**, 257-271.

135. E. Reverchon, I. De Marco and E. Torino, *The Journal of Supercritical Fluids*, 2007, **43**, 126-138.
136. E. Reverchon, *The journal of supercritical fluids*, 1999, **15**, 1-21.
137. F. P. Lucien and N. R. Foster, *The Journal of Supercritical Fluids*, 2000, **17**, 111-134.
138. E. Reverchon, R. Adami, I. De Marco, C. Laudani and A. Spada, *The Journal of supercritical fluids*, 2005, **35**, 76-82.
139. E. Reverchon and I. De Marco, *The Journal of supercritical fluids*, 2004, **31**, 207-215.
140. A. A. Manzoor, L. H. Lindner, C. D. Landon, J.-Y. Park, A. J. Simnick, M. R. Dreher, S. Das, G. Hanna, W. Park and A. Chilkoti, *Cancer research*, 2012, **72**, 5566-5575.
141. E. Reverchon and S. Cardea, *The Journal of Supercritical Fluids*, 2007, **40**, 144-152.
142. L. Benedetti, A. Bertuccio and P. Pallado, *Biotechnology and bioengineering*, 1997, **53**, 232-237.
143. J. D. Holmes, D. M. Lyons and K. J. Ziegler, *Chemistry-a European Journal*, 2003, **9**, 2144-2150.
144. Y. Gao, T. K. Mulenda, Y.-F. Shi and W.-K. Yuan, *The Journal of supercritical fluids*, 1998, **13**, 369-374.
145. Z.-R. Tang, J. K. Bartley, S. H. Taylor and G. J. Hutchings, *Studies in surface science and catalysis*, 2006, **162**, 219-226.
146. P. J. Miedziak, Z. Tang, T. E. Davies, D. I. Enache, J. K. Bartley, A. F. Carley, A. A. Herzing, C. J. Kiely, S. H. Taylor and G. J. Hutchings, *Journal of Materials Chemistry*, 2009, **19**, 8619-8627.
147. F. S. Galasso, *Structure, properties and preparation of perovskite-type compounds: international series of monographs in solid state physics*, Elsevier, 2013.
148. S. Royer, F. Berube and S. Kaliaguine, *Applied Catalysis A: General*, 2005, **282**, 273-284.
149. Y. Wang, X. Cui, Y. Li, Z. Shu, H. Chen and J. Shi, *Microporous and Mesoporous Materials*, 2013, **176**, 8-15.
150. R. Voorhoeve, D. Johnson, J. Remeika and P. Gallagher, *Science*, 1977, **195**, 827-833.
151. A. E. Maegli, T. Hisatomi, E. H. Otal, S. Yoon, S. Pokrant, M. Grätzel and A. Weidenkaff, *Journal of Materials Chemistry*, 2012, **22**, 17906-17913.
152. Z.-X. Wei, Y. Wang, J.-P. Liu, C.-M. Xiao and W.-W. Zeng, *Materials Chemistry and Physics*, 2012, **136**, 755-761.
153. H. Bosch, *Catal. Today*, 1987, **2**, 369-532.
154. J. Zhu, D. Xiao, J. Li, X. Yang and Y. Wu, *Journal of Molecular Catalysis A: Chemical*, 2005, **234**, 99-105.

155. M. Taniguchi, H. Tanaka, M. Uenishi, I. Tan, Y. Nishihata, J. i. Mizuki, H. Suzuki, K. Narita, A. Hirai and M. Kimura, *Topics in Catalysis*, 2007, **42**, 367-371.
156. J. Chen, M. Shen, X. Wang, J. Wang, Y. Su and Z. Zhao, *Catalysis Communications*, 2013, **37**, 105-108.
157. J. Zhu, X. Yang, X. Xu and K. Wei, *Science in China Series B: Chemistry*, 2007, **50**, 41-46.
158. V. Belessi, P. Trikalitis, A. Ladavos, T. Bakas and P. Pomonis, *Applied Catalysis A: General*, 1999, **177**, 53-68.
159. A. Giannakas, A. Ladavos and P. Pomonis, *Applied Catalysis B: Environmental*, 2004, **49**, 147-158.
160. I. Rodriguez-Ramos, A. Guerrero-Ruiz, M. Rojas and J. Fierro, *Applied catalysis*, 1991, **68**, 217-228.
161. Y. Zeng, Y. Lin and S. Swartz, *Journal of membrane science*, 1998, **150**, 87-98.
162. A. Grimaud, K. J. May, C. E. Carlton, Y.-L. Lee, M. Risch, W. T. Hong, J. Zhou and Y. Shao-Horn, *Nature communications*, 2013, **4**, 2439.
163. J. Fierro, *Catalysis Reviews*, 1992, **34**, 321-336.

## 2.0. Experimental

### 2.1. Materials

Source and purity of all materials used, with all being used as received.

Water HPLC - Aldrich

Methanol HPLC - Aldrich

Hydrogen tetrachloroaurate trihydrate - Aldrich

Palladium (II) chloride, 99 % - Aldrich

Chloroplatinic acid hydrate, 99 % - Aldrich

Titania, P25 - Degussa

Titanium (IV) isopropoxide, 99.999 % Aldrich

Lanthanum (III) acetylacetonate hydrate - Aldrich

Manganese (II) acetate tetrahydrate, 99.99 % - Aldrich

Nickel (II) acetate tetrahydrate, 98 % - Aldrich

Cobalt (II) acetate, 99.99 % - Aldrich

Iron (II) acetate, 99.99 % - Aldrich

Zinc, mossy,  $\geq 99$  % - Aldrich

Potassium chromate, 99.95 % - Aldrich

Sodium acetate anhydrous, 99 % -Aldrich

Hydrochloric acid, 37 % - Sigma-Aldrich

Sulfuric acid, 99.999 % - Aldrich

Polyvinyl alcohol, 99 % hydrolysed - Aldrich

Sodium borohydride, 98 % - Sigma

Glycerol,  $\geq 99$  %, Sigma-Aldrich

Sodium hydroxide,  $\geq 97$  % powder, Sigma-Aldrich

## 2.2. Definitions

Conversion;

---

Selectivity;

---

Turn over frequency (TOF);

---

Although the turn over frequency is expressed using the concentration of active sites on the surface of a catalyst, this body of work cannot accurately describe this value. Therefore, the TOF is described by using the total moles of metal on the catalyst used.

Substrate to metal ratio (S:M);

---

By standardising the S:M ratio, it was ensured that all reactions were conducted with the same relative amount of precious metal.

## 2.3. Support Preparation

Supports for novel catalyst preparation were synthesised using Supercritical anti-solvent (SAS) precipitation due to the inherent advantages of the technique, as discussed in the introduction. Supports were prepared through different techniques in order to view the effect that the preparation technique has on reaction in question. FP was chosen as a possible alternative for forming comparable supports whilst BM was chosen as a potentially scalable alternative to SAS precipitation.

### 2.3.1. Supercritical anti-solvent (SAS) preparation

#### 2.3.1.1 Supercritical anti-solvent (SAS) apparatus

The preparation of support materials utilising  $\text{ScCO}_2$  was conducted in a purpose-built SAS rig designed and built by Separex (Figure 1.). There are two modes of operation, batch (GAS) and semi-continuous flow (SAS). Only SAS precipitation was used within this body of work.

The input feed to the system is a liquid  $\text{CO}_2$  cylinder. Upon opening, the liquid  $\text{CO}_2$  transitions to the gas phase due to depressurisation from the vessel. This system requires a liquid  $\text{CO}_2$  input for pumping, and to ensure this happens, a Hitema chiller (C1) is used containing a mixture of demineralised water and glycol (20 % glycol) cooled to  $-4\text{ }^\circ\text{C}$ . The flow rate and pressure of the  $\text{CO}_2$  is controlled with the use of a dual system pump. This enables the flow rate to reach up to 18 kg/h and reaching homogeneous optimum pressures of  $\geq 110$  bar. Prior to the introduction of  $\text{scCO}_2$  to the system, the  $\text{scCO}_2$  is flowed through a heater (H1) to allow thermal equilibrium with the metal precursor solution. The pressure of the system is steadily increased to operating pressure, ensuring that the operating pressure is stabilised prior to introduction of the precursor solution.

The precursor solutions pass through a HPLC pump to allow control over the flow rate at which the precursor solution is introduced to the system. The prepared solution and  $\text{ScCO}_2$  were simultaneously pumped into the precipitation vessel through a co-axial nozzle (Figure 2.1 B – 2.1.C). The co-axial nozzle has an inner and outer tube setup, with the precursor solution flowing through the inner tube and the  $\text{ScCO}_2$  flowing simultaneously through the outer tube.

The co-axial nozzle is affixed to a 1 L stainless steel precipitation vessel equipped with a lip seal and a frit filter disk (pore size 0.5 micron). The precipitation vessel is housed within a stainless-steel basket with heater (H<sub>2</sub>) and pressure transducer. The precipitate is collected on the frit, with all  $\text{ScCO}_2$  soluble material passing through the frit and flowing into the heated solvent collection vessel (H3). A filter between the precipitation vessel and solvent collection vessel prevents clogging of the BPR used to control pressure throughout the system.

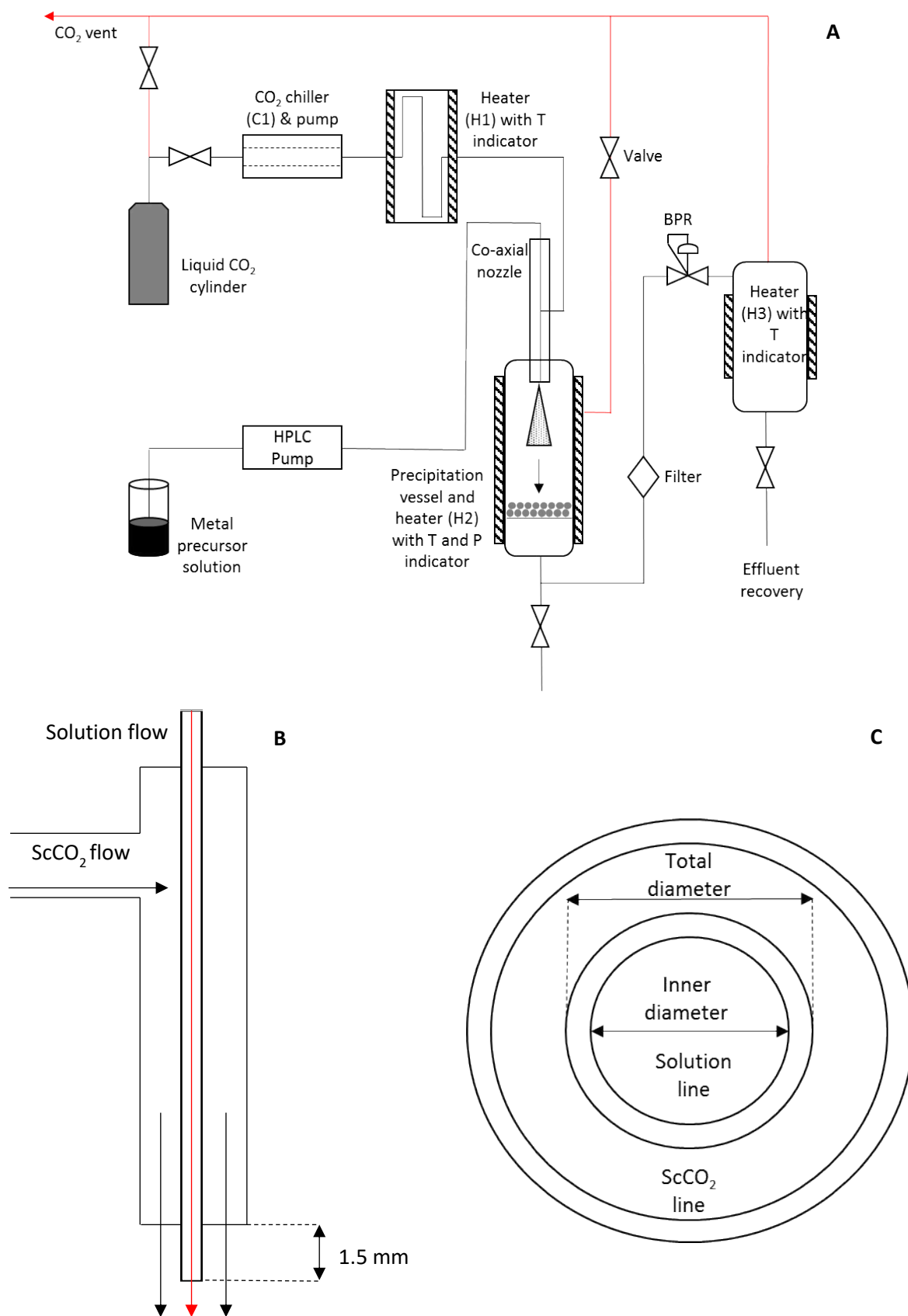


**Figure 2.1** Schematic outlining the SAS operating rig (A), and the co-axial nozzle design from side view (B) and end view (C).

### **2.3.1.2 Supercritical anti-solvent (SAS) support preparation**

Utilising the SAS system, a series of perovskite type mixed metal oxides ( $ABO_3$ ) were synthesised using acetate precursor materials. This was achieved by preparing solutions of A site lanathanum (III) acetylacetonate hydrate precursor along with a corresponding B site precursor, manganese (II) acetate tetrahydrate, Nickel (II) acetate tetrahydrate, cobalt (II) acetate, iron (II) acetate, or chromium (III) acetate in a 1:1 ratio of the cations. The precursors were stirred in methanol until completely dissolved. Exact concentrations are recorded in the subsequent results chapters.

Pure methanol was pumped into the system prior to the precursor solution so as to allow the system to equilibrate. Preparation of the support precursor was achieved by spraying the solution into the rig after pressurisation to 130 bar was stabilised, at a flow rate of 4 ml/min. Once the solution had been fully depleted, the system was sprayed with methanol for a further 5 min, followed by  $ScCO_2$  at a lower flow rate and pressure to ensure the precursor material was dry. The precursor material was then calcined in a flowing air furnace at a pre-determined temperature obtained through TGA analysis.

### **2.3.2. Flame pyrolysis (FP) preparation**

#### **2.3.2.1. Flame pyrolysis (FP) apparatus**

Comparative supports were prepared using a purpose built, small scale flame pyrolysis apparatus (FP) shown in Figure 2. The system uses an oxygen and propane mix, at a controlled ratio, to produce a high velocity flame of varying oxygen concentration. Using an automatic flow meter to control the rate of delivery of the solution, the precursor solution is introduced to an atomiser which sprays the atomised solution into the flame. The rapidly formed particulate is propelled forward by the flame and the resultant solid adheres to a water-cooled quartz collection plate.

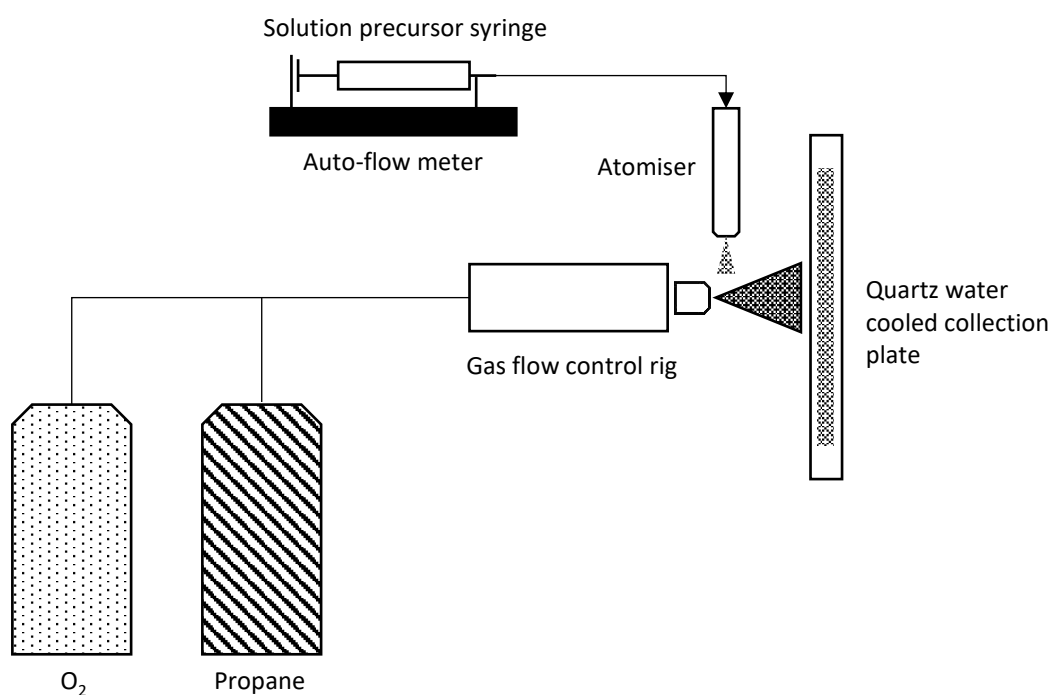


**Figure 2.2 Schematic describing a simple flame pyrolysis apparatus setup**

### 2.3.2.2. Flame pyrolysis (FP) support preparation

Flame pyrolysis was performed using the custom built equipment described above. An aqueous solution containing La/B nitrate salts (0.1 M) were sprayed at a rate of  $0.5 \text{ ml min}^{-1}$  through a Sonozap ultrasonic nebuliser (2.8 W, 130 kHz) directly into a horizontally augmented oxygen-propane mixed flame ( $1.4 - 0.5 \text{ L min}^{-1}$ ) flowing through a stainless steel nozzle (0.082" diameter). The gas flows recorded were controlled through the use of a mass flow controller. The resulting particulate was collected on a water cooled quartz plate, set 10 cm from the nozzle tip. Typical experimental procedure was approximately 10 minutes. Longer durations caused a build-up of particulate that grew closer to the flame causing an increase in particle size distribution.

### 2.3.3. Planetary ball mill (BM) preparation

#### 2.3.3.1. Planetary ball mill (BM) apparatus

The planetary ball mill is a system which utilises a form of high powered mechanical grinding in which precursor materials are added into a vessel containing a grinding ball made of a hard substance, such as zirconia. The system rotates at user controlled RPM around a central point. As the ball mill spins, so does the grinding vessel around its axis, enabling a high-powered mixing of the precursor materials (Figure 2.3).

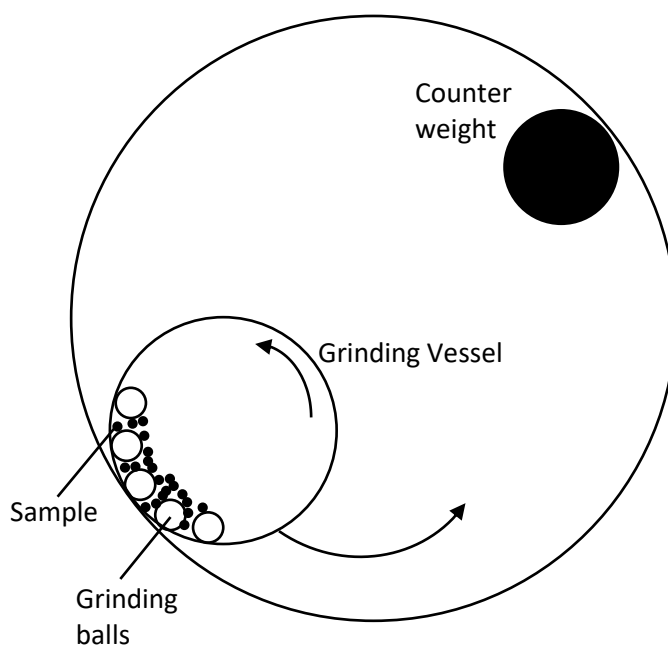


*Figure 2.3 Planetary ball mill schematic.*

#### 2.3.3.2. Planetary Ball Mill (BM) Support preparation

The support prepared was an  $ABO_3$  perovskite type mixed metal oxide and utilised a Retsch PM 100 planetary ball mill. The oxide precursors were added to the grinding vessel to form a ratio of 1:1 A to B site, along with zirconia grinding balls. The vessel was then weighed and the counter weight set. The system was set to 400 rpm for a period of 24 hours, followed by a calcination at a temperature predetermined by TGA analysis. No lubricant was involved in the grinding.

### 2.4. Chromium (II) acetate precursor synthesis

Due to the flexibility of the chromium cations oxidation state, it is necessary to synthesise the precursor within 24 hours of its use. This is achieved through a simple ion exchange in which mossy zinc (20 g) was placed into a sealed boiling tube with potassium

dichromate (4 g). In a separate beaker, a solution of sodium acetate trihydrate was prepared (18 g, 16 ml, 8.26 M). Conc. Hydrochloric acid (40 ml, 12M) was added drop wise to the sealed boiling tube containing the mossy zinc and potassium dichromate with a vent syringe. The solution was left until a blue solution is formed. The resulting blue solution was removed via injection and rapidly added to the sodium acetate trihydrate solution. The resulting red precipitate is then filtered under suction and, washed with ice cold methanol, ensuring the precipitate doesn't fully dry. The resulting precipitate is collected and used within 24 hours of preparation.

## 2.5. Catalyst Preparation

The method of deposition of precious metals on to the surface of the prepared materials was the sol-immobilisation preparation. Sol immobilisation results in a high dispersion of metals with a narrow particle size on the surface of a catalyst; thereby ensuring that the catalyst is working as efficiently as possible.

### 2.5.1. Sol immobilisation preparation

Sol immobilisation is a technique that provides a small particle size distribution of highly dispersed nanoparticles across the surface of a support material. The method involves creating a stable colloid form of a precious metal, reducing the precious metal from its precursor form to a metallic state before depositing the resulting particles upon the surface of a support by manipulating the isoelectric point of the support until a metal surface interaction is induced resulting in a good wetting of the support surface.

A range of Au,Pd,Pt, Au-Pd and Au-Pt catalysts were produced for this body of work in monometallic and bimetallic forms supported on the perovskite materials and P25 titania (80/20 anatase/rutile blend). The general procedure for sol immobilisation is detailed as follows for a 1 g catalyst.

A colloid is formed via the addition of polyvinyl alcohol (0.1 M, 0.65:1, PVA:metal) to an aqueous solution (400 mL) of known concentration Au/Pd/Pt in either monometallic (0.01 g metal) or bimetallic, at a ratio of 1:1 (total 0.01 g). The metal chlorides are then reduced with sodium borohydride (0.1 M), with the molar amount added dependant on the metal used; Au – 5:1, Pd – 5:1, Pt – 10:1, AuPd – 5:1, AuPt – 7.5:1. The solution is left to equilibrate (30 min) before adding the support (0.99 g). The solution can be manipulated by adding H<sub>2</sub>SO<sub>4</sub> to the solution when acidic supports are used (such as titania) to increase the metal support interaction. Supports that are basic in nature do not need to have the isoelectric point altered as the metal surface interaction occurs spontaneously. In the case of the perovskite supports, as they contain both acidic and basic sites, the solution was not acidified. After a period of 1 h the solution is

filtered with appropriate washing (~ 800 mL) to wash away excess acid. The resulting catalyst is dried in a fan oven (16 h, 120 °C).

## **2.6. Catalyst testing**

### **2.6.1. Oxidation of glycerol in water – Standard reaction conditions in a glass reactor**

A 50 ml Radley's round bottom flask was charged with an aqueous solution of glycerol at various concentrations (10 ml) with a varying base (sodium hydroxide) ratio (10 ml) with a varying amount of catalyst (s:m 500 – 2000). The reactor base was brought up reaction temperature using a silicone bath feedback loop to control temperature. The round bottom glass was then sealed, pressurised to the required oxygen pressure (0.5 – 5 bar) and purged 3 times prior to use. The oxygen inlet valve was opened to ensure oxygen pressure remains constant throughout the reaction. The reactor was then heated to temperature and stirrer speed set to the desired rpm (400 – 1000 rpm). Reaction duration varied, with periodic samples taken and analysed by high performance liquid chromatography (HPLC). HPLC analysis was fitted with UV and refractive index detectors. Reactants and products were separated using a Metacarb 67 H column. The eluent was an aqueous solution of phosphoric acid (0.01 M) at a flow rate of 0.25 ml min<sup>-1</sup>. Each sample (0.5 ml) was diluted with eluent (4.5 ml) and products were identified by comparison with purchased samples. Quantification was achieved through an external calibration method.

## **2.7. Characterisation**

This section describes the techniques applied for the characterisation of all the supports and catalysts formed. The gases used in the various techniques were purchased from BOC and were of a high-grade purity.

### **2.7.1. Powder X-ray diffraction (XRD)**

X-ray diffraction (XRD) was initially developed between 1914 – 1919 by Debye and Scherrer, and also separately by Hull<sup>1</sup>. XRD is a technique that relies upon measuring the elastic scattering of monochromatic X-ray photons by atoms in a crystalline structure. The X-rays that are not initially scattered continue to the next layer of atoms, where further elastic scattering occurs and so on through the layers of atoms, causing an overall diffraction pattern. If the X-rays diffracted by two different layers of atoms are in phase, constructive interference will occur, satisfying the Bragg relation (Equation 1. and Figure 2.4.), resulting in the formation of a

reflection. If the X-rays are out of phase, then destructive interference occurs, resulting in no peak.

**Equation 1.**

Where  $n$  is the order of reflection (integer),  $\lambda$  is the wavelength,  $d$  is the spacing between atom layers, and  $\theta$  is the angle of incidence of the X-ray. Therefore, the Bragg relationship allows the calculation of the lattice spacing by measuring the angle of the constructive interference for X-rays exiting the crystal. The lattice spacing corresponds to specific compounds where it is possible to identify the compound's purity by their unique diffraction patterns through comparison with a database of well-defined materials. The purity of the product is found through a semi-quantitative method by analysing the diffraction pattern of the known material and that of any residual impurities. Long range order is essential for diffraction to occur, and therefore only occurs in crystalline solids. Incomplete destructive interference of the scattering X-rays result in peak broadening relating directly to the crystallite size of the corresponding reflecting planes. This relationship is defined by the Scherrer equation (Equation 2.)

**Equation 2.**

---

Where  $L$  is the crystallite size in the direction perpendicular to the reflecting plane,  $K$  is a dimensional shape factor taken as 0.9,  $\lambda$  is the X-ray wavelength,  $\beta$  is the line broadening at the full width half maximum and  $\theta$  is the angle between the beam and normal reflecting plane. The minimum measurement for this method is 5 nm as below this the peaks are too broad to be observed.

All XRD analysis was performed on a ( $\theta$ - $\theta$ ) PANalytical X'pert Pro powder diffractometer with a Ni filtered  $\text{CuK}\alpha$  radiation source operating at 40 KeV and 40 mA. All patterns were recorded between  $10 - 80^\circ 2\theta$  in increments of  $0.016^\circ$ . All samples were prepared using a back filled sample holder.

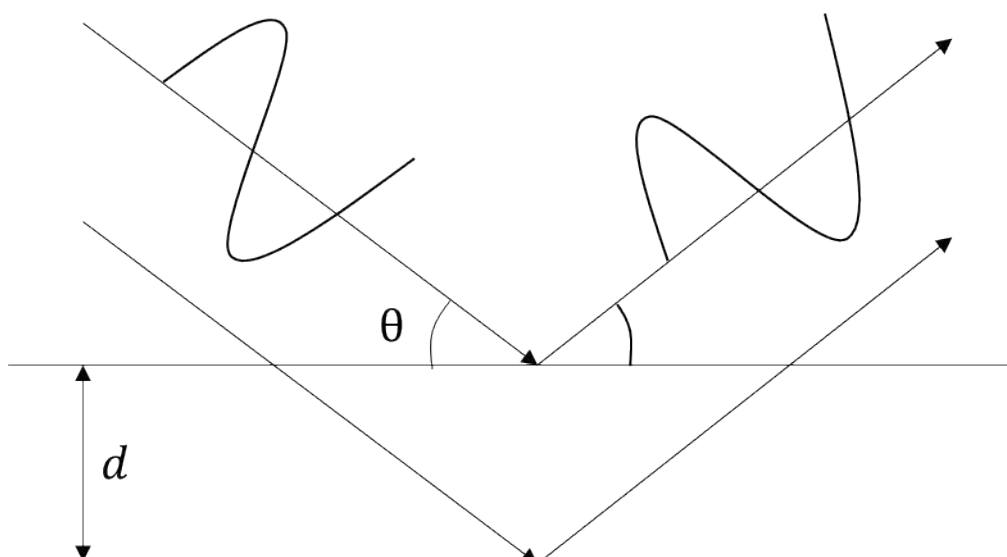


**Figure 2.4.** Graphic representation of the Bragg relationship showing the incident X-ray penetrating the lattice structure of the material and the resulting wave exiting the material.

### 2.7.2. X-ray photoelectron spectroscopy (XPS)

The principle of X-ray photoelectron spectroscopy (XPS) is based upon the photoelectric effect. An atom absorbs a photon of energy ( $h\nu$ ) resulting in the ejection of a core or valence electron, with a specific binding energy ( $E_b$ ) to be ejected at a specific kinetic energy (KE). This relationship is described by the equation 3.

#### **Equation 3.**

When conducting XPS, measuring the kinetic energy gives a fingerprint of the atom corresponding to the specific binding energy associated with each core atomic orbital. The spectra produced by XPS gives information on the electronic state, elemental composition and chemical species that exist on the surface of the sample tested.

All analysis was conducted on a Kratos Axis Ultra DLD spectrometer using a monochromatic AlK $\alpha$  X-ray source (75 W) and analyser pass energy of 40 eV. Samples were run by the XPS manager at the university.

### 2.7.3. Thermogravimetric analysis (TGA)

Thermogravimetric analysis (TGA) is a quantitative characterisation technique that measured the mass loss of a sample as a function of temperature and time. This technique

allows for the use of a variety of atmospheres and generates quantitative data of the sample's composition by correlating specific mass loss with the functional groups associated with decomposition at known temperatures.

All samples were analysed on a Seteram TGA/DTA to acquire the decomposition mass losses of metal acetate/acetylacetonate precursor materials to obtain suitable calcination temperatures in order to form pure phase support materials. Sample masses were approximately 20 mg and used air as the gas flow.

#### **2.7.4. Temperature programmed desorption (TPD)**

Temperature programmed desorption (TPD) is a technique that can be used to define the acidic and basic sites upon the surface of a catalyst. The procedure requires the saturation of a sample (adsorbent) with an adsorbate chemical, followed by gradual heating of the sample to observe the temperature at which desorption of the adsorbent occurs. This allows the strength of the chemisorption to be defined, thus defining the strength of the acid/basic sites.

Acidic sites are investigated with the adsorbent being a basic species, in this case  $\text{NH}_3$ , whereas basic sites are investigated with the adsorbent being an acidic species, in this case  $\text{CO}_2$ . The strength of the acidic/basic sites can be quantified, as the higher the temperature at which the adsorbent is desorbed, the stronger the chemisorption with the peak areas correlating to the quantity of the adsorbate.

Both  $\text{NH}_3$  and  $\text{CO}_2$  TPD were used in this work to analyse catalysts with potentially both acidic and basic sites using a Quantachrome ChemBET Chemisorption analyser with a TCD.

#### **2.7.5. Brunauer Emmett Teller (BET) surface area analysis**

The Brunauer Emmett Teller (BET) technique is applied to measure the specific surface area of a material. The general principle is determined by the physical adsorption of a gas ( $\text{N}_2$ ) as a result of relatively weak van der Waals forces of attraction between the surface of a material and the adsorbate gas. The amount of gas adsorbed on a monomolecular layer of the surface of the material is then calculated which corresponds to the specific surface area.

BET measurements are calculated using a multipoint measurement system and are calculated using the BET adsorption isotherm equation (Equation 3.). By plotting the BET equation in a linear format, the gradient will provide a volume of surface adsorbed gas. This value when taken under consideration along with the surface area of the adsorbate molecule ( $\text{N}_2 \sim 16 \text{ \AA}^2$ ), can be used to determine the surface area of the material.

**Equation 3.**

$$\frac{V_a}{V_m} = \frac{C P}{P_0 - P}$$

Where  $P$  is the specific pressure,  $P_0$  is the saturated pressure of the adsorbate gas,  $V_a$  is the volume of adsorbed gas,  $V_m$  is the volume of gas adsorbed to create a monolayer, and  $C$  is the dimensionless BET constant.

All BET analysis measurements were conducted using a Quadrasorb surface area analyser. A 5 point analysis of each material was performed with  $N_2$  as the adsorbate gas. Samples were degassed at the maximum temperature (250 °C) for 2 hours before analysis. Surface areas calculated are recorded to the nearest  $1 \text{ m}^2\text{g}^{-1}$  due to inherent limitations of the equipment.

**2.7.6. Microwave plasma atomic emission spectroscopy (MP-AES)**

MP-AES is an analytical technique that relies upon the basic principles of atomic emission spectroscopy, shown in figure 2.5. Microwave and magnetically excited nitrogen plasma is heated to approximately 5000 K using a quartz torch. Digested samples are sprayed into the torch causing atomisation, and excitation of the electrons within the sample, leading to a high population of excited states. After the electrons are excited to higher quantised energy levels, they then relax into the lower quantised energy levels releasing photons of a specific energy and wavelength that are characteristic to each element. It is possible, using this apparatus, to analyse individual wavelengths using a monochromator detector and mirror grating, allowing for higher sensitivity for elements with interfering wavelengths.

The higher temperatures used within in the system result in a higher degree of accuracy than lower temperature techniques such as those using flame atomic absorption spectrometers.

All samples were prepared for analysis by adding a known amount of catalyst to a volumetric flask (50 ml) ensuring the sample was fully submerged in freshly prepared *aqua regia* (5 ml). The catalyst was then left for 24 hours to allow full dissolution, followed by dilution with deionised water up to 50 ml. The solutions were filtered using PTFE syringe filters (0.45  $\mu\text{m}$ ). Samples were then analysed using an Agilent MP-AES 4100 series, testing for the metal loading including Au, Pt, and Pd as well as composition of the support material including La, Mn, Co, Fe, Ni and Cr, using multiple wavelength calibrations for each element searched.

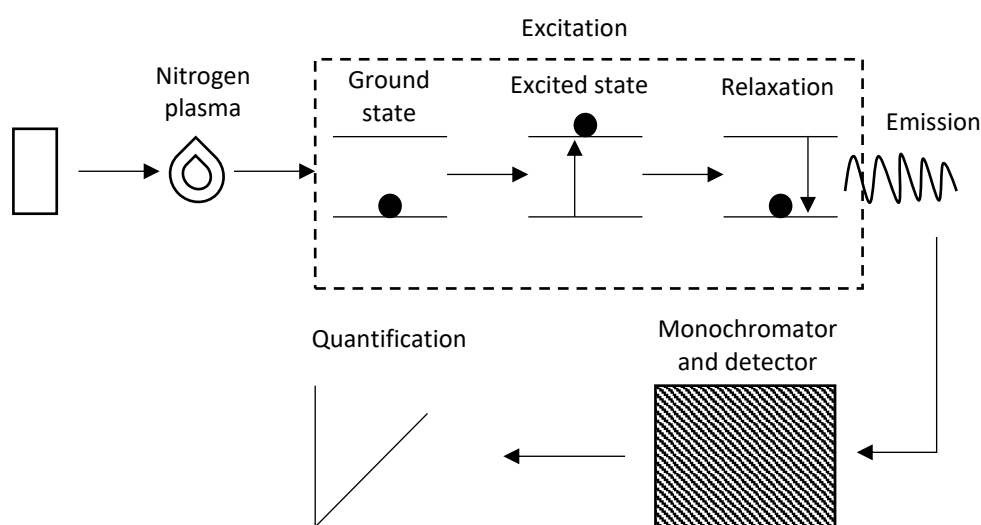


**Figure 2.5 MP-AES Equipment flow schematic**

### 2.7.7. Transition electron microscopy (TEM)

Transition electron microscopy (TEM) is an extremely powerful tool for characterising material morphology. Utilising a high energy electron beam, interactions between electrons and atoms within a material can be observed in order to acquire information about the crystal structure, as well as the resolution being sufficient to view nanoparticles deposited on the surface of a material. TEM works under the same basic principle as a light microscope, utilising an electron beam instead of light (Figure 2.6). This difference is due to the fact that electrons have wavelengths which are orders of magnitude lower than that of light, consequently the resolution of images observed by TEM are orders of magnitude greater than that of light microscopes. It is possible to ascertain the particle size distribution and the morphology of nanoparticles across a catalyst surface, providing information on how a catalyst operates

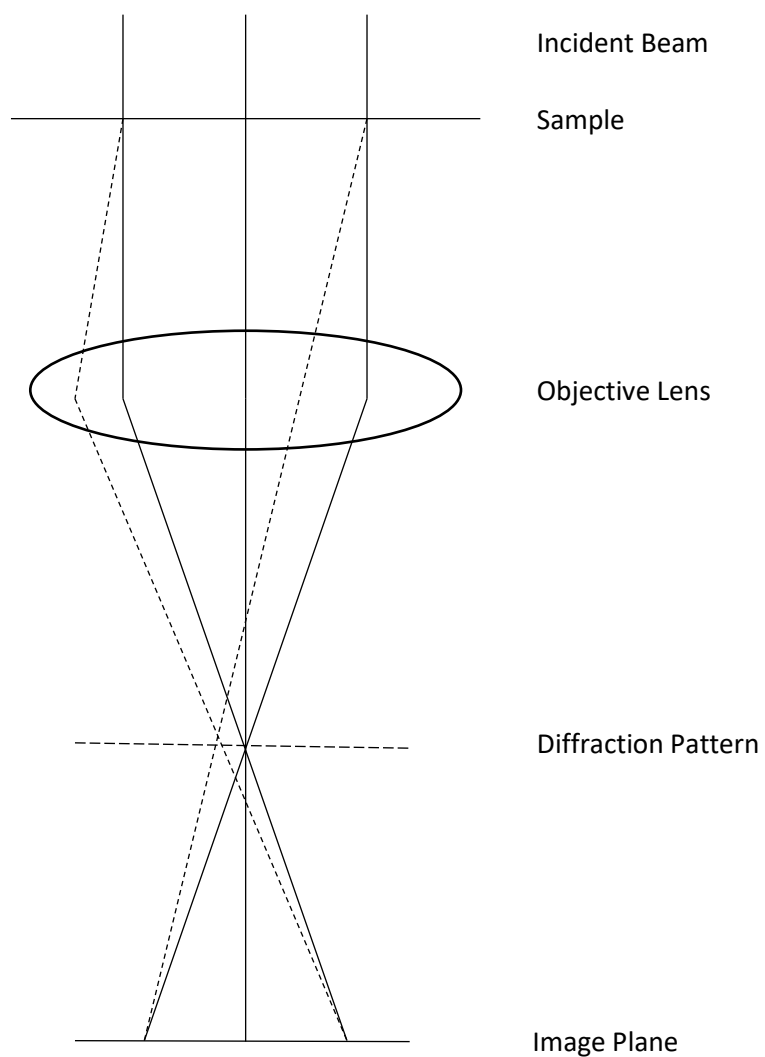


**Figure 2.6. Diagram illustrating the diffraction mechanism of an electron beam**

The TEM was carried out with a Jeol 2100 with a LAB6 filament operating at 200 kV. Each sample was prepared by dispersing the powder catalyst in ethanol and dropping the suspension onto a lacey carbon film over a 300 mesh copper grid. TEM analysis was carried out by an instrument technician.

## 2.7.8. Nuclear magnetic resonance (NMR) spectroscopy

### 2.7.8.1. Nuclear magnetic resonance theory

NMR was originally developed to study the various properties of atomic nuclei, but was also found to be extremely useful at providing an insight into the structure of organic compounds. The theory behind NMR relies on the spin of a nucleus. Just as electrons have  $+\frac{1}{2}$  and  $-\frac{1}{2}$  spin states, particular nuclei can also experience charged spin states that create a magnetic field, known as the magnetic moment. Nuclei that have even numbers of neutrons and protons experience no spin, whereas nuclei with odd numbers of neutrons and protons have integer spins. Nuclei in which the sum of the protons and neutrons equal an odd number (i.e.  $^1\text{H}$  and  $^{13}\text{C}$ ) experience  $\frac{1}{2}$  integer spins. When a magnetic field is applied, illustrated by figure 2.7, the nuclear spins orient themselves either with or against the applied field. The  $\alpha$ -spin state is parallel to the applied force and exhibits a lower energy than the  $\beta$ -spin state that is antiparallel to the applied force. The difference in energy observed between the  $\alpha$ - and  $\beta$ -spin states is dependent on the strength of the applied magnetic field. The energy emitted between these two states produces a measurable NMR signal. The factors governing the alignment of the electron are determined by the value of  $m_s$  and the magnetic field strength,  $B$ , with an associated energy of each orientation described by equation 4 below, where  $g_e$  is the g value of a free electron (2.0023) and  $\gamma$  is the gyromagnetic ration of the electron derived from equation 5.

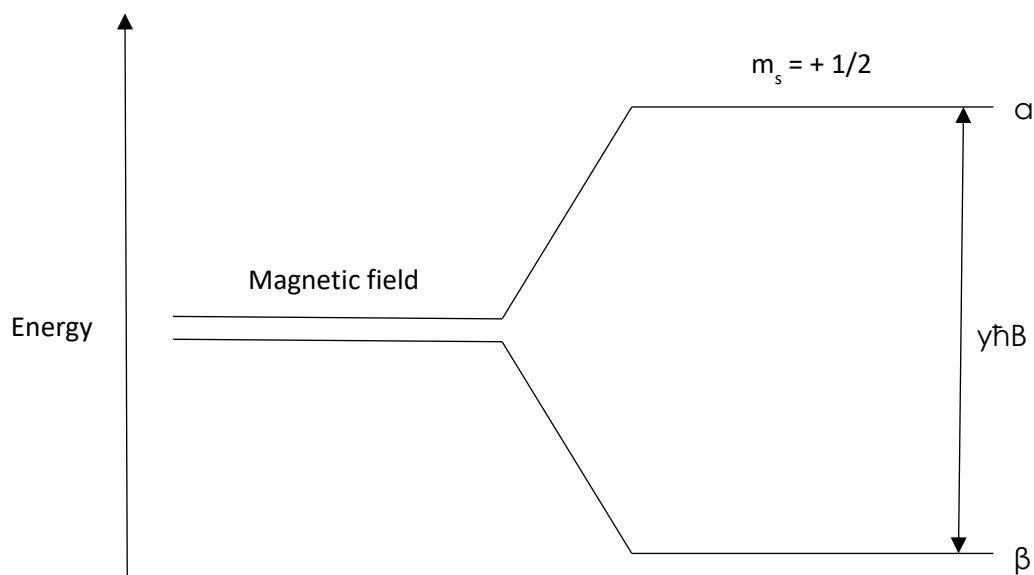


**Figure 2.7.** Energy level diagram representing the spin of a  $\frac{1}{2}$  nucleus in a magnetic field

**Equation 4.**

**Equation 5.**

---

The chemical shift of a nucleus is defined by the difference between its resonant frequency and that of a reference standard. This relationship can be manipulated in a number of ways. There is a proportional relationship between chemical shift and magnetic field strength, thereby increasing the magnetic field strength will increase the chemical shift. There are also shielding effects from the surrounding atoms that alter chemical shift dependent on the nature of the neighbouring groups. The area under each resonance signal is found to be proportional to the number of nuclear occupying the same environment.

An effect known as spin-spin coupling (denoted by the constant  $J$ , Hz) causes splitting of the resonance signals affected by the nuclei within the local field. This constant is independent of magnetic field strength and is specific to each molecule. Splitting is reliant upon the number of neighbouring spin active nuclei, with the general rule,  $N$  equivalent nuclei spin =  $\frac{1}{2}$  split the resonance of a neighbouring atom into  $N+1$  lines, with intensity distributions of Pascals triangle.

#### **2.7.8.2. Nuclear magnetic resonance experimental**

The  $^{13}\text{C}$  and  $^1\text{H}$  NMR spectra were obtained using a Bruker Avance 400 MHz DPX spectrometer, equipped with Silcon Graphics workstation running X win 1.3 with all results recorded in ppm with number of protons, multiplicity and assignment. The chemical shifts for  $^1\text{H}$  NMR were run in deuterated chloroform ( $\text{CDCl}_3$ ) or deuterated dimethylsulfoxide ( $d_6$ -DMSO).

## 3.0 An investigation into glycerol oxidation

### 3.1. Introduction

Glycerol is a C<sub>3</sub> alcohol produced as a significant by-product from the transesterification of triglycerides, the bio-diesel process<sup>1</sup>. As each carbon atom has a functional hydroxyl group, the potential for catalytic production of value added products is possible and highly attractive to companies producing biodiesel<sup>2</sup>; this has led to significant research into heterogeneous catalysts for the production of value added products from glycerol<sup>3-5</sup>. The research conducted has found that several factors attribute to the activity of the catalyst and selectivity profile of the reaction; (i) the choice of support<sup>6</sup>, (ii) the type and size of metal nanoparticles on the surface of the catalyst<sup>7</sup> and (iii) the specific reaction conditions chosen<sup>8</sup>.

The reaction scheme represented in (Scheme 1.6) shows the potential products formed through the catalytic oxidation of glycerol using heterogeneous catalysts<sup>9</sup>. Some of the first Au supported catalysts shown to be active for selectively oxidising glycerol were pioneered by Prati *et al.*<sup>10</sup>. It was found that Au/C could selectively produce glyceric acid through the sequential oxidation of glycerol. Further development of the Au catalysts produced found that the activity of the catalysts could be significantly increased through the addition of Pd<sup>11</sup> or Pt<sup>12</sup>. The most desirable products that can be produced from glycerol oxidation are the either the C<sub>3</sub> oxidation products, glyceric acid (GA) and the sequential oxidation of this product, tartronic acid (TA), or, lactic acid (LA) produced through the opposing dehydration pathway. To achieve the selective production of these products, C-C scission must be limited as much as possible.

Reaction conditions for the oxidation of glycerol have a significant impact upon the selectivity profile for the reaction. C<sub>3</sub> selectivity has been found to increase as temperature increases, where at 60 °C the selectivity towards the oxidation C<sub>3</sub> products<sup>12</sup> increases, whereas an increased reaction temperature of 90 °C enhances the dehydration pathway to lactic acid<sup>13</sup>. It has been suggested that the increased selectivity to C<sub>3</sub> products at higher temperatures is due to the decreased stability of the in-situ produced H<sub>2</sub>O<sub>2</sub>, which can increase C-C scission. The pH of the solution has also been shown to have a significant effect on selectivity, with an increase in pH leading to higher selectivities of C<sub>3</sub> products<sup>14</sup>, due to the base acting as a sacrificial agent, increasing the rate at which the initial deprotonation of the glycerol occurs<sup>15</sup>. Although some promising work has been conducted into the base free oxidation of glycerol<sup>16</sup> and many industrial oxidation processes attempt to eliminate the use of a base within the reaction due to the cost of purification of the products, one of the principal means of transesterification of oils uses a significant amount of KOH<sup>17</sup>, therefore any crude glycerol produced would contain a

significant proportion of base. The O<sub>2</sub> content within the reaction is an important factor to consider, and has been shown to aid in the activation of the catalyst, although there may be a trade-off between the activity and the amount of C-C scission, therefore by altering the oxygen concentration it is possible to find a balance between higher activity and obtaining the highest possible C3 selectivity.

Although a significant amount of research has been conducted upon glycerol oxidation, there are few studies that look in depth at the effect the reaction parameter conditions have on the reaction. This study will attempt to optimise the conditions of the reaction to probe how the highest possible yield to lactic acid can be obtained. AuPt/TiO<sub>2</sub> has been shown to actively promote the formation of lactic acid<sup>13, 19</sup>, with relatively high yields of lactic acid being produced which make AuPt/TiO<sub>2</sub> catalysts ideal for a model study. By modelling a study upon the reaction using a standard catalyst, all other data presented in this thesis will have a basis of comparison on the same reactor setup.

## **3.2. Aims and objectives**

### **3.2.1. Objective**

An investigation in to how the condition parameters affect the selective oxidation of glycerol using a standardised AuPt/TiO<sub>2</sub> catalyst with the goal of selectively producing lactic acid.

### **3.2.2. Aims**

- Provide an insight into how the various reaction parameters effect the selectivity profile of the reaction.
- Investigate a sequential elimination of reaction parameters to produce a map leading to an ideal set of conditions for producing lactic acid from glycerol.
- Use the results produced as a bench mark for further work with novel supports.

## **3.3. Catalyst preparation**

The catalyst chosen to provide a bench mark for the parameter mapping study was the AuPt/TiO<sub>2</sub> as described in the introduction above. The catalyst was prepared by sol-immobilisation due to the small, well dispersed nanoparticles that the method produces to create a model system. An aqueous solution of HAuCl<sub>4</sub> and H<sub>2</sub>PtCl<sub>6</sub> were prepared at specific concentrations (10 mg ml<sup>-1</sup>). Polyvinyl alcohol (PVA, 1 wt% aqueous solution, MW = 10 kDa) was freshly prepared and used as the stabilising agent. NaBH<sub>4</sub> (0.1 M aqueous solution) was also freshly prepared and used as the reducing agent. To an aqueous mixture of the HAuCl<sub>4</sub> and

H<sub>2</sub>PtCl<sub>6</sub> of a concentration to produce 1:1 metal weight ratio, to a total of 1 wt % of total metal in the prepared catalyst, the PVA solution was added (PVA/(Au + Pt) (wt/wt) = 0.65) with vigorous stirring for 2 min. NaBH<sub>4</sub> was subsequently added such that the NaBH<sub>4</sub>:total metal ratio (mol/mol) was 7.5. The resulting solution was stirred for 30 min to allow the stabilisation of the reducing colloidal particles, followed by the addition of the TiO<sub>2</sub> support. The resulting solution was acidified to pH 1 with conc. H<sub>2</sub>SO<sub>4</sub> to increase the surface-metal interaction. The solution was left stirring for a further 1 h, followed by washing with distilled water and drying at 110 °C for 16 h.

### **3.4. Catalyst Characterisation**

#### **3.4.1. Transmission electron microscopy**

A sample of a freshly produced catalyst was analysed by TEM, with the images shown below in (Figure 3.1 (a-c)) with a particle size distribution histogram (Figure 3.1 (d)) showing the average particle size of the nanoparticles on the surface of the catalyst. It was found from the imaging that the majority of the nanoparticles on the surface of the AuPt/TiO<sub>2</sub> were between 0.5 – 2.5 nm, which are particle sizes typical of the sol immobilisation procedure<sup>20</sup>. The particle sizes observed are within the limits defined for active nanoparticles for alcohol oxidation.

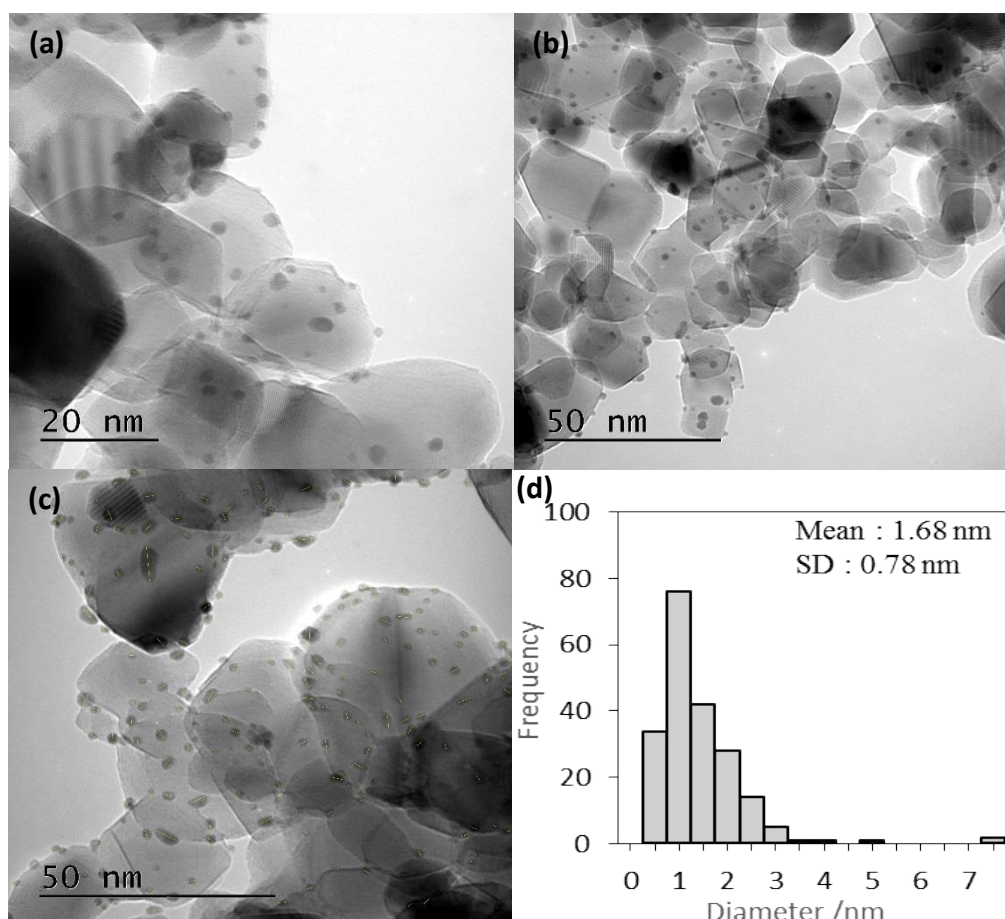


**Figure 3.1** Representative transmission electron micrographs of a sol immobilised 1 wt % AuPt/TiO<sub>2</sub> where (a) and (b) the images at 20 nm and 50 nm respectively, (c) Shows the count for determining the average particle size distribution and (d) shows a histogram to represent the particle size distribution.

### 3.4.2. Phases, loading and surface area of the support

X-ray diffraction (XRD) of the catalyst does not show peaks for the AuPt nanoparticles as there is only a 1 wt % loading, below the detection limit of the equipment used. There are two phases present in the diffraction pattern of the catalyst, one for the anatase phase of TiO<sub>2</sub> and one for the rutile phase of TiO<sub>2</sub>, which is the design of the commercial P25 TiO<sub>2</sub> used as the support for this catalyst.

The loading of precious metals on the surface was conducted by microwave plasma atomic emission spectroscopy, shown in Table 3.1. The microwave plasma atomic emission spectroscopy (MP-AES) results shows that the catalyst contains a total metal loading close to the 1 wt % aimed for, with the ratio of Au:Pt close to the stoichiometry expected, showing the immobilisation of the metal nanoparticles was successful during the catalyst preparation. The

surface area was determined through BET analysis showing a surface area typical of  $\text{TiO}_2$ , allowing its use as a support with a sufficient surface area to disperse the AuPt nanoparticles effectively.

**Table 3.1 The total metal loading and surface area of 1 wt% AuPt/ $\text{TiO}_2$  determined through MP-AES and BET.**

Sample	Total metal loading	Au (molar %)	Pt (molar %)	Surface area / $\text{m}^2\text{g}^{-1}$
AuPt/ $\text{TiO}_2$	0.98	52.75	48.15	61

XPS was also conducted upon the catalyst to view the surface species of the Au and Pt nanoparticles (Figure 3.2). The spectra produced shows that the Au and Pt have formed in their metallic state, which is expected with the sol-immobilisation process. The typical binding energy for Au/ $4f_{7/2}$  is found to be 84.0 eV, however the peaks are observed at 83.2 and 87.1 eV are that of the Au/ $4f_{7/2}$  and Au/ $4f_{5/2}$  species. This slight shifting in the binding energies related to  $\text{Au}^0$  have been previously observed, and have been suggested to be due to either an interaction with the  $\text{Ti}^{3+}$  surface centres in  $\text{TiO}_2$  or potential alloying of Au and Pt nanoparticles on the surface of the catalyst. Although the Ti3s orbital energy overlaps with the Pt4f orbital energies, the Pt/ $4f_{7/2}$  and Pt/ $4f_{5/2}$  were resolved and found to be at 71.0 and 74.4 eV which are indicative of the  $\text{Pt}^0$  species.

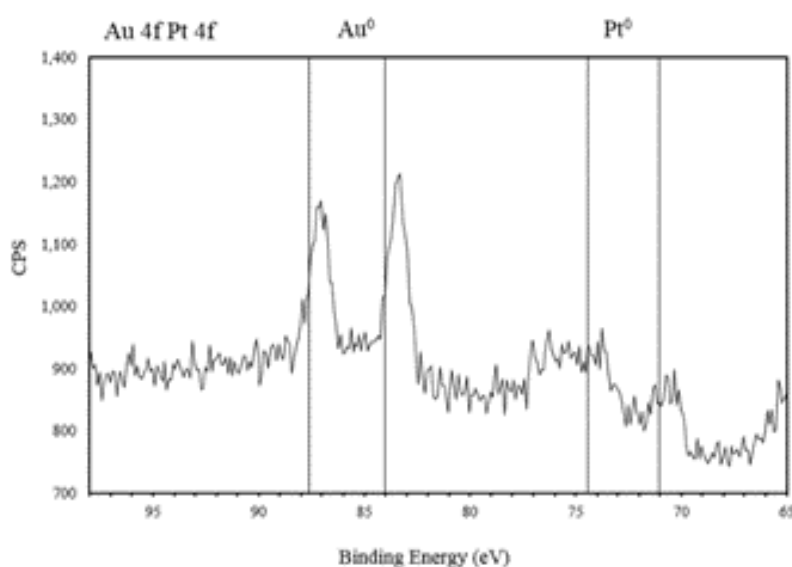


**Figure 3.2 XPS spectra of the Au and Pt 4f regions for a 1wt% AuPt/ $\text{TiO}_2$  catalyst**

### 3.4.3. Isoelectric point of P25 TiO<sub>2</sub>

The isoelectric point is an important factor to consider for acidic supports in sol immobilisation, as the pH of the solution is manipulated to encourage a higher metal-support interaction. Anatase and rutile phases of TiO<sub>2</sub> have been well characterised in literature with the isoelectric point being pH 5.8<sup>21</sup> and 5.2<sup>22</sup> respectively. The zeta potential of P25 was measured at varying pH values shown in Figure 3.3, with the isoelectric point being pH 6.5. The commercial P25 was confirmed to contain 80:20 anatase:rutile phases of TiO<sub>2</sub> by semi quantitative XRD, therefore the isoelectric point is higher than expected, but is still slightly acidic. The acidification of the solution is therefore a viable method to increase the metal support interaction creating a catalyst with higher stability.

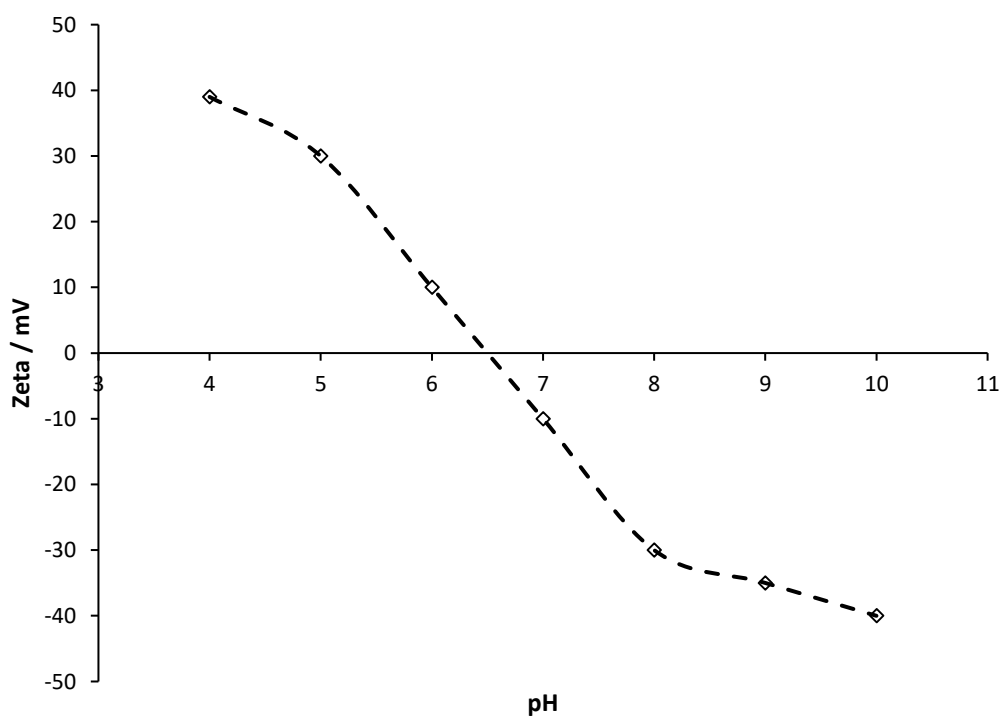


*Figure 3.3 Zeta potential measurements of P25 TiO<sub>2</sub> at varying pH*

### 3.5. Conditional parameter mapping of glycerol oxidation

To gain an effective understanding of the reaction, a systematic approach will be undertaken to the altering the various conditions mentioned above and monitoring the effect the conditions have on the reaction. This approach takes a series of conditions known for

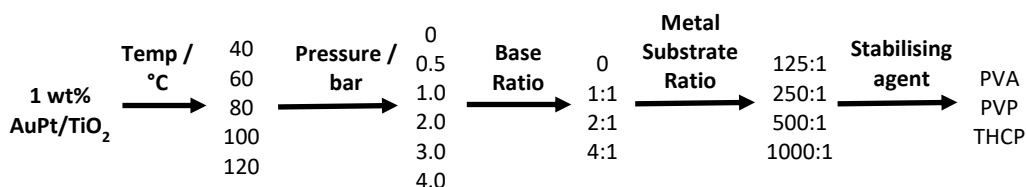


**Figure 3.4** Parameter mapping plan for obtaining an ideal set of conditions for producing higher yields of lactic acid

producing successful yields of 54 % lactic acid at 80 °C, 2:1 base:substrate ratio, 1 bar O<sub>2</sub> pressure, 1000:1 metal:substrate ratio as a starting point, with an attempt to tune the conditions of the reaction by altering the varying parameters; temperature, pressure, base ratio, metal:substrate ratio, and stabilising agent of the catalyst to produce the highest possible yield/selectivity to lactic acid (Figure 3.4) to provide a basis to proceed with novel supports.

A test reaction was conducted under the stated conditions so as to produce a standard set of results for later comparison (Figure 3.5). The catalyst can be seen to be active, with full conversion of glycerol over a 6 h period. The selectivity profile remains fairly constant

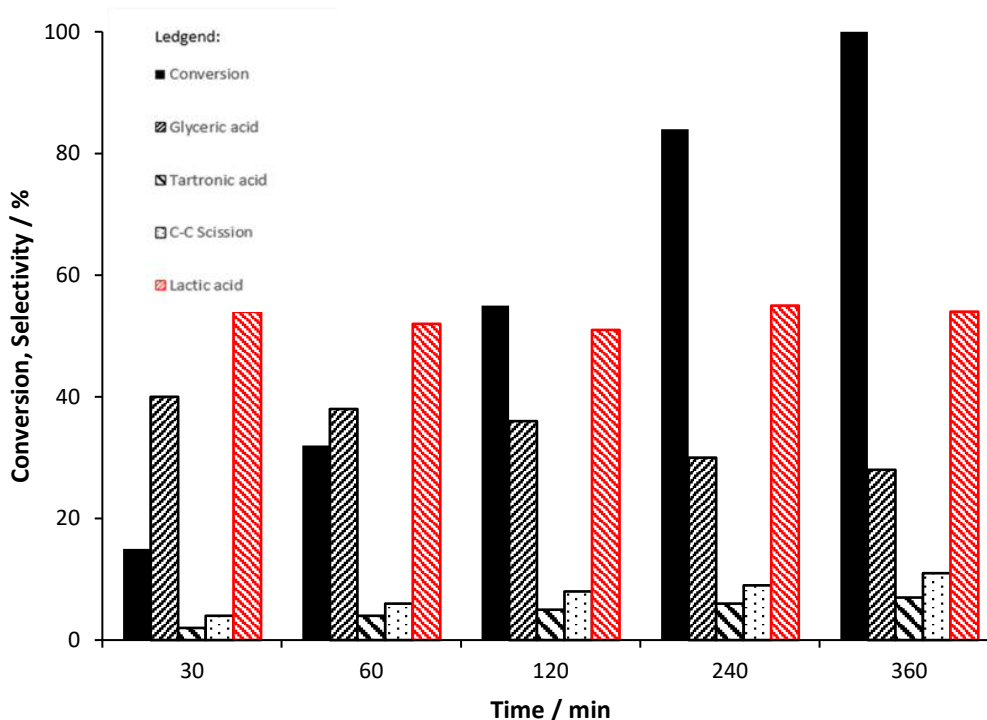


**Figure 3.5** Conversion and selectivity profile of 1 wt % AuPt/TiO<sub>2</sub> sol immobilised catalyst.

throughout, with an almost even distribution of the oxidation and dehydration pathway products at lower conversions, and slightly favouring the dehydration pathway towards the end of the reaction. The glyceric acid can be seen to be further oxidised to tartronic acid, with some C-C scission from the intermediate species, pyruvaldehyde, forming glycolic and formic acid. As the lactic acid remains at a consistent yield of up to 54 % throughout the reaction, it is suggested that the lactic acid is stable under the reaction conditions. These conditions provide a suitable bench mark to work upon allowing a viewpoint on how the distribution of products are affected as the reaction parameters are manipulated.

### 3.5.1. The effect of temperature

The temperatures that glycerol oxidation has been conducted under show a noticeable change in selectivity breakdown of products, with temperatures of 40 - 60 °C favouring the oxidation route to glyceric acid<sup>23</sup> and C-C scission product, and higher temperatures of 90 °C favouring the dehydration route to lactic acid<sup>24</sup>. Not only does the increase in reaction temperature allow for more selective control of product selectivity, but also promotes the catalytic activity. As the temperature has such a profound effect upon the reaction, it was reasoned that it should be the first parameter to be explored, with the results shown in Table 3.2 below.

**Table 3.2** *The effect of temperature upon the conversion and selectivity profile of the products using the sol immobilised 1 wt% AuPt/TiO<sub>2</sub>.*

Temperature / °C	Time / min	Conversion / %	Carbon balance / %	Selectivity / %			
				GA	TA	C-C Scission	LA
40	30	24	100	65	3	21	11
	60	48	99	66	3	19	12
	120	89	100	64	5	21	10
	240	100	100	63	5	21	11
60	30	30	101	62	3	12	23
	60	59	99	61	5	13	21
	120	92	98	61	6	14	19
	240	100	100	59	7	16	18
80	30	28	100	38	6	11	45
	60	64	99	36	8	11	45

	120	97	99	35	11	8	46
	240	100	100	31	15	6	48
<b>100</b>	30	32	99	20	8	4	68
	60	68	101	16	10	5	69
	120	100	98	12	15	5	68
	240	100	100	10	16	6	68
	30	45	95	16	9	4	71
<b>120</b>	60	88	87	14	8	6	72
	120	100	80	12	10	6	72
	240	100	76	11	11	8	70

**Reaction conditions; 10 ml Glycerol (0.3 M), NaOH:substrate (2:1), O<sub>2</sub> pressure (1 bar), metal:substrate ratio 1000:1, 4 h reaction time and varied temperature.**

It was found that there was a proportional relationship between reaction temperature and the rate at which glycerol was converted (Figure 3.5), which is not unexpected and can be explained through conventional collision theory. What is interesting, however, is that a trend develops as the temperature increases, with regard to the product distribution. It was found that as the temperature increased that the amount of C-C scission occurring dropped substantially. As postulated in the introduction section, part of the C-C scission can occur

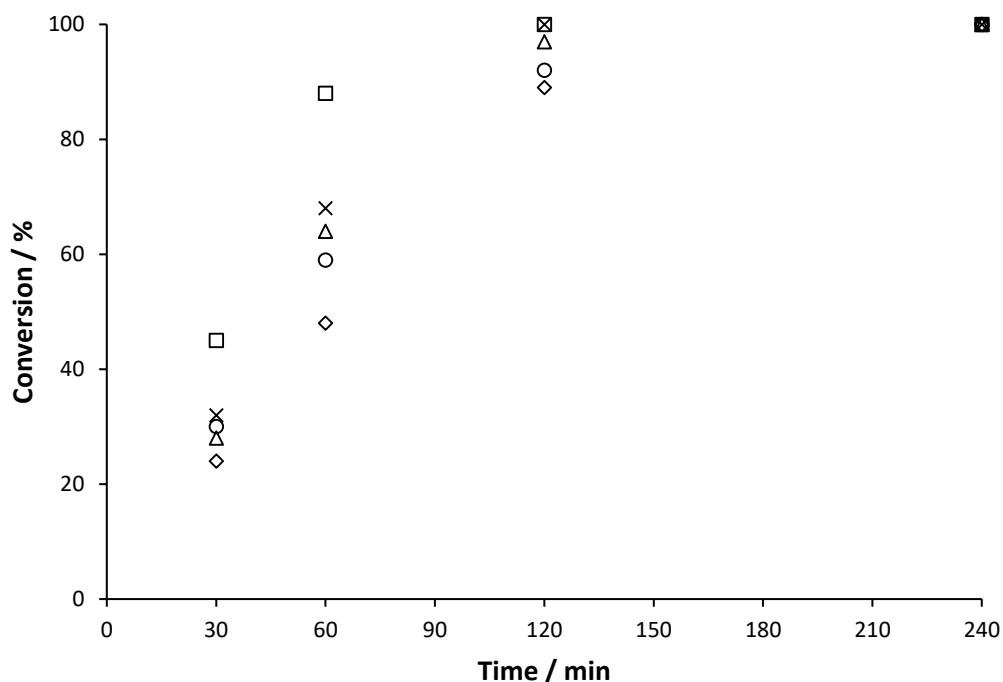


**Figure 3.6 Conversion time on line for varying temperature where; □ is 120 °C, x is 100 °C, ○ is 80 °C, Δ is 60 °C and ◇ is 40 °C.**

through two main routes (i) the over oxidation of glyceric acid, (ii) the formation of  $\text{H}_2\text{O}_2$ . The over oxidation to C1 and C2 products occurs at higher temperatures, however as less of the glyceric acid is formed, it is less obvious, than at lower temperatures. It is unlikely that  $\text{H}_2\text{O}_2$  is the cause of C-C scission at higher temperatures due to the inherent instability exhibited at temperatures above 80 °C, the same point at which the C-C scission is lowered during the experiment (Figure 3.6). It is also apparent that at higher temperatures there is an increase in the selective formation of lactic acid *via* the dehydration pathway of glycerol, where the rate at which the terminal alcohol group is dehydrated increases, and this is believed to be the crucial step in lactic acid formation. There is a clear switch in selectivity as the temperature approaches 100 °C. Above 100 °C the carbon balance is more difficult to maintain in the glass reactor system due to the volatility of water above its boiling point, resulting in a potentially lower yield in lactic acid, despite the increase in selectivity. From these sets of results at these conditions it can be concluded that a higher temperature clearly favours lactic acid production and lowers C-C scission which are two of the most important factors when attempting to selectively produce lactic acid, therefore the temperature carried forward for further reactions will be set at 100 °C.

### 3.5.2. The effect of pressure

The role of oxygen in an oxidation reaction is a variable parameter that can have a significant impact on the selectivity of the products. The oxygen pressure effect on the system involves several key mechanisms and which are complicated further by mass transfer limitations. These can limit the movement of oxygen from the gas phase to the catalyst interface, meaning there are limitations to the oxygen pressure that can be used beyond the simple boundaries of reactor parameters, as going beyond the mass transfer limitations would change the reactions rate limiting step from chemical interactions to oxygen transfer. The role of oxygen pressure in glycerol oxidation has been mentioned in detail in the introduction, and as a key parameter, an investigation into how altering the oxidation pressure affects the production of lactic acid has been conducted.

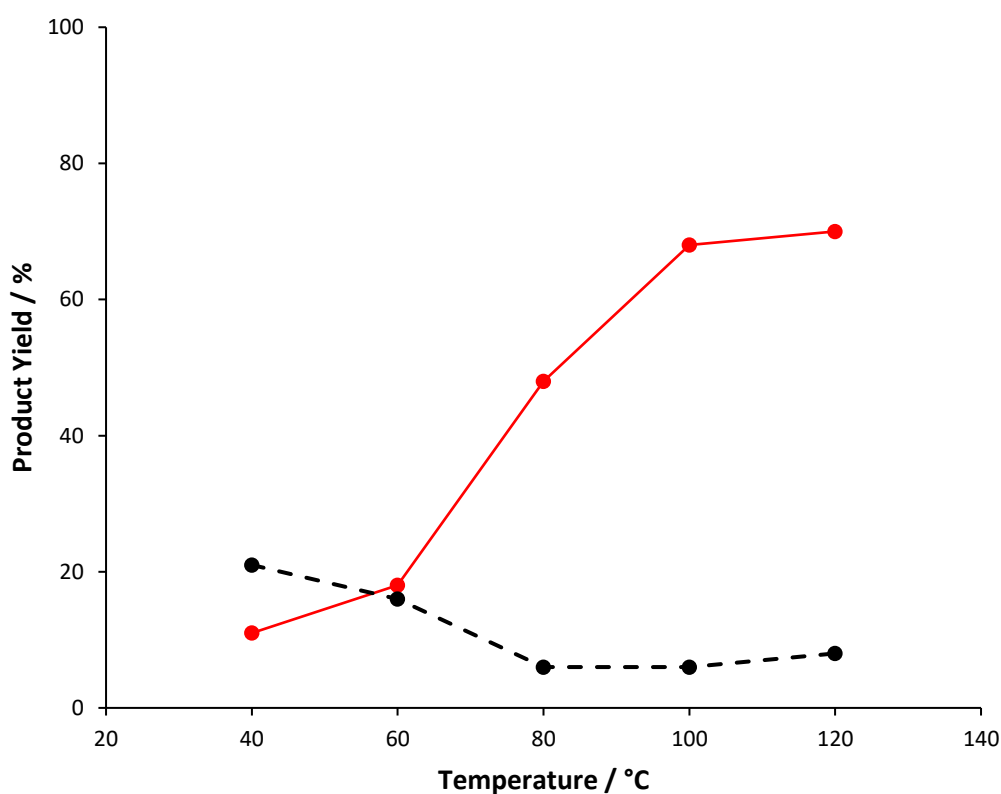


**Figure 3.7** The selectivity towards lactic acid (*red*) and C-C scission (*black*) products as temperature increases.

**Table 3.3** The effect of oxygen pressure upon the conversion and selectivity profile of the products using the sol immobilised 1 wt% AuPt/TiO<sub>2</sub>.

Oxygen		Selectivity / %					
Pressure / bar	Time / min	Conversion / %	Carbon balance / %	GA	TA	C-C Scission	LA
He*	30	1	100	40	0	0	60
	60	1	100	34	0	7	59
	120	2	100	18	0	23	59
	240	3	100	10	1	30	59
0.5	30	14	100	26	0	1	73
	60	28	100	25	0	4	71
	120	67	101	24	1	5	70
	240	78	100	22	1	7	70
1.0	30	16	101	25	0	3	72
	60	36	99	24	1	5	70
	120	72	100	22	1	8	69
	240	88	101	21	2	9	68
2.0	30	18	100	24	0	6	70
	60	44	101	23	1	8	68
	120	84	99	20	2	9	69
	240	94	100	17	3	11	69
3.0	30	33	100	20	1	5	74
	60	73	100	19	1	7	73
	120	96	99	15	2	11	72
	240	100	101	12	4	13	71
4.0	30	42	100	16	1	11	72
	60	79	99	15	2	14	69
	120	100	97	14	3	18	65
	240	100	95	5	12	18	65

**Reaction conditions; 10 ml Glycerol (0.3 M), temperature (100 °C) NaOH:substrate (2:1), metal:substrate ratio 1000:1, 4 h reaction time and varied O<sub>2</sub> pressure. (\* residual oxygen present)**

The data in Table 3.3 shows that the oxygen pressure within the reaction system has a clear effect upon the effective activity of the catalyst. The rate of conversion of glycerol significantly increases as the oxygen pressure increases, an effect that has been observed in many previous oxidation catalysis studies and illustrated more clearly in figure 3.8. It should be noted that this is not a linear trend, and by increasing the pressure further, does not increase the conversion of glycerol by a substantial amount beyond 3 bar.

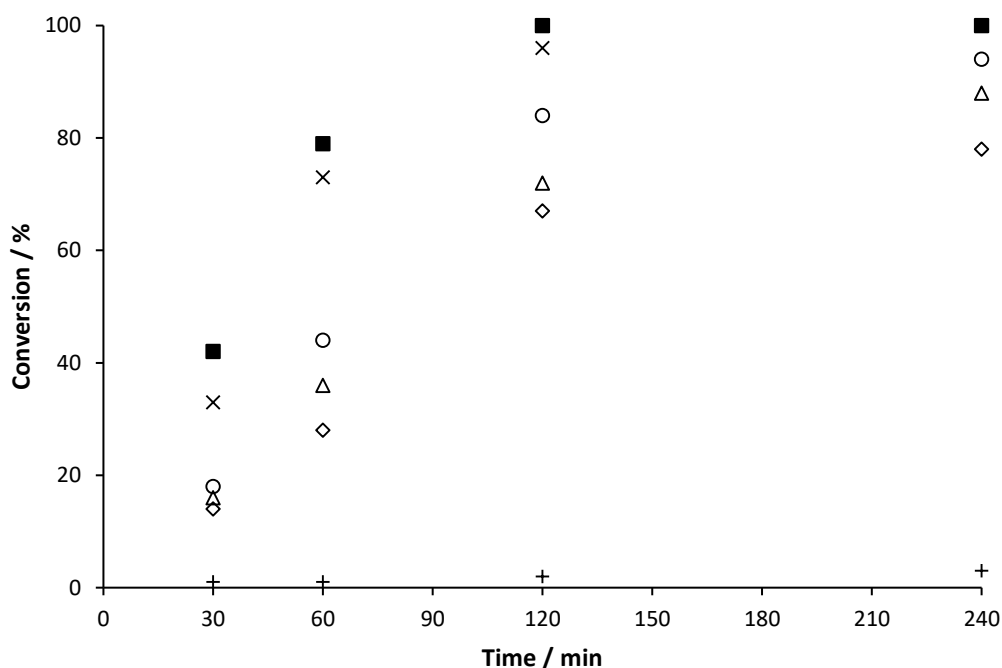


**Figure 3.8 Conversion time on line for varying pressure where; ■ is 4 bar, x is 3 bar, ○ is 2 bar, △ is 1 bar and ◇ is 0.5 bar. The reaction conducted in an inert atmosphere (He) is represented by +.**

The  $O_2$  pressure also shows an increased potential to aid C-C scission, with C1 and C2 products increasing in selectivity as the pressure increases, with this effect becoming more pronounced when conversion of glycerol is complete. It has previously been suggested that  $H_2O_2$  can aid the C-C scission process, and by increasing the pressure, the amount of  $H_2O_2$  would increase as more  $O_2$  would be available which can be reduced by  $H_2O$  forming  $H_2O_2$ , and thus increasing the amount of scission conducted. Whilst this has been observed in studies at lower temperatures (60 – 80 °C)<sup>25</sup>, it is also known that the stability of  $H_2O_2$  at elevated temperatures decreases beyond 80 °C, meaning it is unlikely the cause of the increased scission in these cases. What is more likely is that the glyceric acid produced is being converted in C1 and C2 products as the oxygen pressure increases, which can be observed as the selectivity to glyceric acid decreases as the pressure increases, shown in Figure 3.9. When comparing the glyceric acid and

lactic acid selectivity, it can be seen that whilst the selectivity to glyceric acid decreases significantly at higher conversion, the lactic acid selectivity remains relatively stable. This observation can be explained by the potential stability of the compounds at elevated temperatures, where the glyceric acid is converted through a further oxidation, the lactic acid appears to remain stable under these conditions, despite the increased pressure, shown in Figure 3.9. This trend could partially explain why the selectivity to lactic acid remains remarkably similar throughout the reaction, as the energy required to conduct the C-C scission is likely lower than that of the production of lactic acid, as the C-C scission occurs at an accelerated rate after the glycerol is fully consumed.

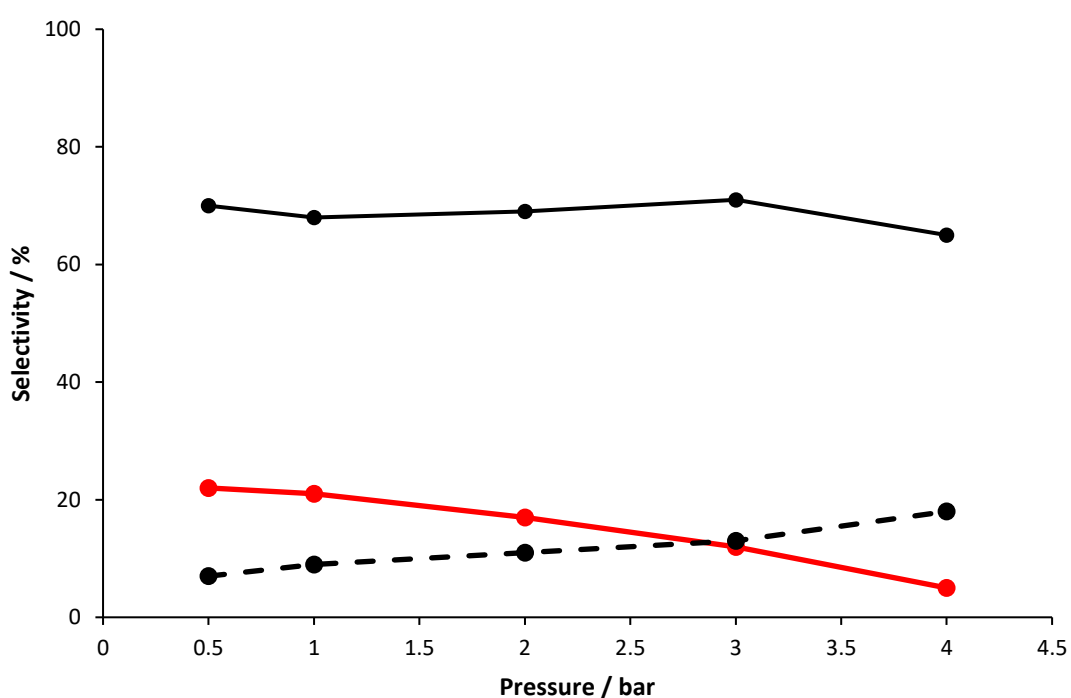


**Figure 3.9** The selectivity towards lactic acid (solid black), glyceric acid (red line) and C-C scission (dashed black) products at  $t = 240$  mins as pressure increases.

By plotting the yield of lactic acid formed at  $t = 240$  mins, shown in Figure 3.10, an interesting observation can be made. Initially the yield of lactic acid produced increases with pressure, however, after 3 bar, it can be seen the selectivity begins to decrease again. If the selectivity to tartronic acid, the sequential oxidation product from glyceric acid, is reviewed it can be seen that the amount of tartronic acid produced is only significant at the higher pressure of 4 bar. Tartronic acid is a product that is rarely seen at lower temperatures due to the increased energy required to further oxidise glyceric acid, which is directly competing with the C-C scission, and therefore often only small quantities of tartronic acid are observed. With a higher oxygen content, the yield of tartronic acid production increases, therefore taking resources from the

competing production of lactic acid, and thus, lowering the yield of lactic acid produced. This means that whilst the conversion of glycerol increases with pressure, the yield of lactic acid decreases above a critical pressure, which in this case is 3 bar. For the areas for further study within the parameter mapping study, 3 bar appears to be the ideal pressure to work at to increase lactic acid production whilst maintaining an appreciable conversion of glycerol.

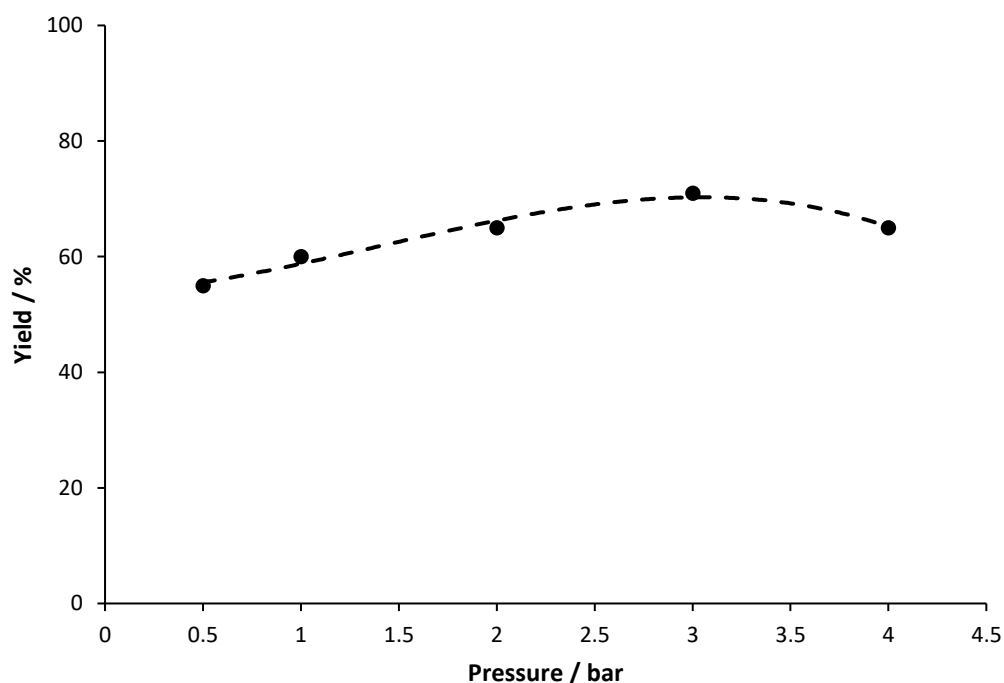


**Figure 3.10** Showing the yield of lactic acid produced at  $t = 240$  mins as the pressure of the reaction is increased

### 3.5.3. The effect of base ratio

As described in the introduction, the base equivalents used with glycerol oxidation have been shown to produce significant changes to the selectivity breakdown. This is due to the fact that the hydroxide anion acts as a promoter within the reaction system as discussed in the introduction. A variety of base ratio tests were conducted using the previously established temperature and pressures.

**Table 3.4** The effect of base ratio upon the conversion and selectivity profile of the products using the sol immobilised 1 wt% AuPt/TiO<sub>2</sub>.

NaOH equivalents	Time / min	Conversion / %	Carbon balance / %	Selectivity / %				
				GA	TA	DHA	LA	C-C Scission
<b>0</b>	30	1	99	10	1	79	0	10
	60	5	100	8	1	67	0	24
	120	8	100	7	2	61	0	30
	240	11	100	5	3	58	0	34
<b>0.5</b>	30	30	100	42	4	0	35	19
	60	64	100	41	5	0	36	18
	120	97	99	35	7	0	37	21
	240	100	100	28	8	0	38	26
<b>1</b>	30	29	99	28	4	0	55	13
	60	59	100	25	7	0	54	14
	120	92	100	18	9	0	55	18
	240	100	100	8	14	0	56	22
<b>2</b>	30	27	99	29	2	0	68	9
	60	55	100	27	7	0	65	10
	120	88	100	29	12	0	58	14
	240	100	100	16	18	0	58	13
<b>4</b>	30	26	100	16	2	0	78	4
	60	52	99	11	6	0	78	5
	120	78	100	5	8	0	79	8
	240	100	100	0	10	0	80	10

**Reaction conditions; 10 ml Glycerol (0.3 M), temperature (100 °C), O<sub>2</sub> pressure (3 bar), substrate:metal ratio 1000:1, 4 h reaction time and varied base ratio.**

It is immediately apparent that base concentration does not have a linear relationship with conversion. The conversion of glycerol remains relatively constant at base equivalents above 0, as can be seen in Figure 3.11. As described in the introduction, base free reactions are much more energy intensive processes, showing that the hydroxide anion almost certainly acts as a necessary promoter for the reaction. Although the activity is relatively close, as the base

equivalents increase, the activity does appear to drop slightly, which can be explained by looking more closely at the selectivity breakdown of the reaction.

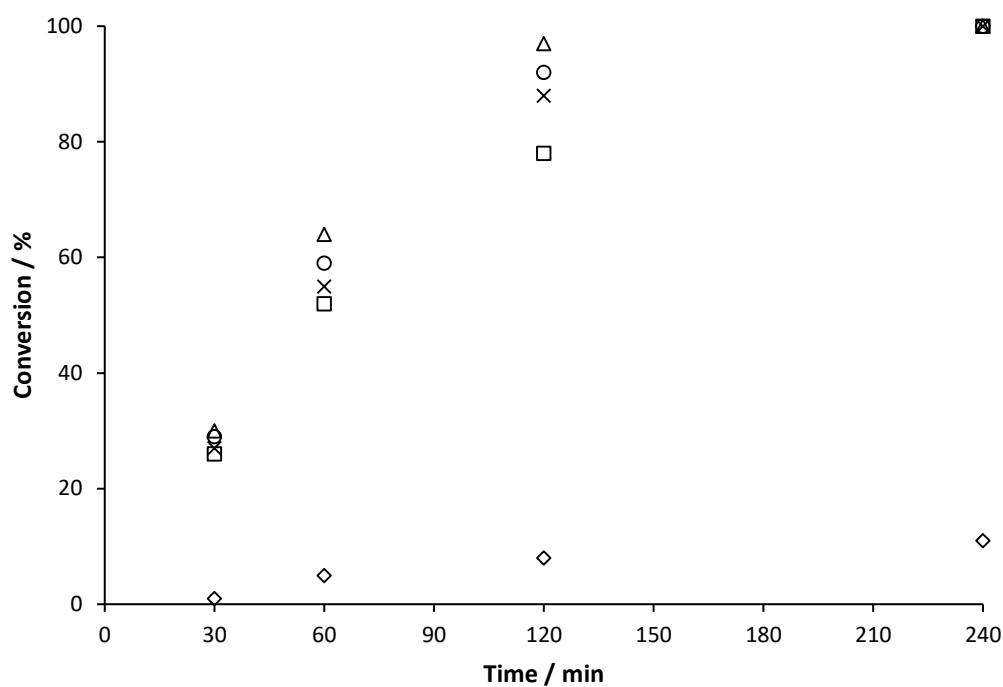


**Figure 3.11 Conversion time on line for varying pressure where; □ is 4 equivalents, X is 2 equivalents, ○ is 1 equivalent, Δ is 0.5 equivalents and ◇ is base free.**

The selectivity breakdown displays a few notable trends as the base concentration is increased, shown in Figure 3.12. Firstly, the selectivity towards lactic acid increases dramatically, which illustrates how significant the role the hydroxide anion interaction is for the formation of lactic acid. Secondly, there is a decrease in C-C scission, and whilst the selectivity to lactic acid remains relatively constant, the selectivity towards glyceric acid decreases. This suggests that the C-C scission is occurring only from the oxidation pathway, where the glyceric acid is either sequentially oxidised to tartronic acid or split into C1 and C2 products.

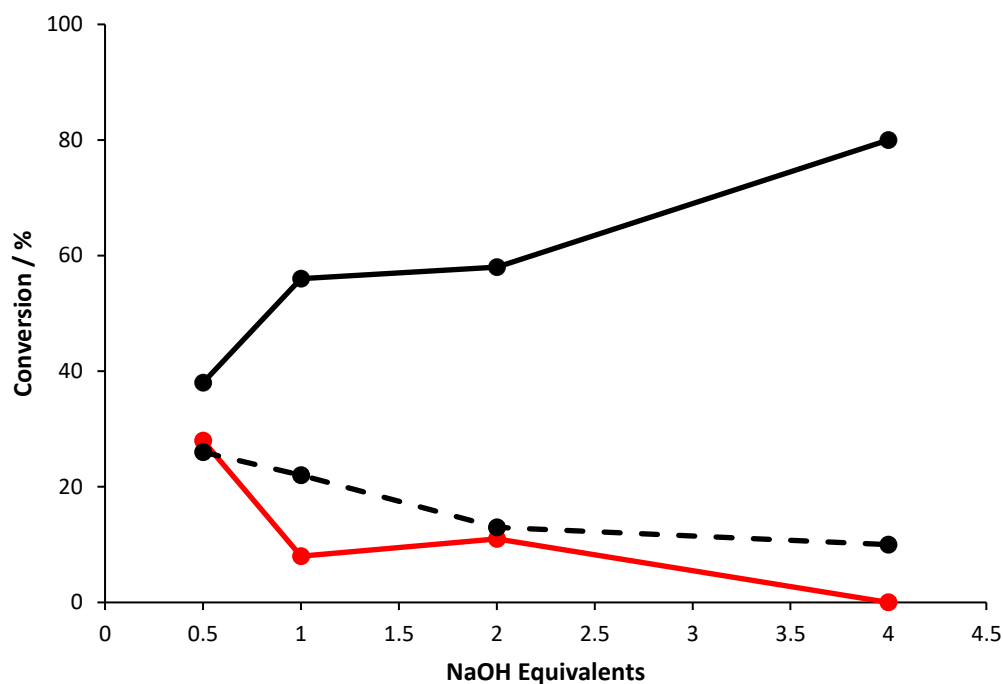


**Figure 3.12** The selectivity towards lactic acid (solid black), glyceric acid (red line) and C-C scission (dashed black) products at  $t$  240 mins as NaOH concentration increases.

The mechanism of formation of lactic acid is a long-contested subject, and therefore the role of base in the formation of lactic acid is unclear and will be addressed along with the mechanism later in this chapter. A factor that has been established, however, is that base has been shown to promote the dehydration pathway of several polyol reactions. One running theory is that base promotes an initial dehydration of the terminal alcohol group on glyceraldehyde (GLD), followed by a dehydration reaction. For the formation of lactic acid this would then require a rearrangement reaction to occur with the intermediate species. It can be seen from the base free reaction that, although the conversion is low, the selectivity to dihydroxyacetone (DHA) is high. This suggests that at higher temperatures, the equilibrium that exists between GLD and DHA shifts in favour of DHA, which implies that the formation of lactic acid actually occurs *via* DHA rather than GLD. If this were the case, a dehydration on the terminal alcohol group would require a base promoted intra/intermolecular Cannizzaro reaction to produce lactic acid.

As it is clear that a higher base concentration is required to optimise the production of lactic acid, the base to substrate ratio selected to continue the parameter mapping will be set at 4:1.

### 3.5.4. The effect of metal substrate ratio

The metal to substrate ratio of a catalyst is an important consideration and can show whether the reaction medium is mass transport limited. By doubling the amount of catalyst, the conversion of substrate should double too. If this is not the case, then the reaction is said to be mass transfer limited. To test the reaction for the metal substrate ratio needed to achieve a system that is not mass transfer limited, a range from a high concentration of 125:1 to lower concentration of 1000:1 have been tested and are shown in table 3.5.

**Table 3.5** *The effect of metal substrate ratio upon the conversion and selectivity profile of the products using the sol immobilised 1 wt% AuPt/TiO<sub>2</sub>.*

Metal substrate ratio	Time / min	Conversion / %	Carbon balance / %	Selectivity / %			
				GA	TA	C-C Scission	LA
125:1	30	62	92	19	1	11	69
	60	88	88	17	1	14	68
	120	100	86	18	2	15	65
	240	100	82	15	2	18	65
250:1	30	55	95	22	1	8	69
	60	72	92	21	2	9	68
	120	95	92	19	2	11	68
	240	100	90	18	3	12	67
500:1	30	42	98	20	2	6	72
	60	59	97	17	2	8	73
	120	92	97	17	2	9	72
	240	100	96	14	4	10	72
1000:1	30	29	99	17	2	3	78
	60	44	100	12	4	6	78
	120	88	100	8	4	8	80
	240	100	100	5	5	9	81

**Reaction conditions; 10 ml Glycerol (0.3 M), temperature (100 °C), O<sub>2</sub> pressure (3 bar), 4:1 base ratio, 4 h reaction time and varied metal substrate ratio.**

The results show that by decreasing the metal substrate ratio, i.e. increasing the amount of catalyst used, that the rate of conversion increases, shown in figure 3.13. This is typical of catalytic reactions as with a higher amount of catalyst more active sites are available. When the catalyst amount is increased from s:m 125 to 1000, the initial rate of conversion at 30 mins increases by a factor of 2, illustrating that the initial rate is not affected by mass transfer limitations. The major change in rate occurs between 60 and 120 mins where the rate dramatically slows, indicating that there is a potential mass transfer limitation whereby the sequential oxidation products are more strongly bound to the catalyst surface, slowing the desorption process and therefore blocking active sites.

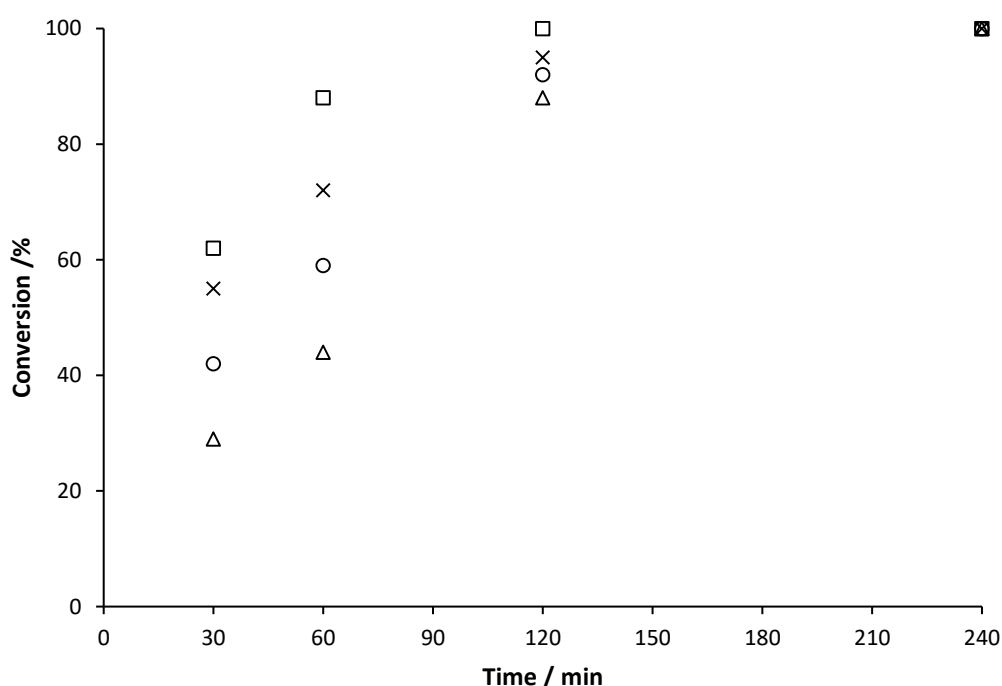


**Figure 3.13 Conversion time on line for varying metal substrate ratio where;  $\square$  is 125:1,  $\times$  is 250:1,  $\circ$  is 500:1,  $\Delta$  is 1000:1.**

There are two issues with using large amounts of catalyst within a reaction medium. Firstly, from a practical and industrial perspective, larger amounts of catalyst are more expensive to produce, and whilst catalysts are theoretically reusable indefinitely, all catalysts in reality will deactivate over time incurring much larger costs. Secondly, using higher amounts of catalyst in at elevated temperatures (100 °C) has a negative effect on the selectivity towards lactic acid. This suggests that due to the increased rate of the initial oxidation, the more stable GLD is formed, and prior to the system being able to equilibrate to DHA, the sequential oxidation to GA occurs. As more of the glycerol is converted, the GLD converts to DHA allowing for lactic acid to form. It can be seen that the lactic acid within the system is stable as the selectivity remains

relatively constant throughout, whereas the GA is converted in to C-C scission products and partially to the sequential oxidation product, TA.

Although the conversion of glycerol is much higher initially with lower metal substrate ratios, the reaction is still complete with all tests within 240 min period. Due to the lower selectivity to lactic acid and increased scission with the lower metal substrate, for further work the metal substrate ratio will be set at 1000:1.

### 3.5.5. The effect of stabilising agent and reusability

When following the sol immobilisation preparation method, the addition of a stabilising agent is a necessary step in forming a stable colloid prior to the addition of the support material. The substrate used as the stabilising agent has the potential to affect the reaction as the stabilising agent exists at the most critical point of reactant interaction, the surface of the catalyst. There are a large number of stabilising agents available, however, there are three stabilising agents that have been proven to produce stable catalysts with bimetallic precious metal catalysts; polyvinyl alcohol (PVA), polyvinylpropylene (PVP) and tetrakis(hydromethyl)phosphonium chloride (THPC). A series of glycerol oxidation reactions were conducted with 4 catalyst samples;

- i) AuPt/TiO<sub>2</sub> with PVA stabiliser.
- ii) AuPt/TiO<sub>2</sub> with PVP (10,000 Daltons) stabiliser.
- iii) AuPt/TiO<sub>2</sub> with PVP (1,200,000 Daltons) stabiliser.
- iv) AuPt/TiO<sub>2</sub> with THPC stabiliser.

The results shown in Table 3.6 show that by altering the stabilising agent, there is a significant effect on how the catalyst interacts with the reactants. When looking at the conversion of glycerol it can be seen that highest activity shown is that of the catalyst made using THPC, and when comparing to the results from previous sections, the selectivity of lactic acid is slightly lower than the other stabilising agents, potentially caused by the higher initial activity forming more of the oxidation products. Both PVP catalysts exhibited lower activity than the PVA and THPC, which is due to the fact PVP has a relatively large nitrogen containing ring within its structure. This nitrogen ring is bulky, and will block active sites on the surface of the catalyst, preventing the reactants from adsorbing and therefore lowering the rate of conversion. The larger chain length on catalyst (iii) when compared to catalyst (ii) can also block active sites on the surface. This observation shows how important it is to consider how the catalyst is prepared for particular reactions. Reactions with bulkier molecules as part of their chemical

make-up are going to be more affected by the orientation they can adsorb to the catalyst surface with. The catalyst produced using PVA shows a lower activity than the THPC, but a higher selectivity to lactic acid, suggesting that by lowering the initial rate, the amount of scission and sequential oxidation products can also be lowered.

**Table 3.6 The effect of stabilising agent used for catalyst preparation upon the conversion and selectivity profile of the products using the sol immobilised 1 wt% AuPt/TiO<sub>2</sub>.**

Stabilising agent	Time / min	Conversion / %	Carbon balance / %	Selectivity / %			
				GA	TA	C-C Scission	LA
PVA	30	31	100	15	2	3	80
	60	45	99	10	4	5	81
	120	89	99	7	4	7	82
	240	100	100	5	4	8	83
PVP (10,000 D)	30	18	99	13	3	2	82
	60	34	100	10	4	3	83
	120	58	100	8	5	4	83
	240	72	100	4	6	6	84
PVP (1,200,000 D)	30	12	100	10	4	1	85
	60	29	100	7	5	2	86
	120	45	99	3	6	3	88
	240	55	100	0	6	4	90
THPC	30	45	98	16	3	6	75
	60	68	97	11	4	8	77
	120	97	98	8	4	10	78
	240	100	97	4	5	11	80

**Reaction conditions; 10 ml Glycerol (0.3 M), temperature (100 °C), O<sub>2</sub> pressure (3 bar), NaOH:substrate (4:1), substrate:metal ratio (1000:1) at 4 h reaction time.**

It is also important to consider the reusability of a catalyst and how an unstable catalyst may affect the reaction medium. Table 3.7 shows the how the conversion of glycerol changes with sequential reactions using the same catalyst. The PVA catalyst shows high stability with little variation over the first 3 runs with a slight increase in activity on the 4<sup>th</sup> run. This is likely

due to the PVA breaking down and leaching the Au and Pt metals into the solution, slightly increasing the activity, but destabilising the catalyst. The 5<sup>th</sup> run shows a clear loss of activity indicating that the metal lost from the surface is no longer present to aid the catalysis process. Both the PVP catalysts maintain the same level of activity throughout the 5 runs, an observation that can be explained by the large polymers thermal stability, meaning that although the PVP partially blocks the surface, the inherent stability is higher than that of the PVA and THPC. Interestingly the THPC has a much lower stability than the other prepared catalysts with activity dropping significantly after a single run. The thermal stability of THPC is higher than that of PVA, and therefore, the temperature of the reaction is not sufficient to remove THCP from the catalyst service. Rather, it suggests that there is a lower metal surface interaction, increasing the leaching of the nanoparticles into the reaction medium, lowering the catalyst stability, thus, eliminating the THPC catalyst as a potential candidate for future work. The stability data plotted in figure 3.14, shows that whilst the PVP stabiliser is the most stable, the lower activity would severely hinder future work and therefore the PVA stabilising agent will be used for the further work.

**Table 3.7 The conversion of glycerol using the same catalyst over 5 runs using the sol immobilised 1 wt% AuPt/TiO<sub>2</sub> synthesised with varying stabilising agent.**

Stabilising agent	Time / min	Conversion / %				
		Run 1	Run 2	Run 3	Run 4	Run 5
PVA	30	31	32	30	38	25
	60	45	46	48	59	32
	120	89	91	87	100	44
	240	100	100	100	100	56
PVP (10,000 D)	30	18	17	17	18	17
	60	34	35	33	35	36
	120	58	56	57	57	56
	240	72	70	73	71	71
PVP (1,200,000 D)	30	12	11	12	11	13
	60	29	28	27	28	28
	120	45	46	45	44	44
	240	55	53	54	55	54
THPC	30	45	31	10	5	3

60	68	42	14	6	4
120	97	55	15	6	4
240	100	62	17	7	5

**Reaction conditions; 10 ml Glycerol (0.3 M), temperature (100 °C), O<sub>2</sub> pressure (3 bar), NaOH:substrate (4:1), substrate:metal ratio (1000:1) at 4 h reaction time.**

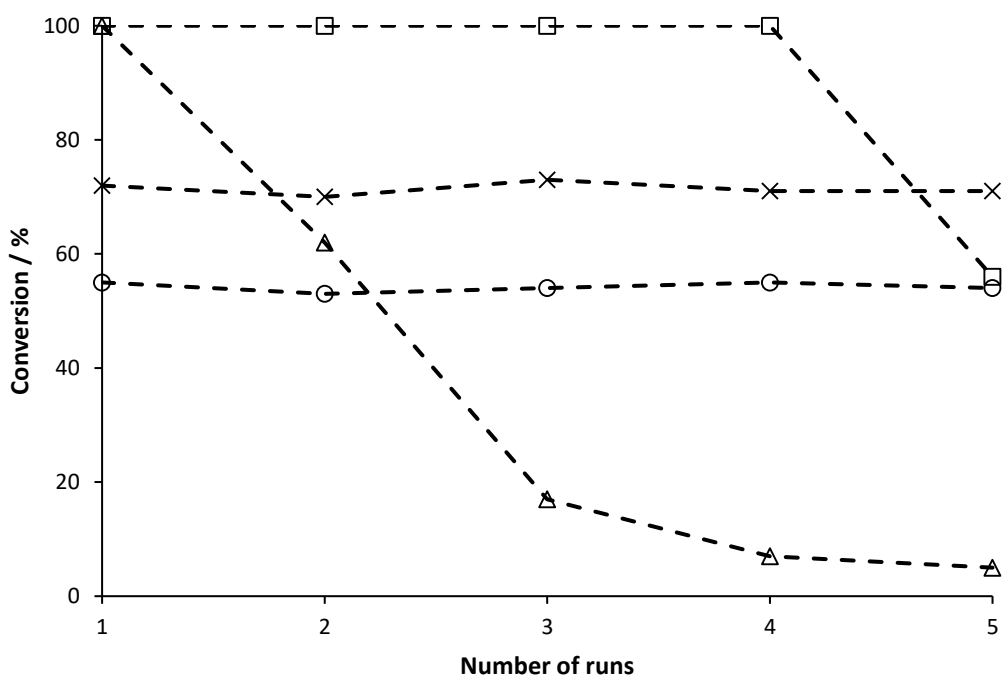


**Figure 3.14 Conversion of glycerol after 240 min period over 5 sequential reactions. Where all the catalysts are AuPt/TiO<sub>2</sub> with differing stabilising agents used in synthesis; □ is PVA, X is PVP (10,000 D), ○ is PVP (1,200,000 D) and Δ is THPC.**

### 3.5.6. Optimised conditions for lactic acid production

The series of experiments previously conducted have sequentially eliminated the varying parameters to attempt to find the highest potential selectivity to form lactic acid from glycerol. The results show that using the series of conditions deduced from the parameter mapping study an appreciably high selectivity to lactic acid was achieved and is illustrated by the molar conversion plot in Figure 3.15. The trend shows that the increase in lactic acid selectivity is directly proportional with the conversion of glycerol, with the selectivity remaining constant throughout the reaction period. Having achieved a positive result for a high selectivity to lactic acid, a study into the mechanism can be conducted to attempt to confirm whether the current theories of the mechanistic route to lactic acid are correct.

**Table 3.8** The conversion of glycerol using a sol immobilised 1 wt% AuPt/TiO<sub>2</sub> synthesised with PVA.

Time / min	Conversion / %	Carbon balance / %	Selectivity / %			
			GA	TA	C-C Scission	LA
30	31	99	14	2	3	81
60	56	100	9	4	5	82
120	89	100	6	4	7	83
240	100	100	5	4	8	83

Reaction conditions; 10 ml Glycerol (0.3 M), temperature (100 °C), O<sub>2</sub> pressure (3 bar), NaOH:substrate (4:1), substrate:metal ratio (1000:1) at 4 h reaction time.

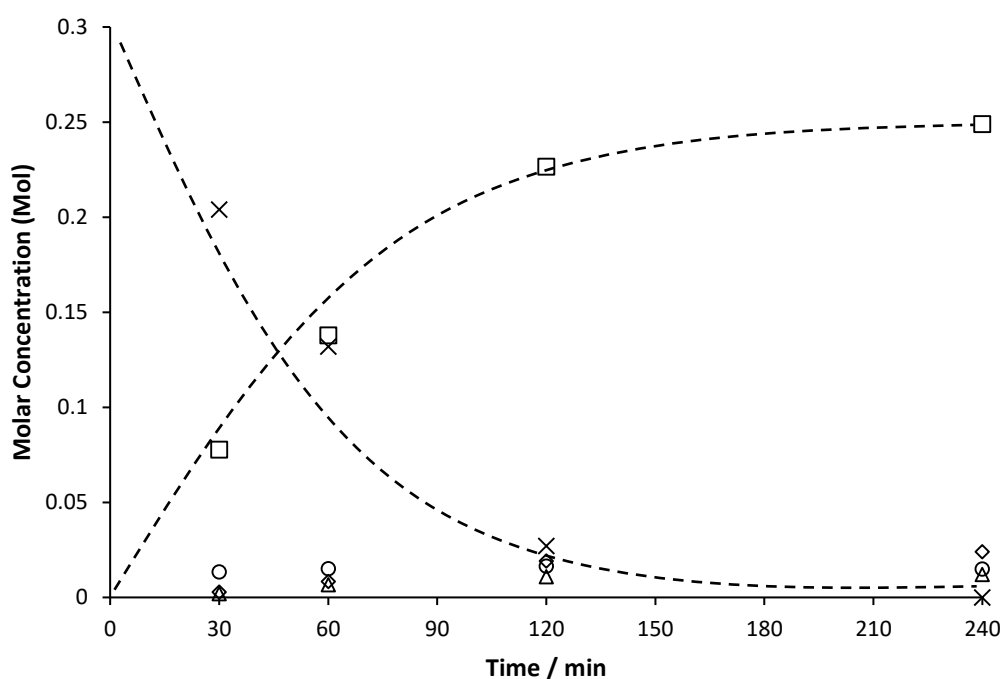
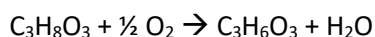


**Figure 3.15** Molar conversion and selectivity plot showing how relationship between converted glycerol and products produced under the predetermined ideal conditions where; □ is glycerol, X is lactic acid, ○ glyceric acid, Δ is Tartronic acid and ∅ is C-C scission products.

### 3.6. The mechanistic pathway to lactic acid

There are two mechanisms proposed as discussed in the introduction; a benzylic rearrangement and an inter/intramolecular Cannizzaro reaction. A benzylic rearrangement would require the coupling of two species for the reaction to proceed to lactic acid. A Cannizzaro reaction would require an intermediate state of pyruvaldehyde to form, which would then

produce pyruvic acid and hydroxyacetone (which itself would dimerise to dihydroxyacetone), which would then require a reduction step to produce lactic acid. Under the conditions the reaction is being run under, a reduction step in the final stages of the reaction is extremely unlikely. To illustrate, the overall reaction (excluding acid-base neutralisations) can be considered as;



As shown in O<sub>2</sub> pressure tests, there is a detrimental effect on the selectivity to lactic acid when adding an excess of O<sub>2</sub> to the reaction system. This could suggest a bifurcation in the reaction at an early stage, with one route leading to lactic acid that is unaffected by oxygen content and the other leading to by-products with a rate dependent on O<sub>2</sub> concentration. The actual involvement of O<sub>2</sub> in the lactic acid route is therefore likely at a later point in the reaction, which could explain why the initial amount of oxidation products produced is much higher than at the latter stages of the reaction.

Theoretically, the reaction could proceed through a dehydration at one end of the glycerol molecule, producing glyceraldehyde/dihydroxyacetone, along with the hydrogenolysis at the other side, producing a methyl compound and water. This would lead to lactaldehyde being produced, which would then be oxidised to lactic acid. There have been studies in which this reaction mechanism occurs, such as benzyl alcohol with a Au/Pd catalyst under similar conditions, showing this methodology is plausible. The possibility of coupling the molecules together in a disproportionation reaction however would be unlikely, as the presence of both base and Pt are known to inhibit disproportionation reactions.

The potential theories for the formation of lactic acid are not simple systems, and therefore require a complex level of reaction design to identify the mechanism of formation. A significant issue with analysing a reaction medium with the number of products produced in the oxidation of glycerol is that identifying the compounds individually is a very difficult task without achieving high selectivity to the product that is the target to identify. The reaction conditions determined by the previous work produce high selectivity towards lactic acid, allowing for a simpler analysis of the products through NMR spectroscopy.

To identify how lactic acid is formed, it would be required to identify the environments each of the carbons are in to view their positions within the lactic acid molecule after the reaction, as different mechanisms will orientate the original carbon molecules in different ways.

An illustration of how the carbon molecules in lactic acid would move dependent on the mechanism of formation I shown in figure 3.16.

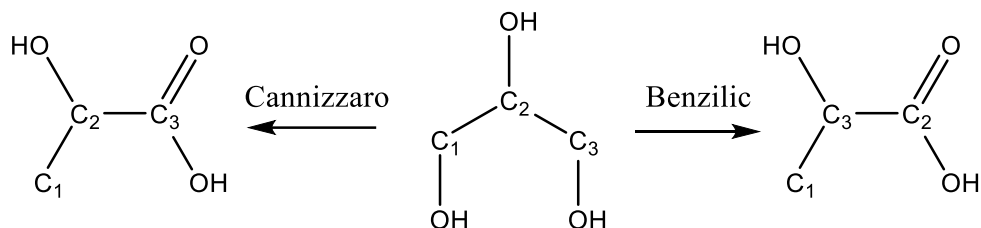


**Figure 3.16 Proposed movement of carbon atoms within glycerol when oxidised to lactic acid.**

An observation that can be seen from these two diagrams is that if the reaction were to proceed through an intramolecular 1,2- shift of either a methyl group or hydrogen, both would proceed through a benzylic rearrangement rather than intramolecular Cannizzaro. If the reaction were to proceed through a Cannizzaro reaction, there would be a hydroxide induced intermolecular hydride transfer between the aldehyde groups. The probability of a Cannizzaro type reaction in this method would be extremely inefficient, requiring energy for each step and therefore making the process much more unlikely, as there would be a requirement for the mechanism to proceed *via* the two extra intermediates (pyruvic acid and lactaldehyde) described above.

The theories described above are hinged on being able to identify how and where the carbons or substituents on the carbons move to within the final lactic acid molecule from the initial glycerol, and also being able to differentiate the products from one another in the analysis. There are two potential methods that could lead to identification of the species present in the synthesised lactic acid molecule. Firstly, the experiment could be conducted using a <sup>13</sup>C labelled sample of glycerol, where either the C<sub>2</sub> carbon or the C<sub>1</sub> and C<sub>3</sub> carbons are labelled, followed by conducting <sup>13</sup>C NMR of the samples produced. Although <sup>13</sup>C NMR is difficult to quantify, the carbons in specific environments would give much stronger signals if they were present in higher quantities. Using the conditions identified in the previous body of work it would therefore be possible to produce a high selectivity of lactic acid, presenting the carbon species in environments that would be easily identified. The second option is by using a deuterated sample of glycerol, and to observe where the deuterium moves throughout the molecule during the reaction. This method presents a series of issues, however, as the deuterium within the sample would likely exchange with the hydrogen in the water or hydroxide medium the reaction is conducted in. This could be solved by conducting the reaction in deuterated water, however this

method would be much more expensive than using a 10 % addition of  $^{13}\text{C}$  labelled sample of glycerol and ultimately, less efficient.

### 3.6.1. Labelled glycerol experiments

A sample of 1,3-di- $^{13}\text{C}$ -labelled glycerol was acquired for the experiments to determine the carbon position using the conditions determined and described in Section 3.5.6. and the results of the reaction shown in Table 3.9, and in molar selectivity plot shown in Figure 3.17. The conversion of the glycerol is slightly lower than in the ideal conditions section above, but this could be due to simple experimental error or potentially a more complex interaction of the  $^{13}\text{C}$  with the catalyst/substrate. The selectivity to lactic acid is still high, however, and therefore should be suitable for  $^{13}\text{C}$  NMR analysis. The NMR spectra were taken at three points throughout the reaction, at  $t = 0$  mins,  $t = 60$  mins and  $t = 240$  mins, to view how the substrate changed through the course of the reaction.

**Table 3.9** *The conversion of 1,3-di- $^{13}\text{C}$ -glycerol using a sol immobilised 1 wt% AuPt/TiO<sub>2</sub> synthesised with PVA.*

Time / min	Conversion / %	Carbon balance / %	Selectivity / %			
			GA	TA	C-C Scission	LA
30	28	99	14	2	5	79
60	49	100	11	4	7	78
120	85	100	8	4	9	79
240	100	100	7	4	10	79

*Reaction conditions; 10 ml Glycerol (0.3 M), temperature (100 °C), O<sub>2</sub> pressure (3 bar), NaOH:substrate (4:1), substrate:metal ratio (1000:1) at 4 h reaction time.*

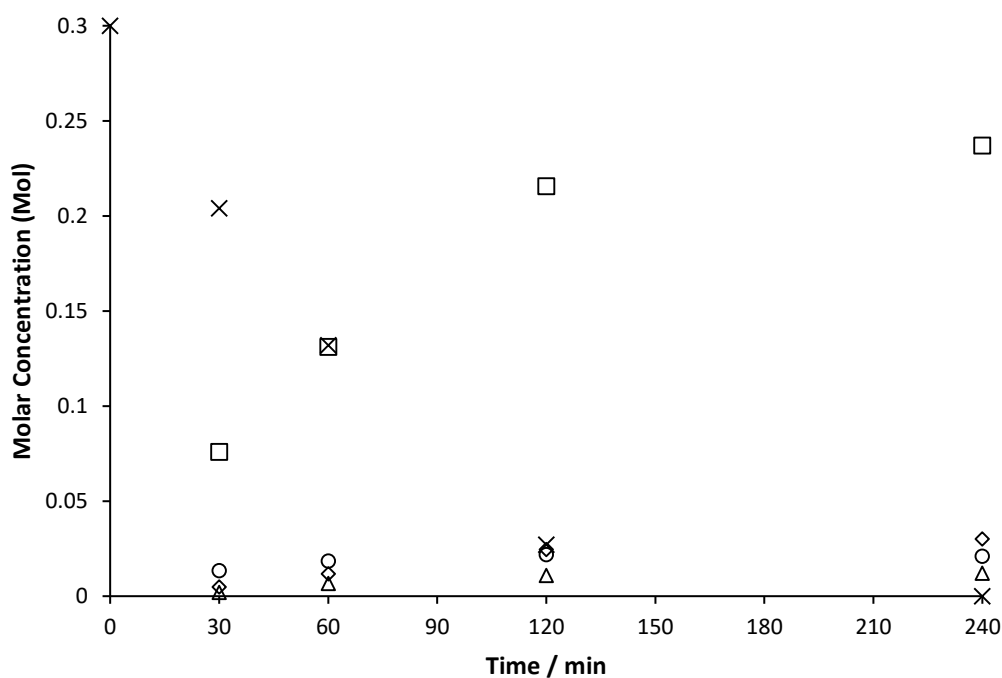


**Figure 3.17** Molar conversion and selectivity plot converted 1,3-di- $^{13}\text{C}$ -glycerol and products produced under the predetermined ideal conditions where;  $\square$  is glycerol,  $\times$  is lactic acid,  $\circ$  glyceric acid,  $\Delta$  is Tartronic acid and  $\diamond$  is C-C scission products.

It can be seen from Figure 3.18 that a strong,  $^{13}\text{C}$  signal is prevalent in the sample, with both of the carbons in the same COH environment as expected. The strength of the  $^{13}\text{C}$  signal increases with the physical quantity of  $^{13}\text{C}$  atoms present in a particular environment, with the COH exhibiting at a chemical shift of 62 ppm.

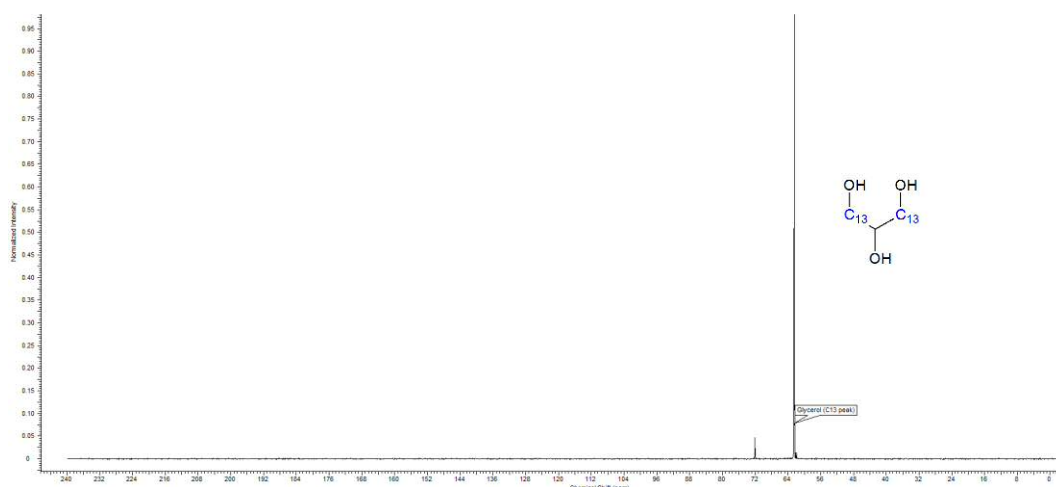


**Figure 3.18**  $^{13}\text{C}$  NMR 1,3-di- $^{13}\text{C}$ -labelled glycerol at  $t = 0$  mins.

In figure 3.19, two new environments of  $^{13}\text{C}$  are observed as the glycerol is converted into what is predominantly lactic acid. Comparing the points in the  $^{13}\text{C}$  NMR and the  $t = 60$  mins point where the molar concentration is equal is can be confirmed as the peak intensity is in the appropriate ratio. The two new  $^{13}\text{C}$  environments correspond to a C=O bond at a chemical shift of 182 ppm and the other peak at 20 ppm indicative of  $\text{CH}_3$ . As the high selectivity to lactic acid corresponds to the high intensity of the  $^{13}\text{C}$  peaks, it is appropriate to label these peaks as the C=O and  $\text{CH}_3$  found within the lactic acid.

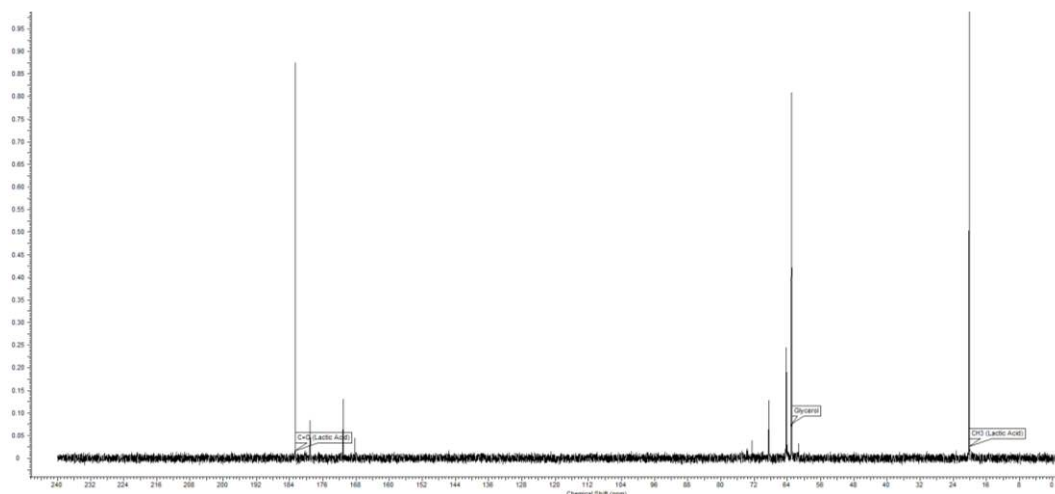


**Figure 3.19**  $^{13}\text{C}$  NMR 1,3-di- $^{13}\text{C}$ -labelled glycerol at  $t = 60$  mins.

The final  $^{13}\text{C}$  NMR taken from a sample at the end of the reaction is shown in Figure 3.20. It can be seen that the intensity of the C=O and  $\text{CH}_3$  peaks in the spectrum have both increased in line with the selectivity observed at the end of the reaction. What is evident is that the original COH environment no longer exists. Looking at figure 3.16, it is evident that the position of the carbon species remains constant. There is no net movement of the  $^{13}\text{C}$  when forming lactic acid, which suggests the reaction proceeds through the less likely Cannizzaro type reaction.

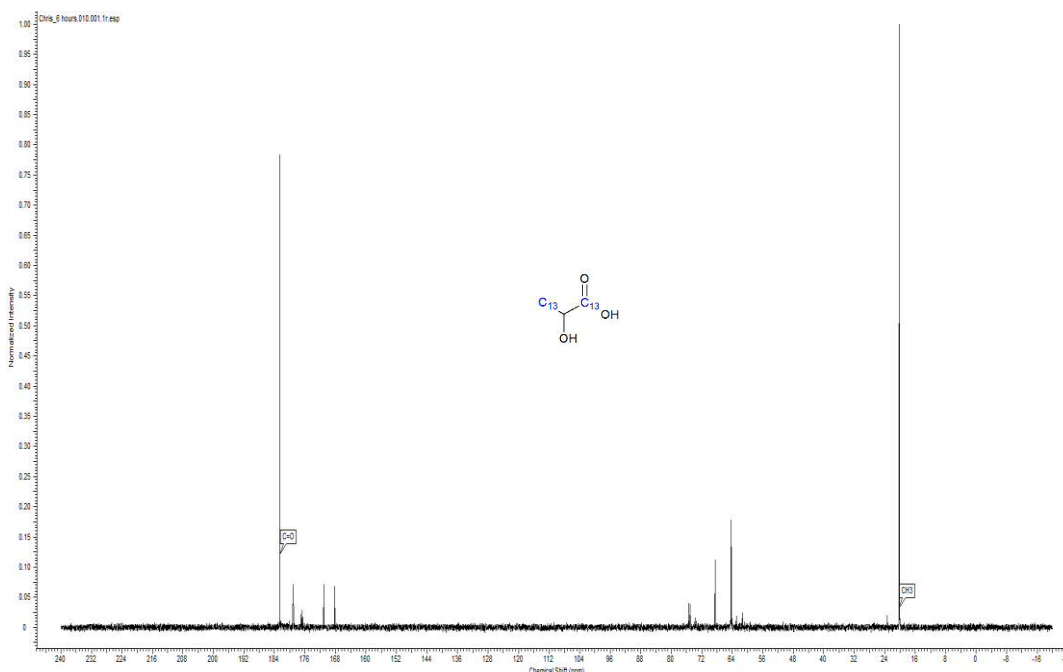


**Figure 3.20**  $^{13}\text{C}$  NMR 1,3-di- $^{13}\text{C}$ -labelled glycerol at  $t = 240$  mins.

There is no evidence of rearrangement of the carbon atoms, eliminating the possibility of a benzylic rearrangement reaction. What is also evident, however, is that for a true Cannizzaro pathway to occur, there would be a hydroxide induced intermolecular hydride transfer. As described above, a Cannizzaro reaction proceeding *via* two extra intermediates is extremely inefficient. The conclusion to these points, with the total lack of carbon movement is the mechanism is actually an intramolecular hydride shift.

### 3.7. Summary and conclusions

During this body of work the aim was determine a set of reaction conditions that would produce a high selectivity to lactic acid and providing an understanding of how the reaction proceeded.

An increase in temperature was found to increase the selectivity to lactic acid and lower the C-C scission observed, up until 120 °C, where the carbon balance decreased substantially, and indicating total oxidation to CO<sub>2</sub>. The temperature that produces the highest yield of lactic acid was therefore 100 °C.

O<sub>2</sub> pressure increased the selectivity to lactic acid up to a limit of 3 bar, beyond this point the O<sub>2</sub> pressure increases the rate of the initial oxidation, creating an equilibrium that favours the production of oxidation products such as glyceric acid. This then increases the scission

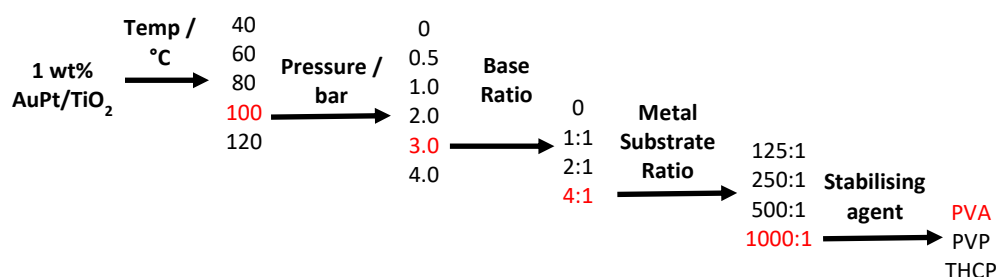
observed in the reaction, and although the selectivity to lactic acid at the end of the reaction is relatively high with 4 bar, the yield is lower than that of the 3 bar reaction.

The base substrate ratio was found to have a profound effect on the selectivity to lactic acid, with lower base substrate ratios producing an excess of oxidation products. As the base ratio increases, so too does the selectivity to lactic acid with 4:1 providing the highest yield overall.

By decreasing the metal substrate ratio, and therefore increasing the amount of catalyst, a negative effect was observed on the selectivity to lactic acid. Again the initial rate of reaction with lower metal substrate ratio produced higher amounts of oxidation products, leading to more C-C scission. The highest yield of lactic acid produced was with a metal substrate ratio of 1000:1.

When observing the effect of the stabilising agent on the catalyst activity, it was found that the bulkier stabilising agents effectively blocked active sites on the catalyst surface leading to lower activity. This did, however, correspond to a higher stability. Overall, the catalyst with an acceptable balance between performance and stability was the catalyst prepared with PVA.

Overall the reaction results obtained through the parameter study produced a maximum selectivity of 83 % to lactic acid using the following conditions; 100 °C, 3 bar O<sub>2</sub>, 4:1 base ratio, 1000:1 substrate metal ratio using a 1 wt% AuPt/TiO<sub>2</sub> produced through the sol immobilisation method using a PVA stabilising agent.



The set of conditions established enabled a study to be conducted on the mechanism of formation for lactic acid, a long-contested subject. This was possible as the high selectivity to lactic acid allowed for a <sup>13</sup>C labelling study to be conducting, with the NMR being adequately clear enough to interpret. Opposed to the theories currently proposed, the mechanism was confirmed to be an intramolecular hydride shift, with no net movement of carbons within the structure of the lactic acid produced.

### 3.8. References

1. W. L. G. d. Silva, P. T. d. Souza, G. G. Shimamoto and M. Tubino, *Journal of the Brazilian Chemical Society*, 2015, **26**, 1745-1750.
2. K. Pathak, K. M. Reddy, N. N. Bakhshi and A. K. Dalai, *Applied Catalysis A: General*, 2010, **372**, 224-238.
3. S. Carrettin, P. McMorn, P. Johnston, K. Griffin and G. J. Hutchings, *Chemical Communications*, 2002, 696-697.
4. E. Sproge, S. Chornaja, K. Dubencovs, V. Kampars, L. Kulikova, V. Serga and D. Karashanova, *IOP Conference Series: Materials Science and Engineering*, 2015, **77**, 012026.
5. G.-Y. Yang, Y.-H. Ke, H.-F. Ren, C.-L. Liu, R.-Z. Yang and W.-S. Dong, *Chemical Engineering Journal*, 2016, **283**, 759-767.
6. A. Namdeo, S. M. Mahajani and A. K. Suresh, *Journal of Molecular Catalysis A: Chemical*, 2016, **421**, 45-56.
7. Y. Li and F. Zaera, *Journal of Catalysis*, 2015, **326**, 116-126.
8. S. Gil, M. Marchena, L. Sánchez-Silva, A. Romero, P. Sánchez and J. L. Valverde, *Chemical Engineering Journal*, 2011, **178**, 423-435.
9. C. D. Evans, S. A. Kondrat, P. J. Smith, T. D. Manning, P. J. Miedziak, G. L. Brett, R. D. Armstrong, J. K. Bartley, S. H. Taylor, M. J. Rosseinsky and G. J. Hutchings, *Faraday Discussions*, 2016, **188**, 427-450.
10. F. Porta and L. Prati, *Journal of Catalysis*, 2004, **224**, 397-403.
11. A. A. Rodriguez, C. T. Williams and J. R. Monnier, *Applied Catalysis A: General*, 2014, **475**, 161-168.
12. A. Villa, N. Dimitratos, C. E. Chan-Thaw, C. Hammond, L. Prati and G. J. Hutchings, *Accounts of Chemical Research*, 2015, **48**, 1403-1412.
13. J. Xu, H. Zhang, Y. Zhao, B. Yu, S. Chen, Y. Li, L. Hao and Z. Liu, *Green Chemistry*, 2013, **15**, 1520-1525.
14. E. G. Rodrigues, M. F. R. Pereira, X. Chen, J. J. Delgado and J. J. M. Órfão, *Industrial & Engineering Chemistry Research*, 2013, **52**, 17390-17398.
15. W. C. Ketchie, Y.-L. Fang, M. S. Wong, M. Murayama and R. J. Davis, *Journal of Catalysis*, 2007, **250**, 94-101.
16. S. A. Kondrat, P. J. Miedziak, M. Douthwaite, G. L. Brett, T. E. Davies, D. J. Morgan, J. K. Edwards, D. W. Knight, C. J. Kiely, S. H. Taylor and G. J. Hutchings, *ChemSusChem*, 2014, **7**, 1326-1334.

17. H. Fukuda, A. Kondo and H. Noda, *Journal of Bioscience and Bioengineering*, 2001, **92**, 405-416.
18. S. Chornaja, K. Dubencov, V. Kampars, O. Stepanova, S. Zhizhkun, V. Serga and L. Kulikova, *Reaction Kinetics, Mechanisms and Catalysis*, 2013, **108**, 341-357.
19. Y. Shen, S. Zhang, H. Li, Y. Ren and H. Liu, *Chemistry – A European Journal*, 2010, **16**, 7368-7371.
20. N. Dimitratos, C. Hammond, C. J. Kiely and G. J. Hutchings, *Applied Petrochemical Research*, 2014, **4**, 85-94.
21. C. E. McNamee, Y. Tsujii and M. Matsumoto, *Langmuir*, 2005, **21**, 11283-11288.
22. J. W. Bullard and M. J. Cima, *Langmuir*, 2006, **22**, 10264-10271.
23. S. Demirel-Gülen, M. Lucas and P. Claus, *Catalysis Today*, 2005, **102–103**, 166-172.
24. C. Zhang, T. Wang, X. Liu and Y. Ding, *Chinese Journal of Catalysis*, 2016, **37**, 502-509.
25. W. C. Ketchie, M. Murayama and R. J. Davis, *Topics in Catalysis*, 2007, **44**, 307-317.

## 4.0. Perovskites for product control

### 4.1. Introduction

The ability to selectively form products from the use of catalysts is highly desirable and is made possible through control of the multiple steps involved in the reaction scheme (Scheme 1.6). To achieve this, a catalyst would need to be developed to promote either the oxidation pathway, to products such as glyceric acid and tartronic acid, or the dehydration pathway to the lactic acid.

It has been well documented that the catalyst support has an influence on the conversion of glycerol and product selectivity in oxidative and basic conditions<sup>2-4</sup>. Single metal oxides and carbon are popular supports for glycerol oxidation, with carbon shown to be more active than supports such as titania and iron oxide<sup>5</sup>. Supports such as Al<sub>2</sub>O<sub>3</sub> and NiO are highly active, but have a large distribution of product selectivity<sup>6</sup>. A study by Villa *et al.* demonstrated the role of acid and base sites on supports used for glycerol oxidation. It was found that basic sites contributed to a higher activity with a poor selectivity breakdown of products, and supports containing acid sites had a lower activity, but higher selectivity to glyceraldehyde and dihydroxyacetone<sup>7</sup>, therefore, controlling this step allows for a greater control over the product selectivity profile of the products. This research clearly shows that the support has a significant role on the activity and selectivity to products, and therefore, tailoring a support with the desired characteristics to enhance a selected mechanistic pathway is the key to selective formation of a desired product.

Perovskite type mixed metal oxides are comprised of two cations in a general ABO<sub>3</sub> formula in which the A site cation is larger than the B site cation. There is a potential to alter the A and B site cations without changing the crystal structure of the compound, allowing the properties to be tuned for specific purpose. The B site cation has been varied to observe the changes in the selectivity profile for the glycerol oxidation reaction. The supercritical antisolvent preparation has been shown to produce high surface area materials due to the inherent intimate mixing of small particle size precipitate allowing for the formation of pure phase material at lower temperature calcinations.

## **4.2. Supercritical antisolvent (SAS) preparation of perovskite type mixed metal oxides**

### **4.2.1. Perovskite synthesis and purity**

The production of a series of LaBO<sub>3</sub> (B site; Cr, Mn, Fe, Co, Ni) perovskite supports was undertaken using the SAS preparation technique. An in depth method for the use of the SAS apparatus has been described in the experimental section. To produce the specific LaBO<sub>3</sub> perovskite, a solution of lanthanum (III) acetylacetonate hydrate (4 mgml<sup>-1</sup>) and the corresponding B site acetate salt (1:1 ratio with La:B molar ratio) were dissolved in methanol and stirred for a period of 60 min. The resulting solution was pumped into the SAS apparatus through a HPLC pump at a rate of 4 ml min<sup>-1</sup> simultaneously with ScCO<sub>2</sub> (held at 130 bar, 40 °C) through a co-axial nozzle at a rate of 12 kg hr<sup>-1</sup>. A stainless steel frit (0.5 micron) was used to collect the resulting precipitate, whilst the ScCO<sub>2</sub> and miscible solvent was recovered down stream in a separate heated vessel. Precipitation continues until the metal solution is fully consumed followed by a system purge with continuously flowing ScCO<sub>2</sub> (80 bar, 40 °C) for a period of 30 min. The apparatus is then slowly depressurised to prevent warping of the frit, and the dried powder collected for calcination.

#### **4.2.1.1. Thermogravimetric analysis (TGA) analysis**

TGA analysis was conducted on the resulting precipitate to ascertain the lowest temperature at which the material could be calcined to produce a pure phase perovskite material. The analysis was carried out up to 900 °C, as typical calcination temperatures are within this range. It can be seen from the TGA analysis (Figure 4.1) that there are multiple mass losses in each perovskite precursor with significant mass loss occurring prior to 450 °C. The significant mass losses can be attributed to the breaking down of the acetate and acetylacetonate ligands present in the precursor materials.

The higher temperature mass losses are attributed to the transitions between various metal oxide and mixed metal oxide phases with the latter number of phases controlled by the versatility of the B site cation oxidation states.

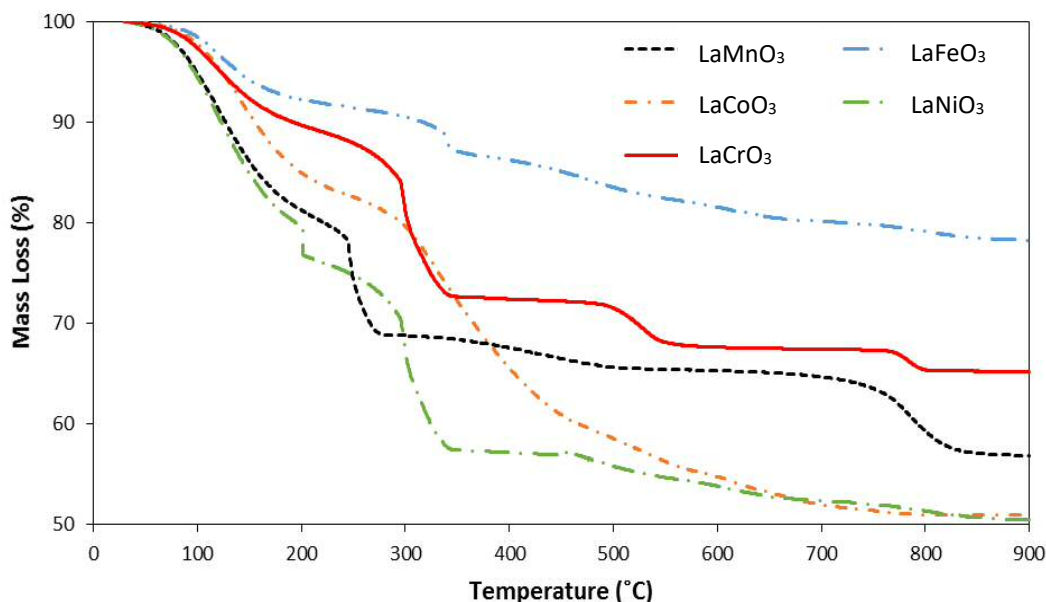


**Figure 4.1 TGA analysis describing the percentage mass loss of the variety of perovskite precursor materials.**

The LaCrO<sub>3</sub> can be seen to undergo several phase boundary changes, indicated by the lower mass losses, due to the chromium cations variable oxidation state. There are several potential ternary oxide phases (LaCrO<sub>4</sub>, La<sub>2</sub>Cr<sub>3</sub>O<sub>12</sub>, La<sub>2</sub>CrO<sub>6</sub> and LaCrO<sub>3</sub>). The chosen temperature for calcination for the perovskite precursors was 750 °C as the final mass loss event begins before this point for Mn, Fe, Co, and Ni and prior to the formation of the La<sub>2</sub>CrO<sub>6</sub> for the Cr sample.

#### 4.2.1.2. X-ray diffraction (XRD) analysis

XRD of the calcined materials was conducted on each of the samples calcined at 750 °C. The semi quantitative data from the each of the diffraction patterns show La<sub>2</sub>O<sub>3</sub> impurities in each of the samples (Table 4.2). The non-stoichiometric precipitation of the precursors occurs due to an inherent difference in precipitation rate of the metal salts used. This is a phenomenon can be ascribed to the solubility of the metal salts within the ScCO<sub>2</sub>/methanol mixture under the conditions described in the experimental section. To increase the phase purity of the perovskite supports, each solution requires a slight excess in the B site salt in order to reduce the amount of La<sub>2</sub>O<sub>3</sub> formed and to increase the stoichiometric ratio that is actually precipitated. The ratio

was increased by the appropriate amount taking in to account the excess in  $\text{La}_2\text{O}_3$  phase for each perovskite (Table 4.1).

**Table 4.1 Phase purity of perovskite material determined through semi quantitative data analysis.**

B Site	$\text{LaBO}_3$ phase purity / %	Crystallite size / nm
Mn	95	25
Fe	75	24
Ni	68	20
Co	72	26
Cr	92	23

**Table 4.2  $\text{La}_2\text{O}_3$  excess and solution correction ratio to improve purity.**

B site	$\text{La}_2\text{O}_3$ Excess / %	Solution ratio / A:B
Mn	5	1:1.1
Fe	25	1:1.25
Ni	32	1:1.3
Co	28	1:1.25
Cr	2	1:1

By increasing the concentration of the B cation acetate salt in the precursor solution, an increased phase purity is observed with a dominant perovskite phase in comparison with the initial sample, as observed in the XRD patterns (Figure 4.2, Table 4.3) A small distribution (approx. 10 wt %) of other by-product phases were found in the  $\text{LaFeO}_3$ ,  $\text{LaCoO}_3$  and  $\text{LaNiO}_3$  samples. The by-products were the single oxides of La and the corresponding B site, the amounts of which could be lowered with a much higher calcination temperature, although this would lower the surface area of the material. As the surface area is a key to the potential activity of the perovskite supports, and the by-product distribution was so low, it was concluded the loss of surface area would overall be detrimental to the aims of using these supports. The  $\text{LaCrO}_3$  species formed showed a small phase distribution of  $\text{La}_2\text{CrO}_6$ , though it was not possible to quantify the phase through a relative intensity ratio method as there is a limited data set for this

particular phase. The principal reflection of this phase at  $28.13\ 2\theta$  was significantly smaller than the principle reflection at  $33\ 2\theta$  indicating that the quantity of the Cr (VI) phase was minimal.

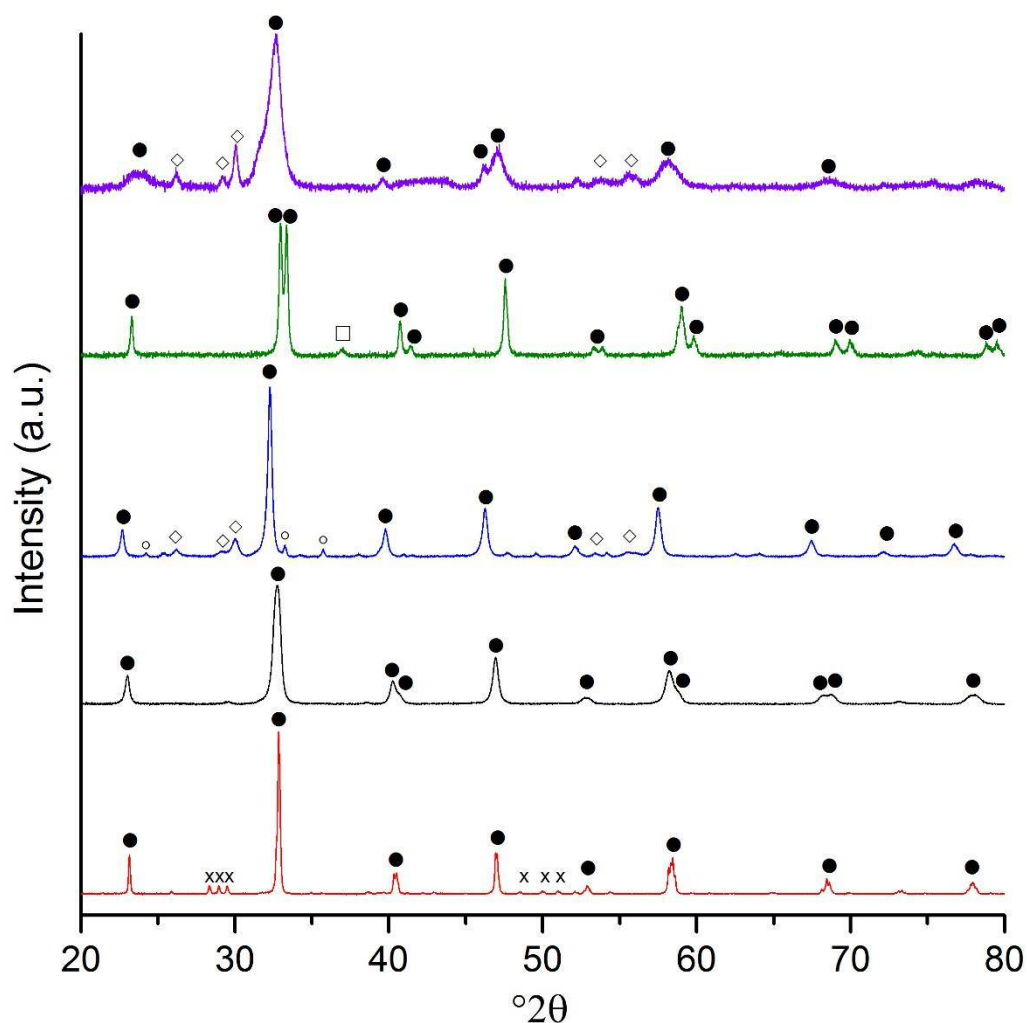


**Figure 4.2 Powder X-ray diffraction patterns of the SAS produced La:B precipitates post  $750\ ^\circ\text{C}$  calcination in descending order of B site; Ni (purple), Co (green), Fe (blue), Mn (black), Cr (red). Phase legend;  $\bullet$  perovskite phases,  $\circ$   $\text{Fe}_2\text{O}_3$ ,  $\diamond$   $\text{La}_2\text{O}_3$ ,  $\square$   $\text{Co}_3\text{O}_4$ ,  $\times$   $\text{La}_2\text{CrO}_6$ .**

The Scherrer equation was used to calculate the crystallite sizes of each of the SAS precipitated perovskite materials, with the resulting range being between 6 and 22 nm (Table 4.3). These crystallite sizes are relatively small in comparison to perovskite materials formed through more traditional means. Cristiani *et al.* obtained crystallite sizes between 50 and 90 nm using the co-precipitation method for a series of  $\text{La}_{0.8}\text{Sr}_{0.2}\text{BO}_3$  perovskites<sup>8</sup>. The small crystallite size obtained is a product of the SAS preparation procedure which produces extremely small

particle precipitates that are extremely well mixed allowing for a lower calcination temperature to form the perovskite phase.

**Table 4.3 Altered precursor ratios and the effect on the purity of perovskite phase.**

Sample	B metal salt		Precursor		Phase composition from XRD	Crystallite size / nm
			solution La:B molar ratio	Precipitated La:B molar ratio*		
LaCrO <sub>3</sub>	Chromium acetate*	(III)	1:1	1:1.06	LaCrO <sub>3</sub> , trace La <sub>2</sub> CrO <sub>6</sub> *	6
LaMnO <sub>3</sub>	Manganese acetate tetrahydrate	(II)	1:1.2	1:1.03	LaMnO <sub>3</sub> (100%),	18
LaFeO <sub>3</sub>	Iron (II) acetate		1:1.4	1:1	LaFeO <sub>3</sub> (85%) La <sub>2</sub> O <sub>3</sub> (9%) Fe <sub>2</sub> O <sub>3</sub> (6%)	21
LaCoO <sub>3</sub>	Cobalt (II) acetate tetrahydrate		1:1.1	1:1.05	LaCoO <sub>3</sub> (90%) Co <sub>3</sub> O <sub>4</sub> (10%)	22
LaNiO <sub>3</sub>	Nickel (II) acetate tetrahydrate		1:1.1	1:1.07	LaNiO <sub>3</sub> (90%) La <sub>2</sub> O <sub>3</sub> (8%) NiO (2%)	15

#### 4.2.1.3. Surface area analysis

The lower calcination temperature coupled with the small particle sizes produced from the SAS preparation allows for relatively high surface area perovskites to be formed, 22 – 52 m<sup>2</sup>g<sup>-1</sup> (Table 4.4). The surface areas obtained in this work are much greater than the perovskites prepared by more conventional techniques, where surface area ranges between 1 – 15 m<sup>2</sup>g<sup>-1</sup> <sup>9, 10</sup>. The combination of small crystallite sizes and higher surface area offers a larger distribution of site defects on the surface of the material, allowing the precious metal nanoparticles to anchor to these defects and increases the perovskite supports viability in liquid phase systems.

**Table 4.4 BET surface area of SAS precipitated perovskites post calcination**

Sample	LaBO <sub>3</sub> phase purity / %	Surface area / m <sup>2</sup> g <sup>-1</sup>
LaCrO <sub>3</sub>	98	52
LaMnO <sub>3</sub>	95	32
LaNiO <sub>3</sub>	90	36
LaFeO <sub>3</sub>	85	26
LaCoO <sub>3</sub>	90	22

The purity of phase and surface area show no real correlation. If the curing temperature is taken into account for each of the perovskites, it can be seen from the TGA plots, shown in figure 4.1, that the final mass loss occurs at a much lower temperature for LaNiO<sub>3</sub>, LaFeO<sub>3</sub> and LaCoO<sub>3</sub> than it does for LaCrO<sub>3</sub> and LaMnO<sub>3</sub>. This illustrates that the surface area decreases once a final mass loss occurs, not just an increased temperature.

#### 4.2.2. Catalyst Preparation

The method chosen for the deposition of the metal nanoparticles was maintained as sol-immobilisation due to the inherently small and well dispersed particle distribution across the surface of the support, hence providing a catalyst with the ideal properties for producing a model reaction. An aqueous solution of HAuCl<sub>4</sub> and H<sub>2</sub>PtCl<sub>6</sub> were prepared at specific concentrations (10 mg ml<sup>-1</sup>). Polyvinyl alcohol (PVA, 1 wt% aqueous solution, MW = 10 kDa) was freshly prepared and used as the stabilising agent. NaBH<sub>4</sub> (0.1 M aqueous solution) was also freshly prepared and used as the reducing agent. To an aqueous mixture of the HAuCl<sub>4</sub> and H<sub>2</sub>PtCl<sub>6</sub> of a concentration to produce 1:1 metal weight ratio, a total of 1 wt % of total metal in the prepared catalyst, the PVA solution was added (PVA/(Au + Pt) (wt/wt) = 0.65) with vigorous stirring for 2min. NaBH<sub>4</sub> was subsequently added such that the NaBH<sub>4</sub>:total metal ratio (mol/mol) was 7.5. The resulting solution was stirred for 30 min to allow the stabilisation of the reducing colloidal particles, followed by the addition of the perovskite material. The solution was left stirring for a further 1 h, followed by washing with distilled water and drying at 110 °C

for 16 h. The acidification of the support was unnecessary and would have been detrimental to the catalyst as the supports are unstable in highly acidic media.

### 4.2.3. Catalyst characterisation

#### 4.2.3.1. Transmission electron microscopy

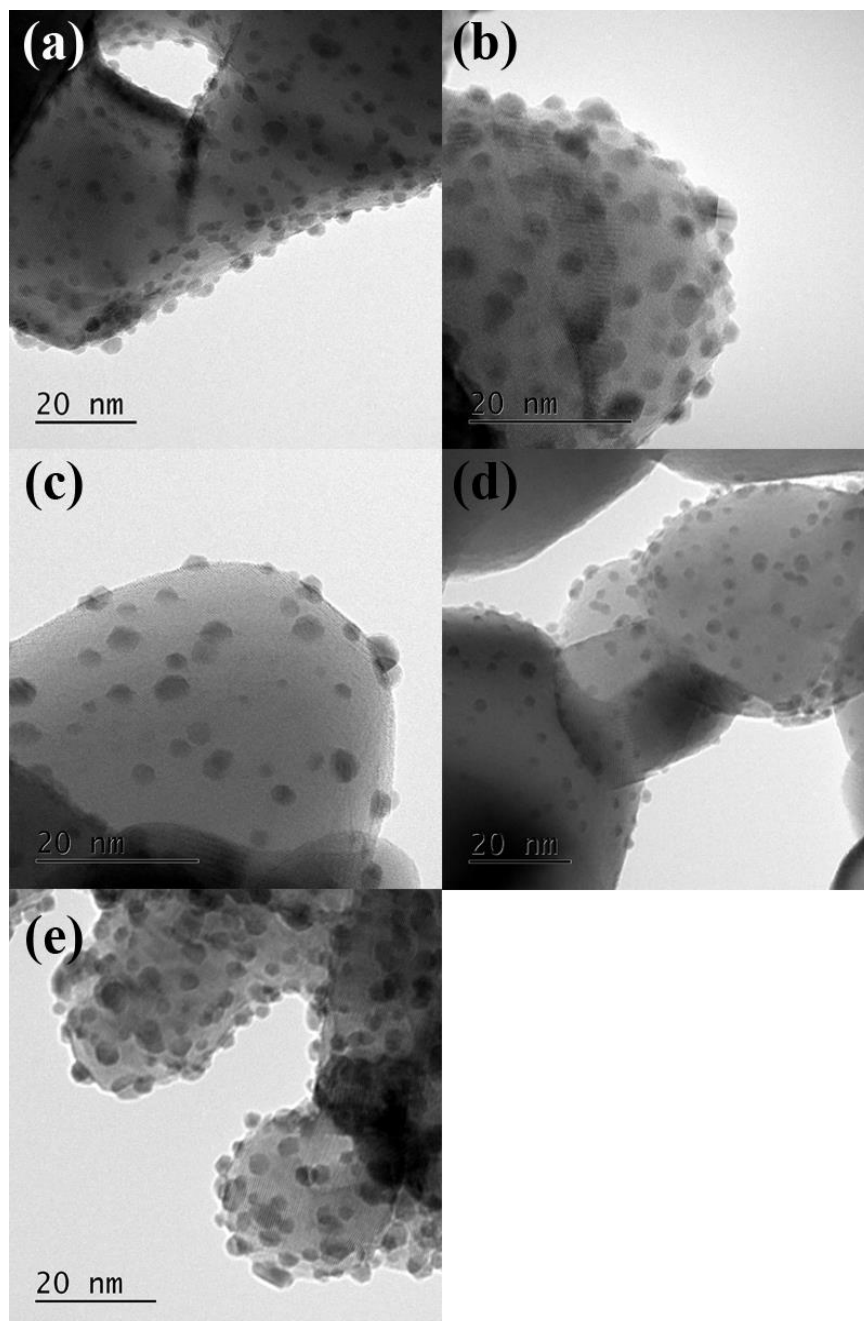


**Figure 4.3** Representative transmission electron micrographs of sol-immobilisation prepared AuPt supported upon the various SAS precipitated  $\text{LaBO}_3$  perovskite supports. Where;  $\text{LaCrO}_3$  (a),  $\text{LaMnO}_3$  (b),  $\text{LaFeO}_3$  (c),  $\text{LaCoO}_3$  (d), and  $\text{LaNiO}_3$  (e).

Transmission electron microscopy was conducted on each of the prepared supports with the images and particle size distribution shown below (Figures 4.3 And 4.4). The deposition of metals *via* the sol-immobilisation preparation was observed in order to view the particle size distribution and mean particle size of the Au and Pt deposited on the surface. For each of the perovskite supports the mean particle size was found to be *ca.* 2 nm with a standard deviation of *ca.* 1 nm. The observed sizes of the metal nanoparticles deposited on the perovskites varied only slightly and appeared to have no strong correlation with either the relative surface area or the specific B site element used. The TEM results obtained show comparable particle size

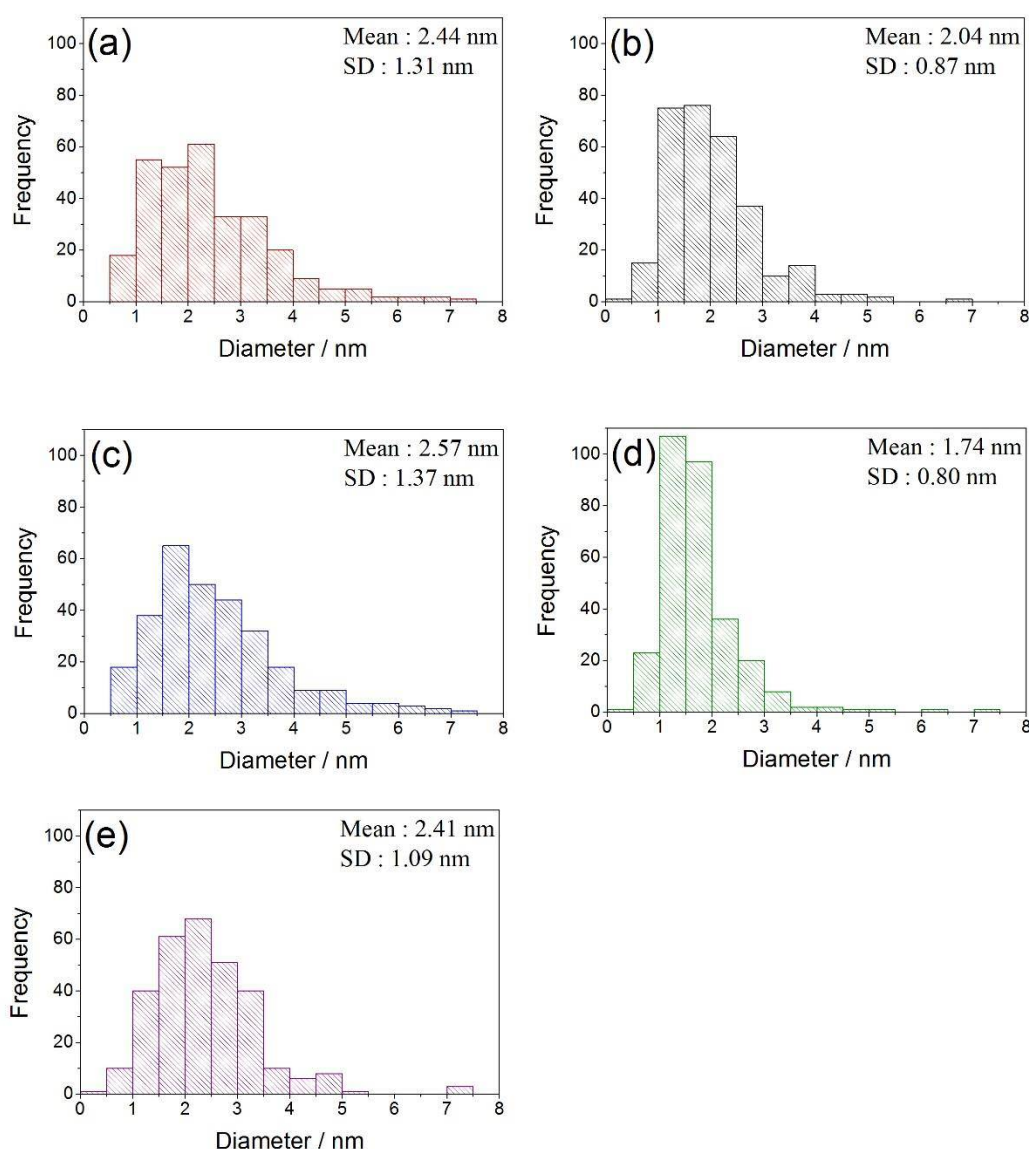


**Figure 4.4** Histograms showing the individual particle size distribution of the AuPt nanoparticles supported on the SAS precipitation prepared LaBO<sub>3</sub> perovskite supports.

Where; LaCrO<sub>3</sub> (a), LaMnO<sub>3</sub> (b), LaFeO<sub>3</sub> (c), LaCoO<sub>3</sub> (d), and LaNiO<sub>3</sub> (e).

distribution and particle size to the single metal oxide supports described in the introduction and the previously tested TiO<sub>2</sub> support.

This may be expected due to the similar surface areas of 50-60 m<sup>2</sup>g<sup>-1</sup>, obtained by utilising the SAS precipitation technique to produce the perovskite supports.

#### 4.2.3.2. Microwave-plasma atomic emission spectroscopy

To view the composition of the Au and Pt nanoparticles and ensure a total loading of 1 wt % had been achieved through the sol-immobilisation preparation, microwave-plasma atomic emission spectroscopy (MP-AES) was conducted on each of the samples. It was found that, within reasonable error, that the Au and Pt wt % contribution was equal with each of the catalysts containing the desired 1:1 ratio of Au:Pt (Table 4.5.).

**Table 4.5 Au and Pt bulk and surface composition for AuPt/LaBO<sub>3</sub> catalysts analysed by MP-AES and XPS**

Support	Au and Pt content (wt.%)	Bulk Au/Pt ratio from MP-AES	Surface Au/Pt ratio from XPS
LaCrO <sub>3</sub>	0.55 (Au), 0.55 (Pt)	1.0	0.6
LaMnO <sub>3</sub>	0.47 (Au), 0.46 (Pt)	1.0	1.4
LaFeO <sub>3</sub>	0.46 (Au), 0.47 (Pt)	1.0	1.0
LaCoO <sub>3</sub>	0.55 (Au), 0.54 (Pt)	1.0	0.6
LaNiO <sub>3</sub>	0.50 (Au), 0.48 (Pt)	1.1	0.9

#### 4.2.3.3. X-ray photon spectroscopy

X-ray photon spectroscopy (XPS) of the prepared perovskite catalysts was used to provide insight into oxidation state of the metal nanoparticle and the relative Au-Pt surface composition. The XPS analysis of the Au and Pt 4f orbitals (Figure 4.5 and Table 4.5) showed that both the Au and the Pt were present in their metallic oxidation states, *i.e.* Au<sup>0</sup> and Pt<sup>0</sup>. It can be seen from Table 4.5 that the surface ratio obtained for the Au and Pt varied throughout the range of perovskite supports, from a minimum Au:Pt ratio of 0.6 for both the Cr and Co B site perovskites up to 1.4 for the Mn B site perovskite. As can be seen from the MP-AES results above, the bulk Au:Pt ratios were found to be the same for all of the prepared catalysts which possibly indicates that the change in surface ratio is influenced by changing the B site of the perovskite which, in turn, alters the metal nanoparticle structure. These changes can be attributed to

possible monometallic phases of the nanoparticles, a change in the composition of the alloying of the nanoparticles or potential formation of core-shell structures dependent on the potential interactions with the various B site cations<sup>12</sup>. Sol-immobilisation is also known to produce both core-shell and random alloys of AuPt nanoparticles, in which the various morphologies are well represented by the observed XPS metal ratios (*i.e.* Au:Pt ratio of 1:1 for random alloy or 0.75:1 for core-shell)<sup>13</sup>. Using Au and Pt makes discerning the reason for the change difficult because of the structural similarities, including close atomic numbers and weights, due to which X-ray spectroscopy techniques find the elements difficult to distinguish.

As shown from the XRD patterns, there are impurities ranging from 2-15 % according to the semi-quantitative phase analysis in the perovskite supports. The impurities must also be considered for their potential to influence the reaction, with the XPS analysis (Figure 4.5) showing a noticeable surface contribution from a La species which could be reasonably assigned to that of the oxide,  $\text{La}_2\text{O}_3$  or the hydroxide,  $\text{La}(\text{OH})_3$ . The B site perovskites with the lowest phased purity (Fe, Co and Ni) were found to have higher contributions of the La phases, which agrees with the data obtained through the XRD analysis.

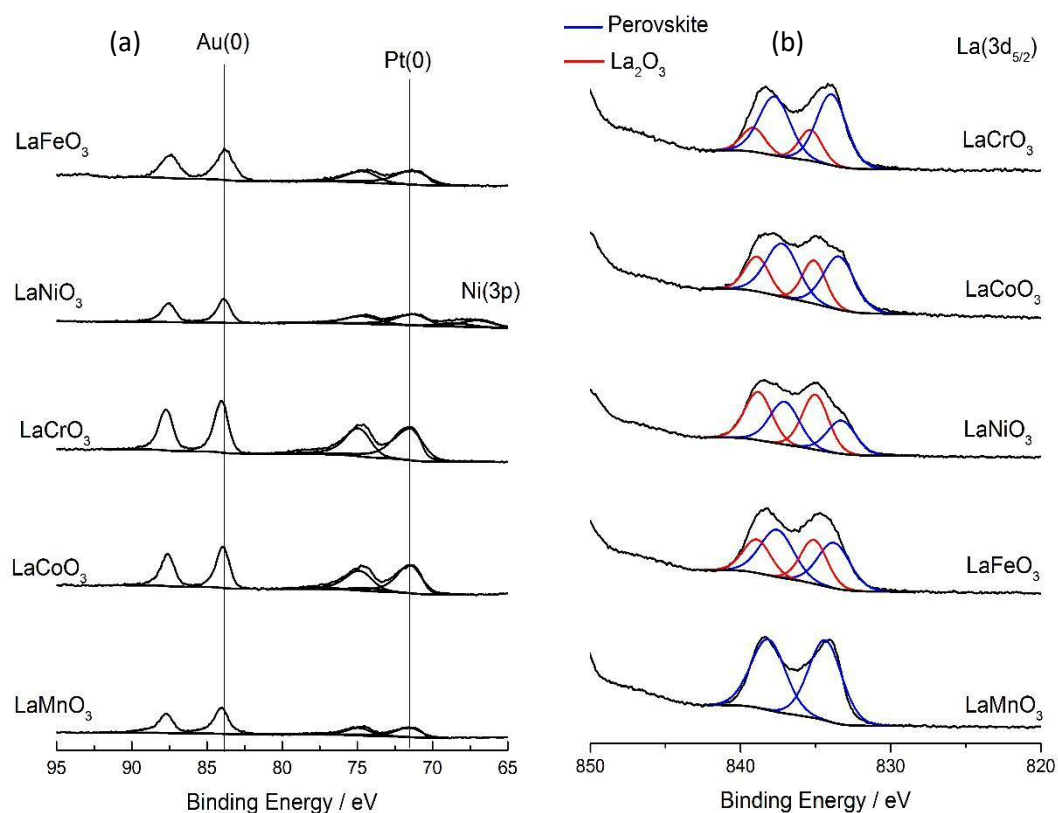


**Figure 4.5 XPS analysis of the prepared AuPt/ $\text{LaBO}_3$  catalysts. Where (a) Au (4f) and Pt (4f) and (b) La (3d<sub>5/2</sub>) spectra.**

#### 4.2.3.4. Ammonia temperature programmed desorption

To investigate the overall acidity of the perovskite supports, ammonia temperature programmed desorption (TPD) was conducted upon each of the samples (Figure 4.6). It has been found from previous TPD-MS studies that lattice oxygen contained within perovskites can potentially oxidise adsorbed ammonia into nitrous oxide and water. This ability to oxidise the ammonia increases the complexity of the desorption profiles as there are four potential desorbed species: (i)  $\text{NH}_4^+$  which is weakly bound to any hydroxyl groups on the surface of the perovskite, (ii)  $\text{NH}_3$  chemisorbed to any available Lewis acidic sites, (iii)  $\text{N}_2\text{O}$  formed *via* oxidation

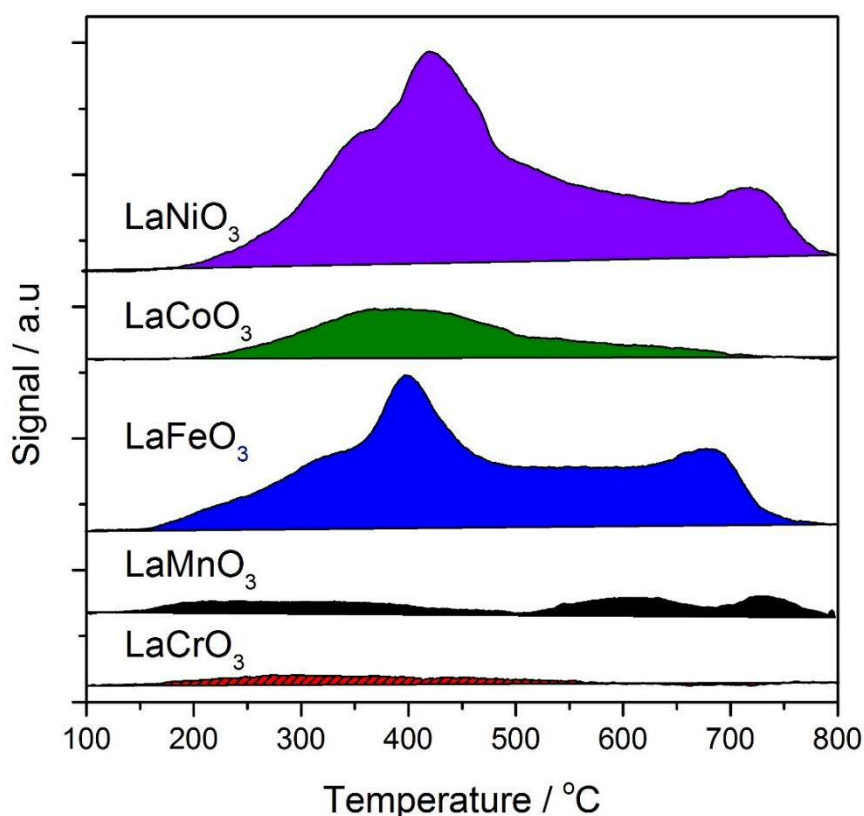


**Figure 4.6** Temperature programmed desorption profiles for the SAS precipitated perovskite supports.

with lattice oxygen and (iv) lattice oxygen desorption. Desorption profiles for type (ii) and (iii) will occur with available Lewis acid sites within the temperature range of 150 – 600 °C. These Lewis acid sites are present at the surface of single metal oxides due to the presence of metal cations which have an unsaturated coordination value. Desorption profiles associated with the loss of lattice oxygen (type iv) occur only with temperatures exceeding 500 °C.

It can be seen from the acid site analysis for Fe, Co and Ni B site perovskites, that a large desorption occurs between 200 – 400 °C, the temperature region associated with Lewis acid sites. The results complement the XRD data (Table 4.4.), in which the 10 – 15 % single oxide

impurities were found for the Fe, Co and Ni containing perovskites. Whilst the  $\text{LaFeO}_3$  and  $\text{LaNiO}_3$  impurities comprise mainly of  $\text{La}_2\text{O}_3$ , the  $\text{LaCoO}_3$  was found to contain the spinel phase  $\text{Co}_3\text{O}_4$  ( $\text{Co}^{\text{II}}\text{Co}^{\text{III}}_2\text{O}_3$ ). As the  $\text{LaMnO}_3$  and  $\text{LaCrO}_3$  contain the lowest impurities (<5 %) and also have very little ammonia desorption within the Lewis acid region, it can be suggested that at least a portion of the ammonia desorption can be attributed to the  $\text{La}_2\text{O}_3$  impurities Lewis acidic nature. The XPS data (Figure 4.5) also shows that in all the perovskites but the  $\text{LaMnO}_3$ , the  $\text{La}_2\text{O}_3$  is present with the  $\text{La}_2\text{O}_3$ :perovskite phase ratio being  $\text{LaNiO}_3 > \text{LaFeO}_3 > \text{LaCoO}_3 > \text{LaCrO}_3$ . Another notable feature of the desorption profiles of the  $\text{LaNiO}_3$ ,  $\text{LaFeO}_3$  and, to some extent,  $\text{LaMnO}_3$  is the exhibition of a desorption at high temperatures (650 – 700 °C), which would allude to the loss of oxygen from within the lattice of the perovskite structures.

### 4.3. Catalyst Testing

The conditions used for the glycerol oxidation testing are the bench mark results for the highest production of lactic acid from chapter 3. The reactions were all conducted within a Radley's starfish reactor. The reaction conditions were as follows; 100 °C, 0.3 M glycerol, 3 bar, 4:1 base ratio (NaOH), 900 rpm stirring speed, with 1000:1 metal:substrate ratio.

### 4.3.1. Unsupported perovskite supports

Prior to conducting any reactions with the supported perovskite catalyst samples it is imperative to know the effect the supports alone have on the reaction. Each of the perovskite supports were run under the bench mark conditions. As can be seen from Figure 4.7, there is no significant conversion of the glycerol over a period of 6 hours, showing that any activation of the reaction will be due to the nanoparticles deposited on to the surface.

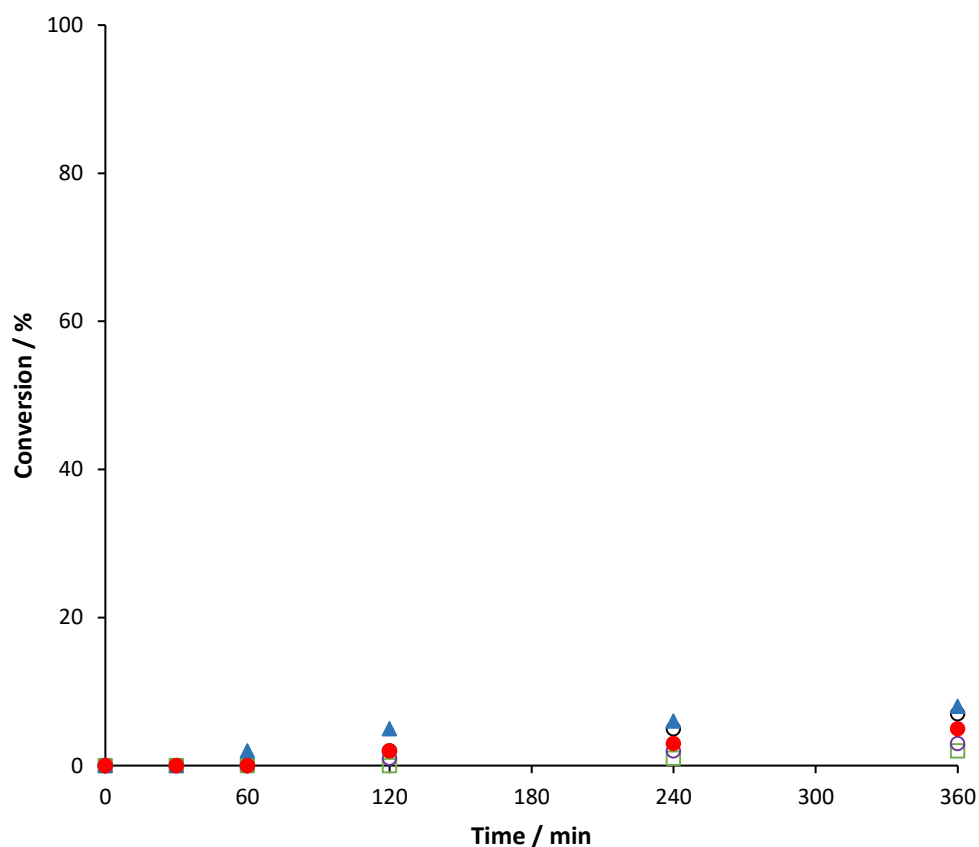


**Figure 4.7** The conversion of glycerol with unsupported perovskite supports where;

*LaCrO<sub>3</sub> (●) LaMnO<sub>3</sub> (○), LaFeO<sub>3</sub> (▲), LaCoO<sub>3</sub> (□) and LaNiO<sub>3</sub> (○).*

### 4.3.2. Supported precious metal catalyst testing

#### 4.3.2.1. Perovskite Supported catalysts

The advantage of the relatively high surface area obtained through utilising the SAS precipitation preparation for the perovskite supports enabled the deposition of Au and Pt on to the surface of each of the supports. This provides a higher availability of active sites for the reaction to proceed, potentially increasing activity. A total of 1 wt % AuPt was deposited on each, characterised in the section above, and tested under the bench-mark conditions for the liquid phase oxidation of glycerol.

The effect of interchanging the B site cation within the AuPt/LaBO<sub>3</sub> catalyst support was investigated, with the glycerol conversion profile reported below (Figure 4.8) and a table with turn over frequency (TOF) and product selectivity profile shown in table 6. The initial rates for each of the catalysts are of a similar magnitude, with AuPt/LaCrO<sub>3</sub> and AuPt/LaNiO<sub>3</sub> boasting the highest TOFs with 620 and 560 h<sup>-1</sup> respectively, with the remaining perovskites having TOFs between 440 – 460 h<sup>-1</sup>. Although there was no correlation between TOF and AuPt nanoparticle size, it is a reasonable assumption that the variation in TOF is due to the variation in specific surface area (Table 4.4), with the perovskites of higher surface area having higher TOFs. All of the calculated TOFs for the AuPt/LaBO<sub>3</sub> are comparable with that of the TOF for a standard 1

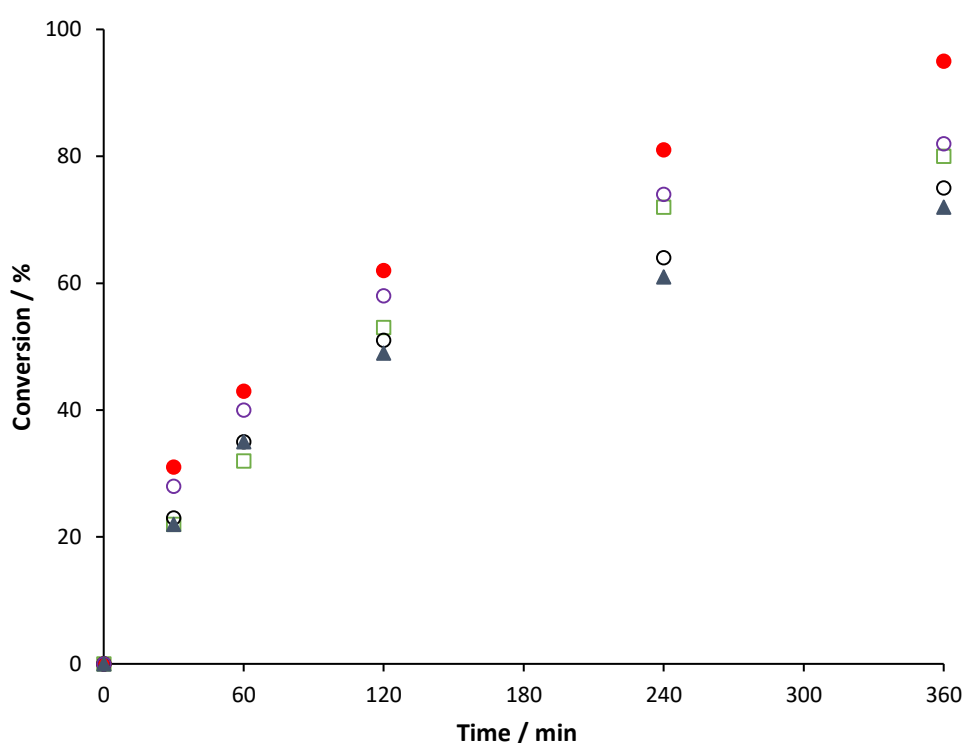


**Figure 4.8 Conversion profile for the AuPt/LaBO<sub>3</sub> where; LaCrO<sub>3</sub> (●) LaMnO<sub>3</sub> (○), LaFeO<sub>3</sub> (▲), LaCoO<sub>3</sub> (□) and LaNiO<sub>3</sub> (○).**

wt% AuPt/TiO<sub>2</sub>, which were calculated to be 520 h<sup>-1</sup> in the above Chapter 3. A comparable study using similar conditions (90 °C and a 4:1 base:substrate ratio) by Shen *et al.* who also utilised a 1 wt% AuPt/TiO<sub>2</sub>, found TOFs of 500 h<sup>-1</sup>.<sup>14</sup>

**Table 4.6 Turn over frequency and selectivity at  $t = 240$  mins for the AuPt/LaBO<sub>3</sub> catalysts.**

Catalyst	TOF (h <sup>-1</sup> )	Selectivity (%)			
		Glyceric acid	Tartronic acid	C-C scission	Lactic acid
<b>Perovskites</b>					
AuPt/LaCrO <sub>3</sub>	620	5	7	2	86
AuPt/LaMnO <sub>3</sub>	460	87	0	13	0
AuPt/LaFeO <sub>3</sub>	440	10	2	19	69
AuPt/LaCoO <sub>3</sub>	440	43	9	24	24
AuPt/LaNiO <sub>3</sub>	560	30	3	26	41
AuPt/TiO <sub>2</sub>	520	5	4	8	83

**Reaction conditions; 10 ml Glycerol (0.3 M), temperature (100 °C), O<sub>2</sub> pressure (3 bar), NaOH:substrate (4:1), substrate:metal ratio (1000:1) at 4 h reaction time.**

Whereas the conversion of glycerol remains fairly consistent between the different AuPt/LaBO<sub>3</sub> catalysts, the product selectivity profile shows a stark difference (Table 4.6). The LaMnO<sub>3</sub> supported catalyst was found to heavily favour the production of C<sub>3</sub> oxidation products, with a high selectivity to glyceric acid over a period of 6 hours and a relatively low selectivity to the potential C-C scission products (oxalic acid, glycolic acid, formic acid and CO<sub>2</sub>). Interestingly, the competing dehydration pathway to the lactic acid is completely turned off, with no lactic acid being observed under the same conditions that a AuPt/TiO<sub>2</sub> was found to produce up to 80 % selectivity in the previous chapter, chapter 3. The effect of increased temperature and base ratio has also previously been reported with the use of AuPt nanoparticles supported on CeO<sub>2</sub> and TiO<sub>2</sub>, giving lactic acid selectivities of values between 60 and 80 %.<sup>14, 15</sup> Conditions that have been shown to favour glyceric acid production have been reported as temperatures of 60 °C with a lower base ratio of 2:1, with the selectivity to glyceric acid achieved of up to 80 %;<sup>13</sup> which are similar results to that of the AuPt/LaMnO<sub>3</sub> catalyst shown here. Selectivity profiles for the AuPt/LaCoO<sub>3</sub> and AuPt/LaNiO<sub>3</sub> show very similar behaviour, maintaining a moderate selectivity to the glyceric acid, a relatively high amount of C-C scission, and a selectivity of 24 and 41 % to lactic acid respectively.

A noticeable feature from the conversion/selectivity profile (Figure 4.9.) is a pointed change in selectivity towards particular products as the glycerol is consumed. The AuPt/LaNiO<sub>3</sub> catalyst (Figure 4.9. (e)) shows a decrease in selectivity towards glyceric acid as the conversion

of glycerol rises from 31 % to 82 %. The decrease in glyceric acid was not observed as the sequential oxidation to tartronic acid, but rather an increase in the production of lactic acid *via* the dehydration pathway, showing an alteration in the preferred pathway from oxidation to dehydration. Although this trend is not followed by each of the supported perovskites, each of them exhibit a change in which pathway is favoured. At lower conversions of glycerol, the AuPt/LaFeO<sub>3</sub> (Figure 4.9 (c)) had no preferential pathway with oxidation products totalling 51 % (25% C-C scission and 25% glyceric acid selectivity) and 50 % lactic acid selectivity. As the reaction progresses with more glycerol converted, the selectivity to glyceric acid drops dramatically due to (i) a lack of production and (ii) C-C scission from the glyceric acid already formed. The lactic acid selectivity increases from 50 % to 69 % over the full duration of the reaction. With a total of 69 % lactic acid selectivity, the AuPt/LaFeO<sub>3</sub> has comparable activity towards previously reported catalysts under similar conditions.<sup>16</sup> The change in the selectivity towards lactic acid was the most pronounced with the AuPt/LaFeO<sub>3</sub> catalyst suggesting that the oxidation sites on the surface of this catalyst are either blocked by reactions intermediates or have low stability.

The catalyst that presented the highest selectivity to lactic acid was the AuPt/LaCrO<sub>3</sub> (Figure 4.9 (a)), producing a yield of 82 % (86 % selectivity to lactic acid and 95 % conversion of glycerol). Whereas the AuPt/LaFeO<sub>3</sub> catalyst was observed to be sensitive to conversion of glycerol, the AuPt/LaCrO<sub>3</sub> had only a slight increase in selectivity to lactic acid, from 80 % - 86 % throughout the whole reaction. With the highest TOF of 620 h<sup>-1</sup>, the highest selectivity to lactic acid of all of the perovskite supported catalysts, and a higher selectivity and yield to lactic acid than the bench mark AuPt/TiO<sub>2</sub> reported in Chapter 3, it can be concluded the AuPt/LaCrO<sub>3</sub> is a highly effective catalyst for the production of lactic acid from glycerol.

It is clear from these results that there is a significant variation in the selectivity profiles at similar activities for each of the perovskite supports, with the alteration of the B site controlling this effect. By using Mn as the B site, there is a clear suppression of the dehydration pathway to lactic acid, with glyceric acid being the dominant product formed. Both the Cr and Fe B site perovskite supports showed an enhanced dehydration pathway, forming the highest selectivity to lactic acid, whereas the Ni and Co B site perovskites had a lower control over the competing pathways, producing both oxidation and dehydration pathway products. As shown in the reaction scheme (Scheme 1), the intermediate product for both glyceric acid/tartronic

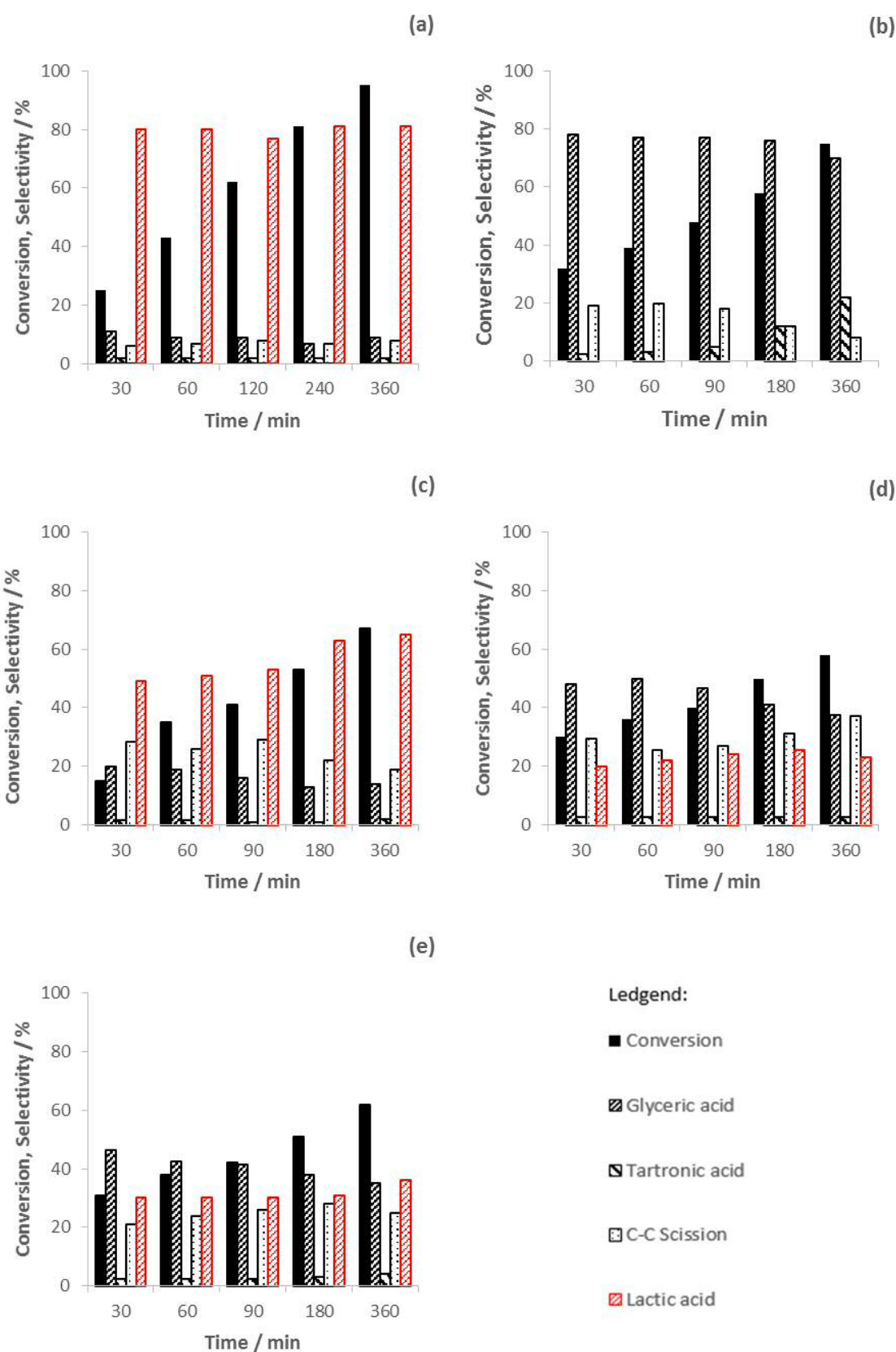


**Figure 4.9 Conversion/Selectivity time on line profiles where; (a) LaCrO<sub>3</sub>, (b) LaMnO<sub>3</sub>, (c) LaFeO<sub>3</sub>, (d) LaCoO<sub>3</sub> and (e) LaNiO<sub>3</sub>.**

acid and lactic acid is glyceraldehyde. The rate limiting step for this reaction can be considered

to be the initial proton abstraction from glycerol, forming the alkoxy intermediate and, as the glyceraldehyde is only observed without a base present, this leads to significant changes in product distribution with the similar catalyst activities.

As mentioned previously in the introduction (Chapter 1), perovskite catalysts have been investigated for the deep oxidation of alkanes, alkenes and CO. It was found that there was a positive link between the activity of the perovskite catalysts and their inherent O<sub>2</sub> coverage profiles, with the perovskites with higher O<sub>2</sub> adsorption capabilities attaining higher activity. The chemisorption of O<sub>2</sub> and isobutene on a range of LaBO<sub>3</sub> catalysts was investigated by Tejuca *et al.* utilising the same range of B site perovskites as those chosen for the above work (Cr, Mn, Fe, Co and Ni). An interesting trend was observed when considering the adsorption data of O<sub>2</sub> on the clean surfaces of the B site perovskites from the work conducted by Tejuca *et al.* and the selectivity profiles of the various AuPt/LaBO<sub>3</sub> perovskite catalysts tested above (at the 6 h end

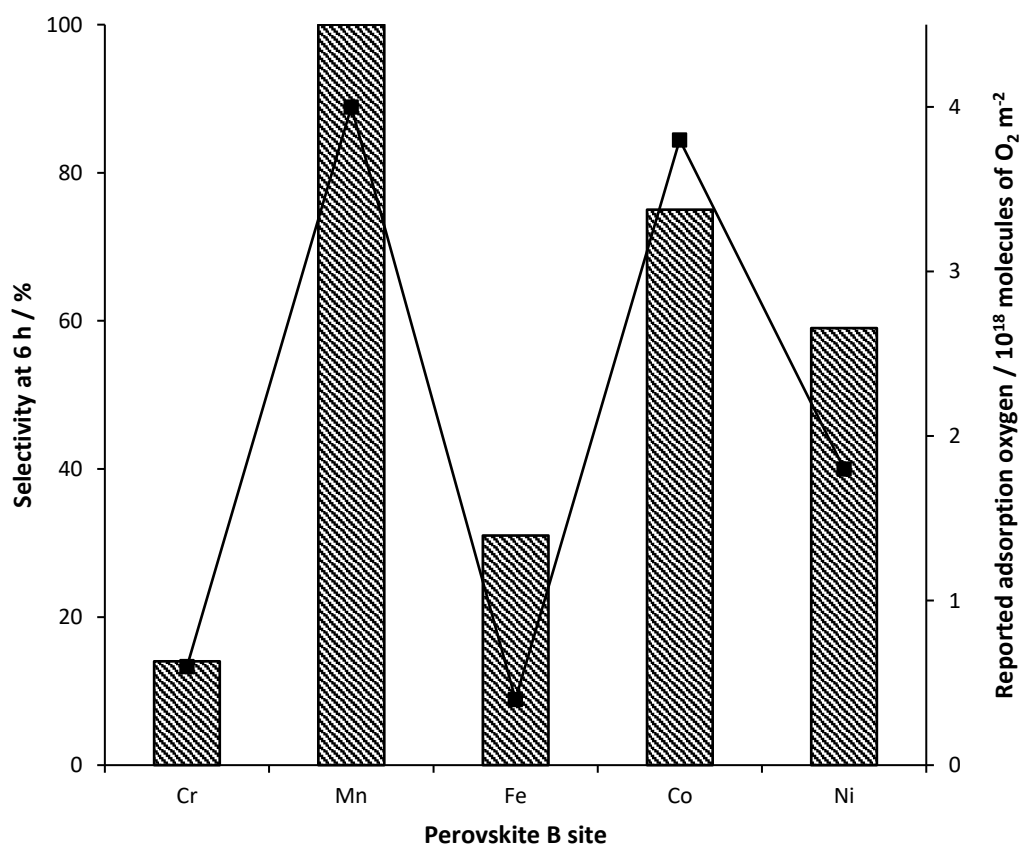


**Figure 4.10** Selectivity profiles of the AuPt/LaBO<sub>3</sub> catalysts against the reported oxygen adsorption values for the corresponding perovskite phases<sup>1</sup>. The sum of the C3 products (glyceric acid, tartronic acid and C-C scission) are shown by the black dashed lines. Read from the right-hand y axis is the reported oxygen adsorption values of the B site perovskites (■).

point of the reaction). By plotting the adsorption of oxygen to a clean perovskite surface against the total selectivity of oxidation products (glyceric acid, tartronic acid and C-C scission products) a correlation between the data can be seen (Figure 4.10). If C-C scission products are assumed to be produced from an oxidation process, the sum of the oxidation pathway products correlate well with the reported oxygen adsorption capacities. The most selective catalyst towards the oxidation pathway used the  $\text{LaMnO}_3$  support, which has the best oxygen adsorption capacity. The  $\text{LaCrO}_3$  and  $\text{LaFeO}_3$  supports, with poor oxygen adsorption characteristics, were found to yield catalysts that favour the production of lactic acid, which is formed from an initial oxidation followed by dehydration to pyruvaldehyde and rearrangement. The  $\text{LaCoO}_3$  and  $\text{LaNiO}_3$  supported catalysts were found to produce both oxidation and the dehydration products that correspond to the intermediate oxygen adsorption capacities. An interesting point highlighted in Tejuca and co-workers' paper was that  $\text{O}_2$  capacities were enhanced on the addition of the iso-butane substrate for all B site perovskites, but disproportionately across the period (i.e. the effect was more significant for Co than Mn B sites).

#### 4.3.2.2. Supported single oxide supports

Having discovered such a vast difference in the selectivity profile between the ranges of B site perovskite supports, it was important to investigate if this was potentially due to the single oxide phases present within the impurities of the perovskite samples. A series of sol immobilised 1 wt % AuPt catalysts were prepared upon the corresponding single metal oxide supports ( $\text{MnO}_2$ ,  $\text{Fe}_2\text{O}_3$ ,  $\text{Co}_3\text{O}_4$  and  $\text{NiO}$ ), also prepared *via* the SAS precipitation technique. Each of the supports were calcined at the same temperature as the perovskites (750 °C) to ensure similar surface areas and tested under the same conditions for glycerol oxidation as described above (Table 4.7).

Immediately it can be seen that the TOFs for the single metal oxides have a much wider range (180 – 700  $\text{h}^{-1}$ ) than their perovskite supported counterparts, with noticeably higher TOFs for the  $\text{NiO}$  and  $\text{MnO}_2$  single metal oxide supported catalysts than their perovskite counterparts. None of the tested single metal oxide counterparts had better selectivity control than the supported perovskites, especially in the case of the  $\text{MnO}_2$  which produced a 33 % selectivity to glyceric acid, whereas the  $\text{AuPt/LaMnO}_3$  produced 87 % of the glyceric acid or the high lactic acid selectivity produced by the  $\text{AuPt/LaFeO}_3$  (69 %) against the  $\text{Fe}_2\text{O}_3$  (21 %).

**Table 4.7 Turn over frequency and selectivity at t = 240 mins for single metal oxide catalysts.**

Catalyst	TOF (h <sup>-1</sup> )	Selectivity (%)			
		Glyceric acid	Tartronic acid	C-C scission	Lactic acid
<b>Single metal oxides</b>					
AuPt/MnO <sub>2</sub>	560	33	3	33	31
AuPt/Fe <sub>2</sub> O <sub>3</sub>	240	19	2	58	21
AuPt/Co <sub>3</sub> O <sub>4</sub>	180	23	4	24	49
AuPt/NiO	700	30	10	39	21

**Reaction Conditions; 10 ml Glycerol (0.3 M), temperature (100 °C), O<sub>2</sub> pressure (3 bar), NaOH:substrate (4:1), substrate:metal ratio (1000:1) at 4 h reaction time.**

Comparative studies with Au/NiO have been conducted by Villa *et al.* in which they found that the NiO supported catalyst was highly active, but had a poor selectivity distribution.<sup>17</sup> It can be concluded from these results that the effect of controlling the selectivity distribution is a unique effect with the perovskite supports and not the single metal oxides.

#### 4.4. Selective formation of value added products

The ability to control the selectivity distribution of specific products for a reaction is highly desirable. Two of the perovskites tested show promising results for the ability to selectively produce glyceric acid/tartronic acid and lactic acid (LaMnO<sub>3</sub> and LaCrO<sub>3</sub> respectively). The conditions were kept the same for each of the reactions as previous testing (100 °C, 4:1 base: substrate, 3 bar O<sub>2</sub>, 900 rpm stirring, 1000:1 metal:substrate). Although there is a clear difference between the two supports, it is extremely difficult to observe exactly why this is the case, as it is likely due to a surface interaction between the support and substrate material which would likely involve some complex molecular modelling to resolve clearly. This would be my next step of investigation, if the resources were available in the scope of this thesis.

##### 4.4.1. Selective control for the production of glyceric and tartronic acid

One of the most significant results from the initial testing was that the AuPt/LaMnO<sub>3</sub> appeared to completely inhibit the dehydration pathway to lactic acid under the same conditions that would usually favour said pathway. This effect presents itself by selectively promoting a more strenuous oxidation pathway, allowing the further oxidation of glyceric acid to tartronic acid at relatively low selectivity over a 6 h period. These results suggest that a longer reaction time may

lead to an increased conversion of glyceric acid to form a higher yield of tartronic acid, which, given the functionalisation of the molecule, make tartronic acid a high value added product, which is desirable to form selectively.

#### **4.4.1.1. Effect of metal ratio on selectivity**

As the catalytic effect of the support is purely a control of the selectivity breakdown and not the activity of the catalyst itself, the ratio of the Au:Pt deposited on the surface of the  $\text{LaMnO}_3$  was altered to observe the effect on the selectivity profile.

It can be seen from the conversion/selectivity profiles (Figure 4.11.) that the Au/ $\text{LaMnO}_3$  (Figure 4.11. (a)) produces the highest selectivity towards tartronic acid at 71%, but the conversion of glycerol plateaus at 62 %. This is potentially due to the inability to remove substrate from the surface of the catalyst, a characteristic enabled by the addition of Pt. As the ratio of Pt increases, so too does the activity of the prepared catalyst, with the overall conversion over a 6 h period increasing from 62 % (Au only, Figure 4.11 (a)) to 88 % (Pt only, Figure 4.11. (e)). The detrimental effect of increasing the activity of the catalyst is twofold, (i) the production of C2 and C1 C-C scission products increases, (ii) the barrier to the dehydration pathway becomes less pronounced, beginning to form small amounts of lactic acid. It was found that the ideal balance between the ratios tested was the 1:1 Au:Pt/ $\text{LaMnO}_3$ , in which the conversion maintained a steady increase towards the 6 h end point (75 % conversion of glycerol), whilst still suppressing the formation of lactic acid, and maintaining a low selectivity to the C-C scission products.

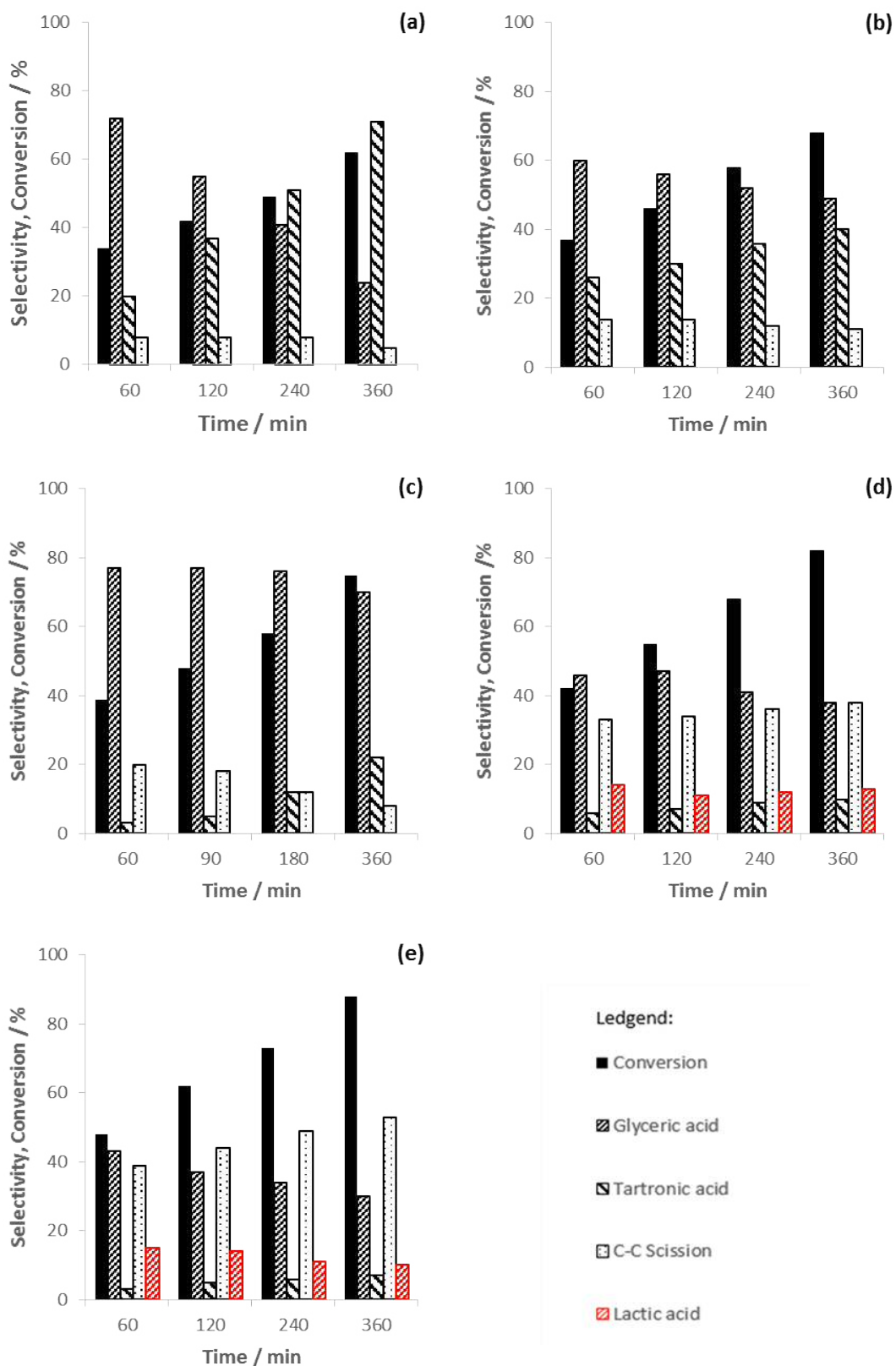


**Figure 4.11 Conversion and selectivity profiles of various AuPt/LaMnO<sub>3</sub> ratios where; (a) Au, (b) 1:3 Au:Pt, (c) 1:1 Au:Pt, (d) 3:1 Au:Pt and (e) Pt.**

#### 4.4.1.2. Selective formation of tartronic acid

Whilst low selectivities of tartronic acid were obtained at low conversion, the majority of tartronic acid is formed as a further oxidation of glyceric acid at higher conversions of glycerol. The hypothesis that obtaining a higher yield of tartronic acid was tested by extending the reaction from 6 h to 24 h to view how the selectivity profile altered (Figure 4.11/12/13). After 10 h it can be seen that the conversion of glycerol has reached 100 %, with the selectivity of glyceric acid being 66 % and the tartronic acid at 22 %. During this time there is only a marginal increase in the selectivity to tartronic acid from the 6 h point, where the total selectivity was 18 %. Once the glycerol had been entirely consumed at the 10 h point, the molar concentration (Figure 4.12) clearly indicates the glyceric acid is being converted to tartronic acid. It can be seen that by using harsher reaction conditions than would traditionally be used for the formation of glyceric acid (60 °C, 2:1 base:substrate ratio) that the sequential oxidation is promoted, allowing

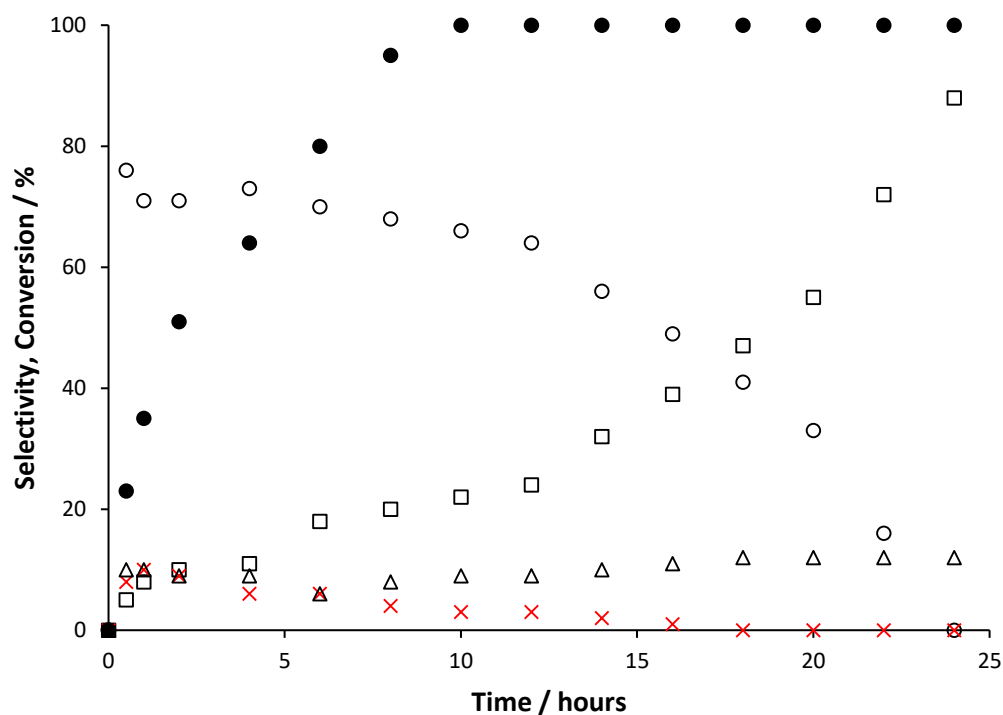


**Figure 4.12 Conversion/selectivity profile for the 24 h extended time line for AuPt/LaMnO<sub>3</sub> where; Conversion (●), glyceric acid (○), tartronic acid (□), C-C scission (Δ) and lactic acid (x).**

for high yields of tartronic acid to be formed. Over the 24 h period a total selectivity of 88 % tartronic acid was obtained, with the remaining 12 % being C-C scission products. At 100 % conversion, the selectivity of tartronic acid translates to an 88 % yield, which compared to current literature, is an exceptionally high yield that is enabled by the use of harsher conditions

(100 °C, 4:1 base:substrate ratio) and the ability of the catalyst to selectively promote the oxidation pathway.

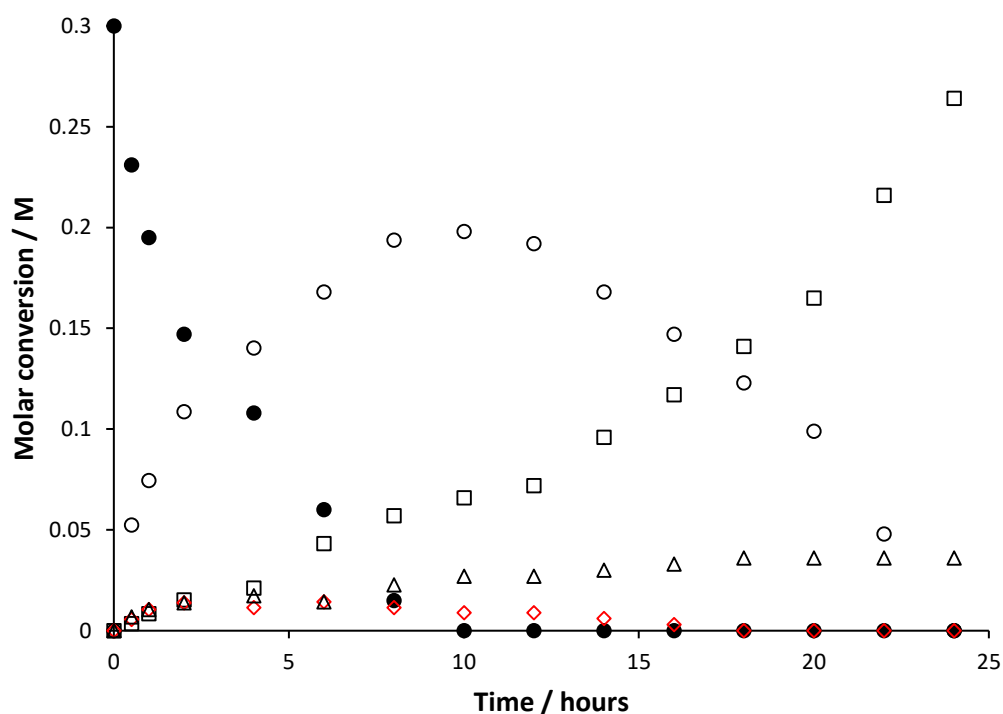


**Figure 4.13** Molar concentration plot for AuPt/LaMnO<sub>3</sub> where; Conversion (●), glyceric acid (○), tartronic acid (□), C-C scission (Δ) and lactic acid (◇).

#### 4.4.1.3. Kinetic model for AuPt/LaMnO<sub>3</sub> from initial rates

Understanding the specific reason why the LaMnO<sub>3</sub> perovskite support has the ability to enhance the oxidation pathway is a challenging problem, as viewing the surface of the support is virtually impossible through readily available techniques such as IR drifts and UV spectroscopy due to the support being a deep black, essentially absorbing the radiation and producing no discernible signal. The problem becomes more difficult in that the Au and Pt are indistinguishable using X-ray techniques, and therefore viewing the morphology of the nanoparticles would be extremely challenging without a computational model to support current findings. By producing a kinetic model through the initial rates method, the activation barrier to the oxidation pathway can be observed and compared to the kinetic model calculated in chapter 2, showing the activation energy of lactic acid.

The reaction order with respect to the reactants can be written in the following form;

The reaction order with respect to the reactants was found to be 1<sup>st</sup> order for each through the initial rates method (Figure 4.14.). The % conversion for the base ratio (Figure 4.14. (c)) was corrected with a blank reaction, as the conversion of glycerol can occur under base free conditions.

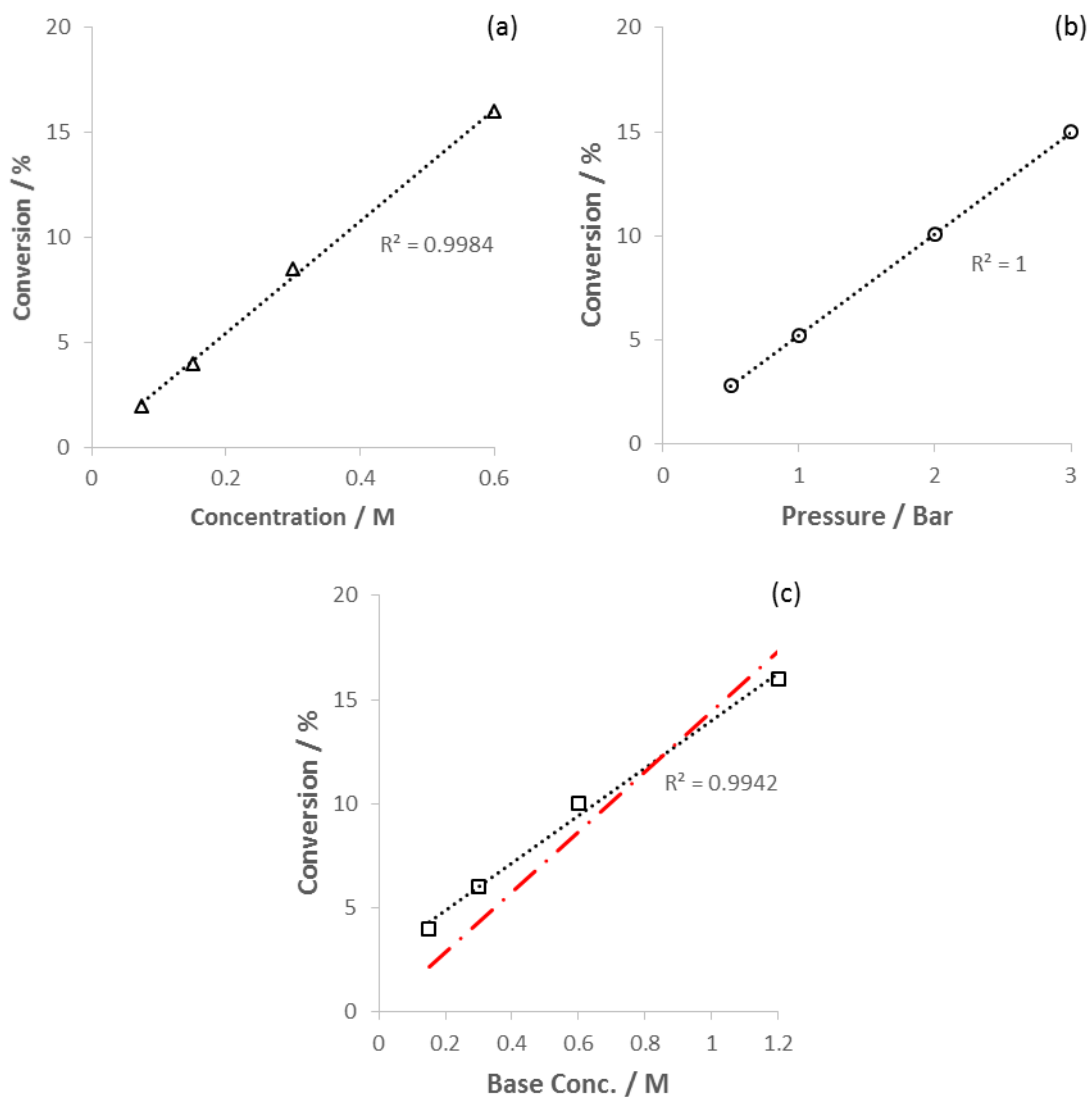


**Figure 4.14 Initial rates at  $t = 30$  mins for AuPt/LaMnO<sub>3</sub> at standard conditions altered singularly to determine rate with respect to each reactant where; (a) Altering glycerol concentration, (b) altering O<sub>2</sub> pressure, and (c) altering base:substrate ratio.**

An Arrhenius plot (Figure 4.15) was then used to determine the activation energy for the oxidation pathway. The dehydration pathway is not considered in this energy calculation as the breakdown of products for the 1:1 AuPt/LaMnO<sub>3</sub>, show no formation of lactic acid. This method also makes the assumption that the rate limiting step is the initial oxidation to the

glyceraldehyde, as this product is never viewed within the selectivity profile. The activation can be found by rearranging the Arrhenius equation from;

To the form;

— —

Therefore;

As was found in chapter 3, the activation energy for the formation of lactic acid on a AuPt/TiO<sub>2</sub> was 41.99 KJ mol<sup>-1</sup>, and although the values are not for the same catalyst, it can be seen that the energy barrier to glyceric acid/tartronic acid for the AuPt/LaMnO<sub>3</sub> is lower than that for the formation of lactic acid under the same conditions with one of the leading catalysts for lactic acid production. This is potentially due to the ability to adsorb oxygen to the surface on the AuPt/LaMnO<sub>3</sub>, as demonstrated in Figure 4.10, lowering the activation energy barrier for the production of glyceric/tartronic acid.

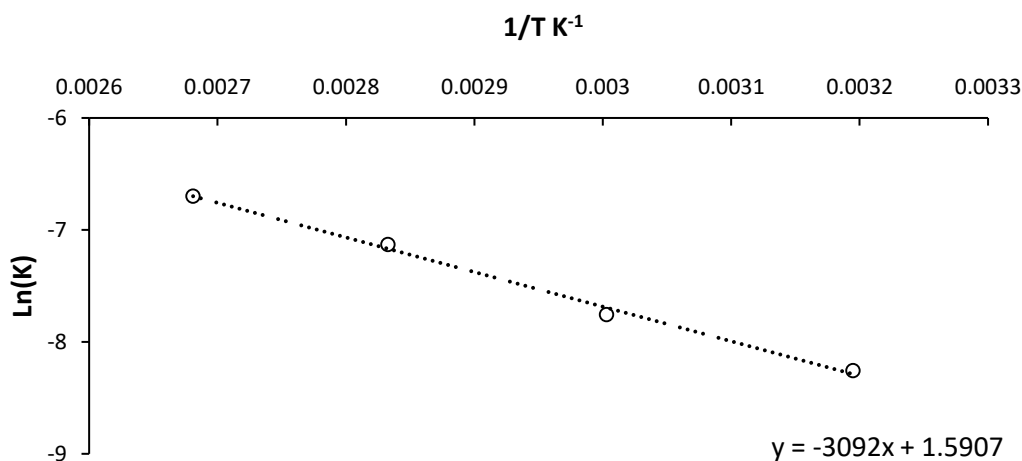


**Figure 4.15 Arrhenius plot for AuPt/LaMnO<sub>3</sub>**

#### 4.4.2. Selective formation of lactic acid

Selectively forming lactic acid from glycerol is also a highly sought after commodity due to its uses for biodegradable plastics. It can be seen from the previous results that the AuPt/LaCrO<sub>3</sub> showed promising results for producing high yields of lactic acid.

#### 4.4.2.1. The effect of metal ratio

As previously mentioned, the effect of the support appears to control the route by which the reaction proceeds, either the further oxidation or the dehydration pathway to lactic acid. To view the effect of the Au:Pt ratio a series of catalysts were prepared with varying ratios (Au only, 3:1 Au:Pt, 1:1 Au:Pt, 1:3 Au:Pt, and Pt only).

It can be seen from the conversion and selectivity profiles (Figure 4.16.), when using the Au/LaCrO<sub>3</sub> that there was a very high selectivity towards lactic acid at 6 h (91 %), however, a similar issue with deactivation appears to occur, resulting in the yield of lactic acid to only be at 58 % (Table 4.8.).

Metal Ratio / Au:Pt	Yield of lactic acid at 6h / %
1:0	58
3:1	65
1:1	77
1:3	77
0:1	60

**Table 4.8 Percentage yields of lactic acid for the various Au:Pt ratios supported on LaCrO<sub>3</sub> at 6 h.**

As the ratio of Pt increases, the activity of the catalysts increases, reaching a conversion of 95 % of glycerol in 6 h with the 1:1 AuPt/LaCrO<sub>3</sub>, with a selectivity of 81 % and a 77 % yield. As the amount of Pt increases in the 1:3 AuPt/LaCrO<sub>3</sub>, there is an increased proportion of C-C scission products, and a lowering of the selectivity to lactic acid, indicating that under these conditions, the C-C scission is occurring on the lactic acid also. This only seems to be the case with the addition of an excess of Pt, with the Pt/LaCrO<sub>3</sub> causing a largest proportion of C-C scission overall at the detriment to the production of lactic acid, with a yield of only 60 %.

The results indicate that a 1:1 AuPt/LaCrO<sub>3</sub> is the most selective catalyst, with the highest yield of lactic acid from the range tested, as the Pt enhances the activity of the catalyst, but with an excess causing C-C scission, which are undesirable for the selective formation of lactic acid.

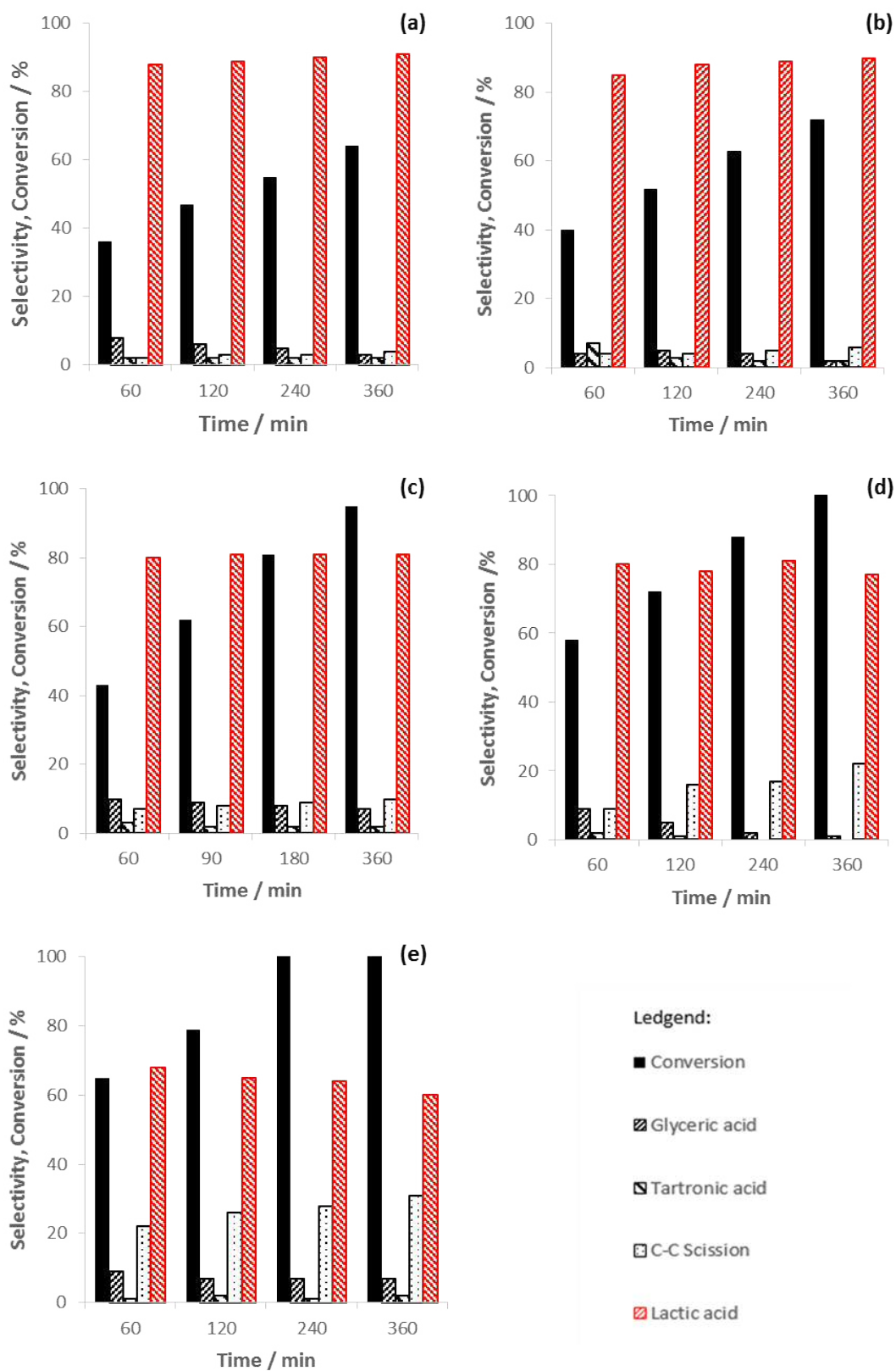


**Figure 4.16 Conversion and selectivity profiles of various AuPt/LaCrO<sub>3</sub> ratios where; (a) Au, (b) 1:3 Au:Pt, (c) 1:1 Au:Pt, (d) 3:1 Au:Pt and (e) Pt.**

#### 4.4.2.2. Selective formation of lactic acid

Utilising the 1:1 AuPt/LaCrO<sub>3</sub>, a 24 hour time on line study was conducted in order to view how the lactic acid selectivity was affected after the catalyst had converted the glycerol completely. It can be seen that the selectivity to lactic acid is maintained around 80 % as the glycerol is being consumed, with the highest selectivity and yield of lactic acid reaching 85 % at 100% conversion (Figure 4.17). After this point, the C-C scission begins to increase steadily as the lactic acid selectivity decreases; which when viewed in a molar conversion plot (Figure 4.18) can be seen to be a reciprocal relationship in which the lactic acid is being converted to C2 and C1 products, although the conversion of lactic acid stabilises around 60 %. This relationship suggests two effects working in tandem, (i) the lactic acid is relatively unstable under the reaction conditions at higher concentrations and (ii) the energy required to cause the C-C scission is higher than that of the glycerol conversion to lactic acid as the C-C scission only increases significantly once the glycerol concentration is severely depleted.

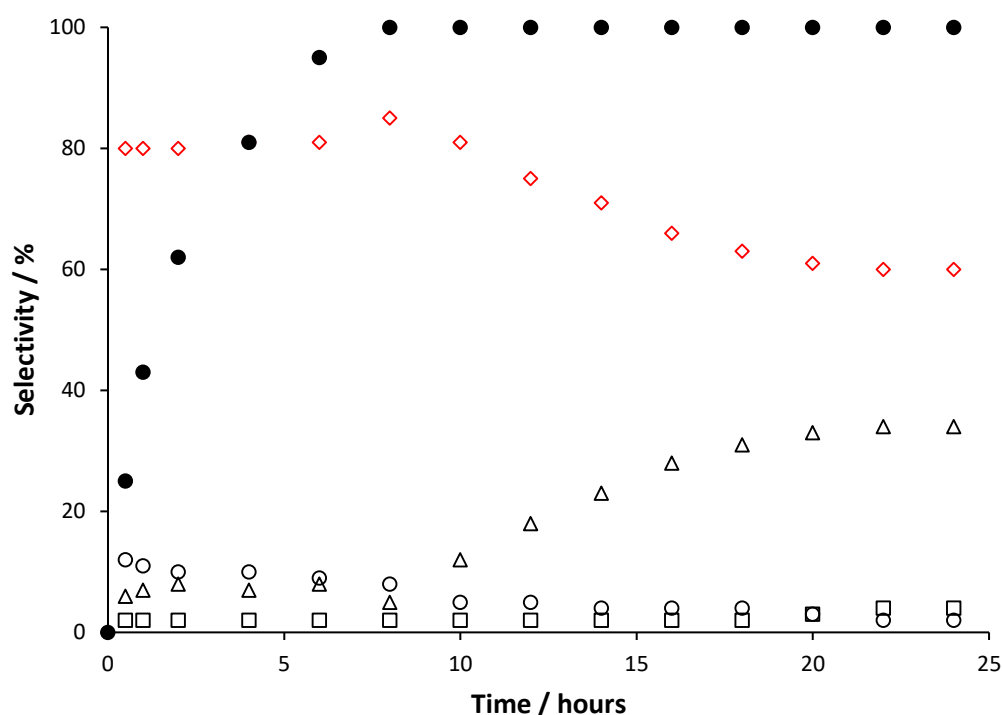


**Figure 4.17 Conversion/selectivity profile for the 24 h extended time line for 1:1 AuPt/LaCrO<sub>3</sub> where; Conversion (●), glyceric acid (○), tartronic acid (□), C-C scission (Δ) and lactic acid (◇).**

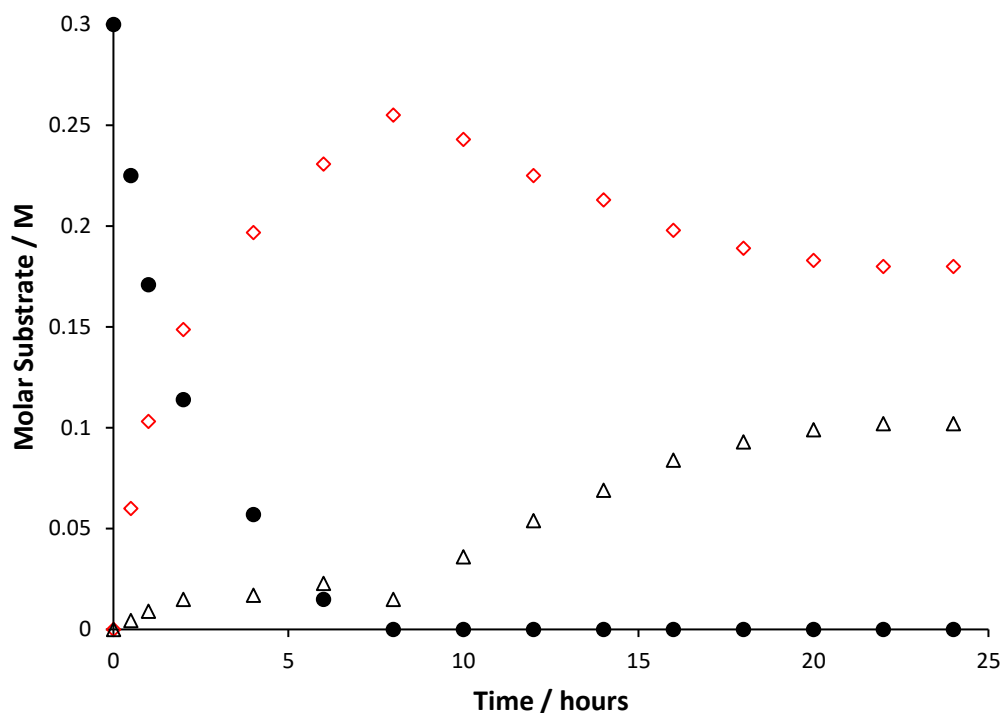


**Figure 4.18** Molar concentration plot for AuPt/LaMnO<sub>3</sub> where; Conversion (●), glyceric acid (○), tartronic acid (□), C-C scission (Δ) and lactic acid (◇).

#### 4.5. Comparing support preparation techniques

The SAS precipitation technique provides several advantages including the access to higher surface area perovskite supports as the energy barrier to form the pure phases for the perovskites is lowered when compared to other methods, allowing for lower calcination temperatures. A comparison between other preparation techniques was needed to observe whether the trend observed was unique to the SAS precipitated perovskite supports, with mechanochemical synthesis (planetary ball milling) utilising the single metal oxides and flame pyrolysis using metal nitrate solutions chosen as the comparative techniques

The planetary ball milling (BM) preparation was chosen as the method, which, in theory, should contain minimal impurities as the only precursors used are the single metal oxides, with no organic residual species present. Flame spray pyrolysis (FP) was chosen as another technique as it has been shown to produce materials of low crystallite size and high surface areas<sup>18</sup>. XRD analysis of the LaMnO<sub>3</sub> prepared by three methods (Figure 4.19) showed that all the prepared

samples have the same perovskite phase present, although the phase purity ranged between 90 – 100 % (Table 4.9).

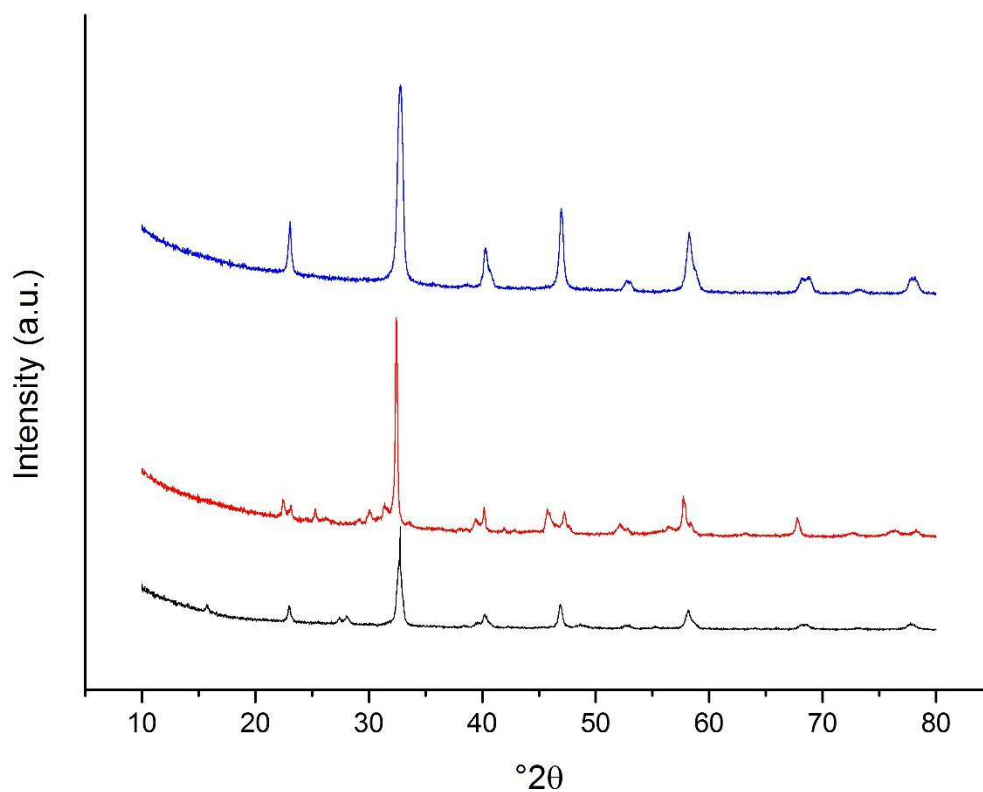


**Figure 4.19** Powder X-ray diffraction patterns of  $\text{LaMnO}_3$  prepared by SAS precipitation (blue), Flame pyrolysis (red) and ball milling (black).

**Table 4.9** Comparative physical properties of  $\text{LaMnO}_3$  prepared through SAS, FP and BM

*\*Determined through XRD analysis*

Preparation method	$\text{LaMnO}_3$ purity(%)*	phase	Crystallite size (nm)*	Surface area ( $\text{m}^2\text{g}^{-1}$ )
SAS precipitation	100		18	32
Flame spray pyrolysis	95		25	15
Mechanochemical	90		40	1

The preparation methods provide different physical properties to the perovskite supports, with the BM preparation producing the highest crystallite sizes and lowest surface areas which are comparable with typical perovskite materials. The surface area produced *via* FP method was found to be much higher than the BM preparation at  $15 \text{ m}^2 \text{ g}^{-1}$ , although this value was still lower than the perovskites developed through the SAS precipitation method.

These perovskite samples were used as supports for 1 wt % AuPt by the same method as previously reported followed by testing under the same conditions for glycerol oxidation as conducted above (Figure 4.11). As the surface areas of the comparative methods were lower than that of the SAS precipitation, it is theorised that the activity of the FP and BM catalysts would be lower than that of the SAS precipitated catalysts. Having a reduced surface area decreases the number of available sites on which to deposit AuPt nanoparticles, thereby reducing dispersion of the metals which effectively reduces the number of active sites available of the surface, resulting in a lower conversion. This effect had been demonstrated in Figure 4.20.

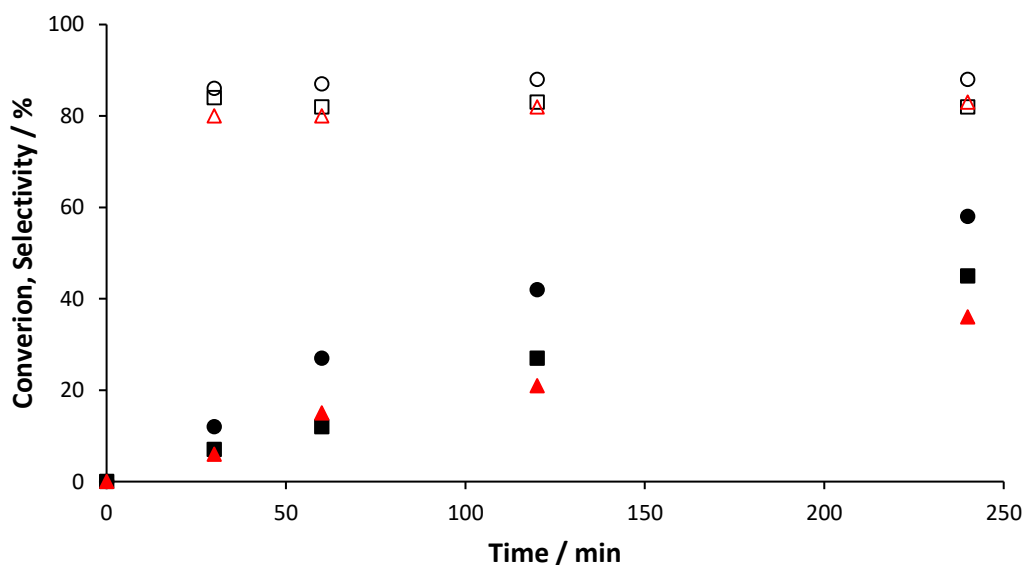


**Figure 4. 20 Conversion, selectivity plot showing the conversion of glycerol in solid markers where; SAS (●), FP (■) and BM (▲) and the selectivity to C<sub>3</sub> oxidation products where; SAS (○), FP (□) and BM (△).**

Where the conversion of the glycerol was lower with the other preparation methods, a fact that is likely linked to the lower surface area having fewer active sites available, the key observation is that the specific preparation method doesn't significantly alter the selectivity profile, with almost identical selectivities to the C<sub>3</sub> oxidation products, *i.e.* glyceric acid and tartronic acid. This finding illustrates an important factor; that the inhibition of the dehydration

pathway (or promotion of the oxidation pathway) is not specific to the SAS preparation technique, therefore, provided a sample of  $\text{LaMnO}_3$  can be produced with a sufficiently high surface area, a catalyst with a strong and selective oxidation capability can be produced.

#### 4.6. Conclusions

Perovskite type mixed metal oxides traditionally have low surface area due to the necessity for high temperatures to form the pure phase. Low surface area makes these materials unsuitable for use as supports for nanoparticles, as it has been shown that well dispersed nanoparticles are active catalytically and stable. By utilising the SAS precipitation technique, a series of perovskite type mixed metal oxides have successfully been formed with sufficient surface area to be used as supports for precious metal nanoparticles in the liquid phase oxidation of glycerol. The range of  $\text{LaBO}_3$  supports were B site substituted with a variety of transition metal cations (where B is Cr, Mn, Fe, Co and Ni), with surface areas ranging between 22 and  $52 \text{ m}^2 \text{ g}^{-1}$ .

The addition of 1 wt % AuPt nanoparticles was achieved through sol-immobilisation, as this preparation method allows for excellent dispersions of a low distribution of nanoparticles upon the surface of a support to make active glycerol oxidation catalysts. Utilising the conditions obtained through the experimental work conducted in chapter 3, the selectivity profile of the reaction was controlled allowing for the selective production of glyceric acid/tartronic acid through the oxidation pathway, or the selective production of lactic acid through the dehydration pathway.

The ability to control which pathway was favoured was enabled by selecting a particular B site perovskite, where Co/Ni formed a broad selectivity distribution, Cr/Fe favoured the dehydration pathway enabling a high selectivity to lactic acid, and Mn provided an enhanced oxidation route forming high selectivities to glyceric acid with longer reaction times further oxidising to tartronic acid. The use of single metal oxide counterparts resulted in a loss of control to the selectivity breakdown of the products.

The use of AuPt nanoparticles was found to be necessary as the perovskite supports were almost completely inactive for glycerol oxidation, with the choice of B site in the perovskite structure having no discernible effect on the AuPt nanoparticle size.

A strong correlation was found between the reported oxygen adsorption capability of the various B site perovskite supports and the selectivity distribution from glycerol oxidation. Low oxygen adsorption capacity was found to highly favour the dehydration pathway, producing

the highest selectivities to lactic acid with the opposite being found for high oxygen adsorption capacity, which was found to produce high selectivities to oxidation pathway products.

Longer reaction times with the AuPt/LaMnO<sub>3</sub> catalysts were found to give an exceptionally high yield to tartronic acid, totalling 88 % over a 24 h period, with the tartronic acid being formed predominantly as a sequential oxidation product of glyceric acid.

Overall, the work conducted in this chapter has allowed for the selective production of highly desirable, value added products from a renewable resource by the design and synthesis of novel AuPt heterogenous catalysts.

#### 4.7. References

1. G. Kremenec, J. M. L. Nieto, J. M. D. Tascon and L. G. Tejuca, *Journal of the Chemical Society, Faraday Transactions 1: Physical Chemistry in Condensed Phases*, 1985, **81**, 939-949.
2. A. Namdeo, S. M. Mahajani and A. K. Suresh, *Journal of Molecular Catalysis A: Chemical*, 2016, **421**, 45-56.
3. C. Xu, Y. Du, C. Li, J. Yang and G. Yang, *Applied Catalysis B: Environmental*, 2015, **164**, 334-343.
4. B. Katryniok, H. Kimura, E. Skrzynska, J.-S. Girardon, P. Fongarland, M. Capron, R. Ducoulombier, N. Mimura, S. Paul and F. Dumeignil, *Green Chemistry*, 2011, **13**, 1960-1979.
5. N. Dimitratos, J. A. Lopez-Sanchez, J. M. Anthonykutti, G. Brett, A. F. Carley, R. C. Tiruvalam, A. A. Herzing, C. J. Kiely, D. W. Knight and G. J. Hutchings, *Physical Chemistry Chemical Physics*, 2009, **11**, 4952-4961.
6. S.-S. Liu, K.-Q. Sun and B.-Q. Xu, *ACS Catalysis*, 2014, **4**, 2226-2230.
7. A. Villa, S. Campisi, K. M. H. Mohammed, N. Dimitratos, F. Vindigni, M. Manzoli, W. Jones, M. Bowker, G. J. Hutchings and L. Prati, *Catalysis Science & Technology*, 2015, **5**, 1126-1132.
8. C. Cristiani, G. Dotelli, M. Mariani, R. Pelosato and L. Zampori, *Chemical Papers*, 2013, **67**, 526-531.
9. H. Zhu, P. Zhang and S. Dai, *ACS Catalysis*, 2015, **5**, 6370-6385.
10. S. Ponce, M. A. Peña and J. L. G. Fierro, *Applied Catalysis B: Environmental*, 2000, **24**, 193-205.
11. J. A. Lopez-Sanchez, N. Dimitratos, P. Miedziak, E. Ntainjua, J. K. Edwards, D. Morgan, A. F. Carley, R. Tiruvalam, C. J. Kiely and G. J. Hutchings, *Physical Chemistry Chemical Physics*, 2008, **10**, 1921-1930.
12. N. Dimitratos, J. A. Lopez-Sanchez, D. Morgan, A. F. Carley, R. Tiruvalam, C. J. Kiely, D. Bethell and G. J. Hutchings, *Physical Chemistry Chemical Physics*, 2009, **11**, 5142-5153.
13. S. Carrettin, P. McMorn, P. Johnston, K. Griffin, C. J. Kiely and G. J. Hutchings, *Physical Chemistry Chemical Physics*, 2003, **5**, 1329-1336.
14. Y. Shen, S. Zhang, H. Li, Y. Ren and H. Liu, *Chemistry – A European Journal*, 2010, **16**, 7368-7371.
15. P. Lakshmanan, P. P. Upare, N. T. Le, Y. K. Hwang, D. W. Hwang, U. H. Lee, H. R. Kim and J. S. Chang, *Appl. Catal. A: Gen.*, 2013, **468**, 260-268.

16. C. Zhang, T. Wang, X. Liu and Y. Ding, *Chinese Journal of Catalysis*, 2016, **37**, 502-509.
17. A. Villa, C. E. Chan-Thaw, G. M. Veith, K. L. More, D. Ferri and L. Prati, *ChemCatChem*, 2011, **3**, 1612-1618.
18. A. I. Y. Tok, F. Y. C. Boey and X. L. Zhao, *Journal of Materials Processing Technology*, 2006, **178**, 270-273.

## 5.0. Conclusions and future work

### 5.1. Conclusions

#### 5.1.2. Ideal conditions for lactic acid production

Using a AuPt/TiO<sub>2</sub> as a standard catalyst, an investigation as to how the reaction conditions affect the rate and selectivity of glycerol oxidation was conducted. The aim of conducting these experiments was twofold. Firstly, the conditions were manipulated sequentially so as to produce the highest potential yield to lactic acid. Secondly, to gain an insight into how the conditions affect the selectivity and rate of the reaction. The reason for establishing a set of reaction conditions was to reduce the considerable variables for the later work within this thesis.

Altering the reaction conditions sequentially seemed like the most efficient way of reaching the ideal conditions for the production of lactic acid within this particular reaction system. The temperature was the first parameter to be altered and it was found that by increasing temperature, the rate of reaction was also increased. This observation is expected and has been seen in many catalytic reactions. As the temperature was increased, the selectivity to lactic acid also increased up to 100 °C. Above this temperature, the carbon balance decreased substantially, indicating a loss of carbon from the system which can be explained by the production of CO<sub>2</sub>, which lowered the yield of lactic acid produced. The second parameter to be altered was the oxygen pressure, increasing from an inert atmosphere up to 4 bar. It was found that the selectivity to lactic acid increased as the oxygen pressure increased up to 3 bar. Above this point, the oxygen pressure increases the initial rate of the reaction, causing an increase in oxidation products at lower reaction times, leading to an increase in C-C scission. The base substrate ratio used in the reaction showed that the amount of base used increases, so too does the selectivity to lactic acid, alluding to the fact that OH<sup>-</sup> plays an integral role in the formation of lactic acid. This result yielded an interesting question as to how the results could be used to further the understanding of the mechanistic pathway to lactic acid. The mechanism has long been debated, and by producing a series of reaction conditions that could provide substantial yields to lactic acid, it may be possible to tease the mechanistic data out of the reaction. To achieve this, a series of conditions to produce a high yield to lactic acid would be necessary to have clear results to interpret.

The parameter mapping work was continued by decreasing the metal substrate ratio, and therefore increasing the amount of catalyst. A negative effect was observed on the

selectivity to lactic acid. Again, the initial rate of reaction with lower metal substrate ratio produced higher amounts of oxidation products, leading to more C-C scission. The highest yield of lactic acid produced was with a metal substrate ratio of 1000:1.

When observing the effect of the stabilising agent on the catalyst activity, it was found that the bulkier stabilising agents effectively blocked active sites on the catalyst surface leading to lower activity. This did, however, correspond to a higher stability. Overall, the catalyst with an acceptable balance between performance and stability was the catalyst prepared with PVA.

Overall the reaction results obtained through the parameter study produced a maximum selectivity of 83 % to lactic acid using the following conditions; 100 °C, 3 bar O<sub>2</sub>, 4:1 base ratio, 1000:1 substrate metal ratio using a 1 wt% AuPt/TiO<sub>2</sub> produced through the sol immobilisation method using a PVA stabilising agent.

### 5.1.2. Determining the mechanistic route to lactic acid

The mechanistic route to lactic acid has been a subject of debate in literature for some time<sup>1</sup>. There is a general agreement that the initial steps involve an initial oxidation of glycerol to glyceraldehyde, which isomerises to dihydroxyacetone. The steps following the initial oxidation are the debated factors. It has been postulated that the reaction proceeds through dehydration to pyruvaldehyde which then undergoes a base catalysed benzylic rearrangement to form lactic acid<sup>2</sup>. This theory could be rationalised through the observations found in the parameter mapping study, where an increase in the concentration of base in the reaction medium produced a higher selectivity to lactic acid. The other popular theory is that the reaction proceeds through what is referred to as an intramolecular Cannizzaro type reaction<sup>3</sup>. This suggests that dihydroxyacetone is converted to pyruvaldehyde under acid exposure, using the acidic media to favour the dehydration pathway in the reaction. The nomenclature used for this explanation can be somewhat confusing, as a true Cannizzaro reaction is a hydroxide induced intermolecular hydride transfer between aldehyde groups.

Several experimental designs were theorised to attempt to resolve the mechanism of formation of lactic acid. Based on the initial theories, two potential models were developed to describe the carbon environments as the glycerol is converted to lactic acid. The design of the labelling study, in which the possible labelling would have either been deuterated samples of glycerol or <sup>13</sup>C labelled glycerol, with either the terminal carbons labelled or the central carbon. When deciding which experiments to conduct to confirm the mechanism, the simplest method initially was thought to be the deuterated sample, and viewing how the base interacted with the glycerol to form lactic acid. After consideration, the likelihood of the D species exchanging with

the solvent was too high to warrant a conclusive test. Labelling the carbon species would require a high yield to lactic acid, so as to differentiate the lactic acid produced from any other products. The initial parameter mapping study had provided the means to achieving a high yield to lactic acid, and therefore  $^{13}\text{C}$  labelling was chosen as the potential starting point of the reaction. A 1,3-di- $^{13}\text{C}$ -glycerol sample was used, opposed to the 2- $^{13}\text{C}$ -glycerol, as the environments of the terminal carbons would confirm the mechanism, provided there was no net movement. NMR of the produced sample showed no net movement of the terminal carbons, proving that the benzylic rearrangement was definitively not the mechanistic route, as the carbon environments would change during the coupling, as illustrated in the curly arrow diagram in the introduction. As to the Cannizzaro route, if considered as a true Cannizzaro type reaction, with an intermolecular hydride transfer between aldehyde groups, the environments would again not show the correct result. The mechanism could therefore only be an intramolecular hydride shift, requiring both base and a Lewis acid to proceed effectively, thereby solving the debate of the formation of lactic acid.

### 5.1.3. Controlling product distribution with perovskites

The formation of perovskite type  $\text{ABO}_3$  mixed metal oxides was achieved through the use of the SAS precipitation technique. This method of production enabled the synthesis of relatively high surface area perovskite materials, which typically have surface areas lower than  $10 \text{ m}^2 \text{ g}^{-1}$ . The range of perovskites formed were La based materials with varying B sites, i.e. Cr, Mn, Fe, Co and Ni. The perovskites were formed to act as supports in glycerol oxidation, to view how the support could alter the reaction.

Using sol-immobilisation, 1 wt% AuPt nanoparticles were deposited on the surface. Initially, the method did not work as intended due to the nature of the supports, therefore requiring the elimination of the acidification step. Conditions for the reaction were established in the parameter mapping study and were used for the subsequent reactions in the perovskite work. The conditions used showed high yields to lactic acid with a standard AuPt/ $\text{TiO}_2$  catalyst. This was not the case when using the perovskite supports, however, where it was found that the B site substitution had a significant effect on the selectivity profile of the reaction.

Depending on the B site used, it was found that it was possible to control the reaction pathway using the same conditions. It was found that by substituting Co/Ni into the B site, that the product distribution was varied, with a wide selectivity distribution of the products. Cr and Fe were found to favour the dehydration pathway of the reaction, of which both exhibit Lewis acidic sites, therefore promoting the intramolecular hydride shift identified in the mechanism

study. Mn showed a high affinity to the oxidation pathway, initially resulting in high yields to glyceric acid, which then further oxidised to tartronic acid, which is an extremely difficult to produce product.

It was found that the perovskites were only active when used as supports for AuPt, as when they were tested alone, there was virtually no activity for glycerol oxidation. The B site also had no discernible effect on the AuPt particle sizes/morphology, alluding to the supports having a direct effect on the substrate, that is only activated in the presence of supported nanoparticles.

There was a strong correlation found between reported oxygen adsorption of the B site perovskite supports and the selectivity distribution of the products from the oxidation of glycerol. Whilst low oxygen adsorption was found to favour the dehydration pathway, high oxygen adsorption was found to favour the oxidation pathway.

The two most promising catalysts produced were the AuPt/LaMnO<sub>3</sub> and the AuPt/LaCrO<sub>3</sub>. AuPt/LaMnO<sub>3</sub> was found to produce an unprecedented 88 % yield of tartronic acid at extended reaction times, with the higher temperature conditions allowing for the sequential oxidation of glyceric acid. AuPt/LaCrO<sub>3</sub> produced an 86 % yield to lactic acid, which is currently the highest reported yield.

## **5.2. Future work**

### **5.2.1. A site Doping**

During this thesis, the effect of the B site of perovskite materials has been investigated for the oxidation of glycerol. The next logical step would be to see how changing the A site of the perovskite affects the reaction. When thinking about the perovskite structure, it is important to consider the ionic radius of the A and B site cations, to ensure the lattice strain does not exceed a point at which the perovskite structure will no longer form. The first step would be to consider cations with similar ionic radius to that of La, which logically leads to the lanthanide metal series. One could work through the lanthanide series sequentially, characterising the materials formed, however, this method would be inefficient. The simplest method would be to observe the cations that have an affinity for the 3/4<sup>+</sup> oxidation states, as these oxidation states are the most favourable for the B site cations that would be selected for further work, i.e. Mn or Cr. Unfortunately, Cr has a stigma from the extremely toxic 6<sup>+</sup> oxidation state, and whilst the 3<sup>+</sup> state would be found in the perovskite structure, the risk of Cr<sup>6+</sup> being formed is too high for

it to pass industrial standards of production. Therefore, when considering Mn, which is most stable in its  $2/3^+$  state, cations such as Ce or Sm would be ideal substitutions for further study.

Another method would be to dope lanthanides into the A site alongside La, to try and introduce a mixed metal oxide where the oxidation states continuously balance each-other as oxygen is absorbed into the lattice structure, potentially creating an environment where the oxygen is continuously absorbed and desorbed to the substrate. This could increase the oxidation potential of the catalyst, resulting in a more efficient catalytic process.

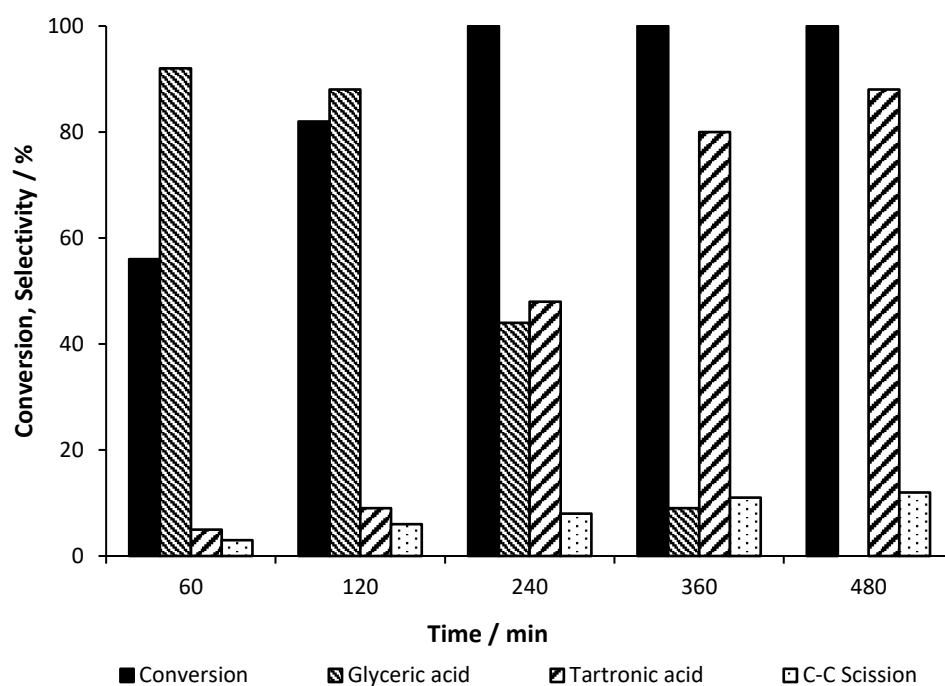


**Figure 5.1 Product distribution for glycerol oxidation using a 1 wt % AuPt/La<sub>(0.8)</sub>Ce<sub>(0.2)</sub>MnO<sub>3</sub>. Reaction conditions; 10 ml Glycerol (0.3 M), temperature (100 °C), O<sub>2</sub> pressure (3 bar), NaOH:substrate (4:1), substrate:metal ratio (1000:1) at 8 h reaction time.**

Initial studies of this idea have been conducted, where Ce was doped into the A site of the LaMnO<sub>3</sub> structure at 20% of the A site. Interestingly this was found to increase the rate of conversion by a factor of 2, and producing an 88 % yield to tartronic acid in half the time it took the LaMnO<sub>3</sub> alone. These results led to an initial study in flow studies on the doped catalyst, shown in Figure 5.1.

The AuPt/LaCeMnO<sub>3</sub> was also tested for 1,2-propanediol oxidation, in which lactic acid can form from both the dehydration or oxidation pathways. The catalyst was found to produce a 98 % yield to lactic acid over 4 hours, as shown in the product distribution table, Figure 5.2.

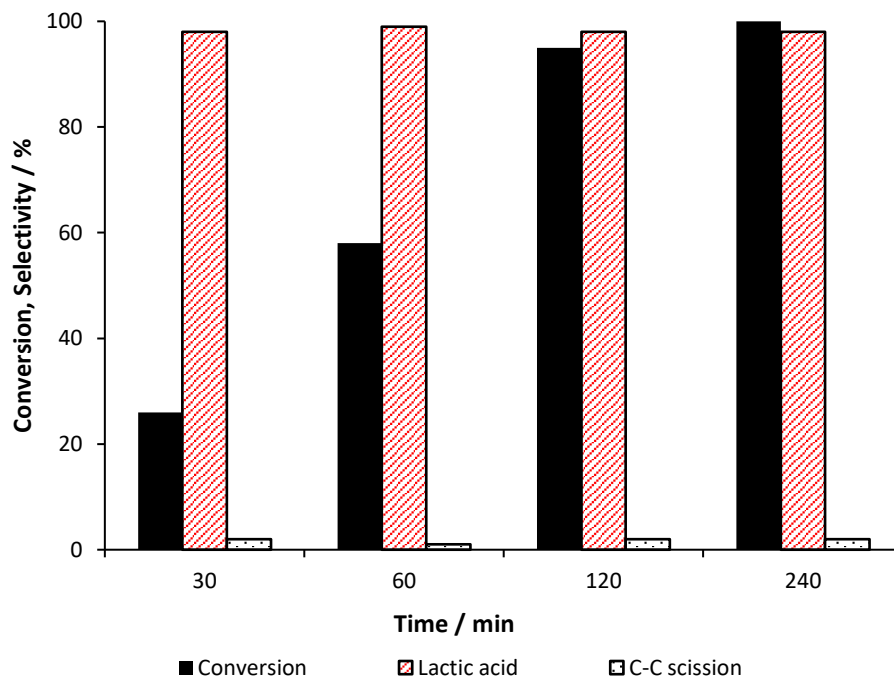


**Figure 5.2 Product distribution for 1,2-propanediol oxidation using a 1 wt % AuPt/La<sub>(0.8)</sub>Ce<sub>(0.2)</sub>MnO<sub>3</sub>. Reaction conditions; 10 ml propanediol (0.3 M), temperature (100 °C), O<sub>2</sub> pressure (0.3 bar), NaOH:substrate (4:1), substrate:metal ratio (1000:1) at 4 h reaction time.**

### 5.2.2. Glycerol in flow

Conducting oxidation in flow is the ultimate goal for the selective production of products, as industrially, this provides the most effective route to continuous production. The issue with the perovskite catalysts investigated in this project is that the activity at early reaction times is too low to be effectively used in a flow system. The development of the AuPt/LaCeMnO<sub>3</sub>, with the much higher activity allowed for initial studies into a flow system to be conducted. A simple trickle bed reactor setup was used to find if the newly developed catalyst would be viable for further flow testing.

Initial testing was successful, showing a 30 % conversion of glycerol with a combined 100 % selectivity to the oxidation products glyceric acid and tartronic acid. The bed volume was increased to increase contact time on the catalyst. It was found that by doubling the bed volume that the conversion also doubled to 60 % conversion whilst maintaining a high selectivity to the

oxidation products. A proposal to continue this work has been accepted beginning in October 2017.

### 5.3 References

1. J. Xu, H. Zhang, Y. Zhao, B. Yu, S. Chen, Y. Li, L. Hao and Z. Liu, *Green Chemistry*, 2013, **15**, 1520-1525.
2. M. Tao, D. Zhang, H. Guan, G. Huang and X. Wang, *Scientific reports*, 2016, **6**.
3. S. Lux and M. Siebenhofer, *Chemical and biochemical engineering quarterly*, 2016, **29**, 575-585.